

1 GRACE, time-varying gravity, Earth system 2 dynamics and climate change

3 **B. Wouters^{1,2}, J.A. Bonin³, D.P. Chambers³, R.E.M. Riva⁴, I.
4 Sasgen^{5,6}, J. Wahr²**

5 ¹ Bristol Glaciology Centre, School of Geographical Science, Bristol, UK

6 ² Department of Physics, University of Colorado at Boulder, Boulder, Colorado, USA

7 ³ College of Marine Science, University of South Florida, St. Petersburg, Florida,
8 USA

9 ⁴ Department of Geoscience and Remote Sensing, Delft University of Technology,
10 Delft, Netherlands

11 ⁵ German Research Centre for Geosciences, Potsdam, Germany

12 ⁶ Department of Geosciences, The Pennsylvania State University, University Park,
13 USA

14 **Abstract.**

15 Continuous observations of temporal variations in the Earth's gravity field have
16 recently become available at an unprecedented resolution of a few hundreds of
17 kilometers. The gravity field is a product of the Earth's mass distribution, and these
18 data – provided by the satellites of the Gravity Recovery And Climate Experiment
19 (GRACE) – can be used to study the exchange of mass both within the Earth and
20 at its surface. Since the launch of the mission in 2002, GRACE data has evolved
21 from being an experimental measurement needing validation from ground truth, to a
22 respected tool for Earth scientists representing a fixed bound on the total change and
23 is now an important tool to help unravel the complex dynamics of the Earth system
24 and climate change. In this review, we present the mission concept and its theoretical
25 background, discuss the data and give an overview of the major advances GRACE has
26 provided in Earth science, with a focus on hydrology, solid Earth sciences, glaciology
27 and oceanography.

28 **1. Introduction**

29 Gravity is one of nature's fundamental forces. Although most people tend to think of
30 gravity – or, more precisely, the gravitational acceleration g at the Earth's surface – as
31 a constant of approximately 9.81 m/s^2 , it is not uniform around the globe. The Earth's
32 rotation and its equatorial bulge cause deviations from the mean value of about half a
33 percent, which can be well predicted from theory. Because the Earth's gravity field is
34 a product of its mass distribution, variations in the density of the Earth's interior and
35 topography cause further regional deviations of a few tens of a millionth of g (Figure 1).
36 These are much harder to model, since this requires knowledge of the Earth's structure.
37 However, mass transport in the interior is a slow process, so that these deviations can be
38 considered to be more or less constant on human timescales. Water, on the other hand,
39 is much more mobile than rock and its constant movement on the Earth's surface and
40 in the atmosphere will cause changes in the gravity field on a wide range of time scales.
41 These variations are minute, but measuring them accurately means literally 'weighing'
42 changes in the Earth's water cycle and could help unravel the complex dynamics of
43 the Earth system and climate change. The list of possible applications of time-variable
44 gravity measurements is abundant: tracking changes in the water held in the major
45 river basins, observing variations in the hydrological cycle, measuring the ice loss of
46 glaciers and ice sheets, quantifying the component of sea level change due to transfer of
47 water between the continents and oceans, detection of water droughts and the depletion
48 of large groundwater aquifers due to unsustainable irrigation policies, and much more,
49 would all be possible. And even processes within the solid Earth would be measurable,
50 provided that they occur fast enough and their gravitational signal is strong enough
51 (e.g., mega-thrust earthquakes). As we will see, all of this and more has become reality
52 at a global scale since the launch of the Gravity Recovery And Climate Experiment
53 (GRACE) satellites.

54 Although the temporal gravity variations associated with the phenomena listed
55 above are extremely small ($\sim 10^{-8} \text{ m/s}^2$), they can be measured with dedicated
56 instruments. Locally, time variations in gravity can be recorded accurately on the
57 ground by gravimeters [1], but global, satellite-based, measurements of time-variable
58 gravity have long been restricted to mapping large-scale variations only. These
59 early observations were mainly based on satellite laser ranging (SLR), which involves
60 measuring the position of satellites orbiting the Earth, with a precision of a few cm or
61 better. Such a high precision is obtained by emitting a laser pulse to a dedicated satellite,
62 covered with reflectors, and measuring the round-trip travel-time once the reflected pulse
63 is received. By collecting a sufficient amount of such position measurements, the orbit
64 can then be determined, which is for a large part determined by the Earth's gravity
65 field. However, these satellites – such as the Laser Geodynamics Satellites (LAGEOS
66 [2]), launched in the 1970s and 1990s and still operational today – orbit the Earth at
67 a high altitude ($\sim 6000 \text{ km}$) to minimize atmospheric drag. Because the sensitivity to
68 the Earth's gravity field decreases with increasing altitude, the determination of time-

69 variable gravity with SLR is restricted to scales of typically 10,000 km [e.g., 3]. For
70 a higher resolution, satellites at a lower altitude are required, such as the Challenging
71 Minisatellite Payload (CHAMP; [4]) satellite, which allowed continental-scale gravity
72 observations at seasonal periods (2000–2010), and in particular GRACE, the subject of
73 this review article.

74 Like many space missions, GRACE had a long history of negotiation and
75 deliberation before the satellites saw daylight. For at least two decades prior to its
76 launch, the Earth Science community had been calling for a dedicated gravity satellite
77 mission to provide an improved determination of the Earth's static, global gravity
78 field [e.g., 5, 6, 7, 8]. While that message had always been well received by NASA
79 and other space agencies, the arguments had not been persuasive enough to lead
80 to an approved mission. A combination of events in the late 1990's changed that
81 situation, and culminated in the acceptance of GRACE. One was the innovative GRACE
82 measurement concept itself, which permits the recovery of monthly global gravity
83 solutions of unprecedented accuracy down to scales of a few hundred km. Originally,
84 though, the focus of GRACE was still to be on the static field. But officials at NASA,
85 wondering about the possible scientific payoff of time-variable gravity measurements,
86 commissioned the US National Research Council to undertake a study to look into this.
87 Prior to that study, it was known that a mission like GRACE could recover the secular
88 gravity changes due to vertical land-motion to useful accuracy, but there had been
89 virtually no work done on the possible use of time-variable satellite gravity to study
90 other processes. The resulting NRC committee, chaired by Jean Dickey, discovered a
91 multitude of possible applications that were well suited to the expected spatial and
92 temporal resolution of GRACE [9]. The proposed GRACE mission design and science
93 plan were subsequently adjusted to focus on the time-variable field, rather than on the
94 static field. The usefulness of these time-variable applications and their relevance to such
95 a wide variety of Earth science disciplines, as well as the perceived ability of GRACE
96 to recover those signals, were certainly among the factors that influenced the decision
97 by NASA and DLR, the German space agency, to fund the mission. Relatively soon
98 after funding was approved, the mission was launched on March 17, 2002, from Plesetsk
99 Cosmodrome in Russia.

100 GRACE has lead to important new insights in many scientific fields, ranging from
101 verifying the 'Lense-Thirring effect' of general relativity [10] to the detection of a
102 giant meteorite impact crater underneath the Antarctic ice sheet [11], to observing
103 tropospheric density changes during geomagnetic storms [12], but it has greatly
104 advanced our understanding of how masses move within and between the Earth's
105 subsystems (land, ocean, ice and the solid earth, in particular [13, 14]). Before reviewing
106 the progress made in time-variable gravity research since the launch of GRACE, we
107 briefly discuss the mission design, some essential equations and the GRACE data.

108 1.1. The GRACE satellites & data

109 Although every satellite mission is a mammoth, complex operation, the basic principle
110 of GRACE is beautiful in its simplicity. GRACE consists of two satellites in a low,
111 near-circular, near-polar orbit with an inclination of 89° , at an altitude of about 500
112 kilometres, separated from each other by a distance of roughly 220 kilometres along-
113 track (Figure 2). The mission does not measure gravity directly with an active sensor,
114 but is based on the satellite-to-satellite tracking concept, which tracks variations in the
115 inter-satellite distance and its derivatives to recover gravitational information. Suppose
116 the satellites approach a sizeable mass located on the Earth's surface (e.g., an ice
117 sheet): since the two GRACE satellites are separated by a certain distance, and the
118 gravitational pull of the mass is inversely proportional to the squared distance to each
119 satellite, the orbit of each of the satellites will be perturbed slightly differently. The
120 leading satellite will be pulled slightly more towards the mass than the trailing one and
121 the separation between the satellites will increase. Although these changes are minute
122 – in the order of a few micrometres, or 1/100th of the width of a human hair – they can
123 be measured by means of a dual-one way ranging system, the K/Ka band microwave
124 ranging system (KBR). Non-gravitational forces, such as atmospheric drag will also alter
125 the relative distance, and are accounted for using onboard accelerometer measurements.
126 The orientation in space of the satellites are mapped by two star-cameras. Since the
127 KBR measurements provide no information on the position in the orbit, the satellites
128 are equipped with Global Positioning System (GPS) receivers so that their location is
129 known.

130 From these data, called the Level-1 data, variations in the Earth's gravity field
131 can be recovered. This is generally done through an iterative procedure: first, an
132 a-priori model of the Earth's mean (static) gravity field in combination with other
133 'background' force models (e.g., representing luni-solar and third body tides, ocean
134 tides, the pole tide, etc.) is used to determine the orbit of both satellites. Importantly,
135 the gravitational effects of ocean and atmosphere mass variations are removed from
136 the measurements at this step using numerical models, because otherwise their high-
137 frequency contributions would alias into longer periods and bias the results. Next,
138 this predicted orbit is compared to the GPS and KBR observations and residuals are
139 computed. Linearized regression equations are constructed, which relate the gravity
140 field (more specifically, the spherical harmonic coefficients as we will see next) and
141 other parameters to the residuals and are used to update the orbit. By combining
142 data of a sufficiently long period – about a month, which guarantees a sufficient ground
143 track coverage of the satellites – these equations can be used to relate the Level-1
144 observations to variations of the gravity field in a least square sense (see [15, 16]). The
145 GRACE data are processed at three main science data centers, i.e., the Center for Space
146 Research (CSR) and the Jet Propulsion Laboratory (JPL), both located in the USA.,
147 and the German Research Centre for Geosciences (GFZ) in Germany. Differences in
148 the approaches of the processing centers lie in the background models used, the period

149 over which the orbits are integrated, weighting of the data, the maximum degree of
 150 the estimated gravity harmonics, etc. [17, 18, 19]. Other institutes are also providing
 151 independent gravity solutions nowadays, often based on alternative approaches [e.g.,
 152 20, 21, 22].

153 Next, we discuss the basic equations behind temporal gravity and the GRACE data.
 154 For the casual reader, it suffices to know the GRACE data generally are distributed as
 155 (*Stokes*) coefficients of spherical harmonic functions of degree l and order m , which can
 156 be related to variations in water height at the Earth's surface. The maximum harmonic
 157 degree of the data depends on the analysis center, but in all cases it is sufficient to
 158 provide a spatial resolution of roughly 300 km.

159 The Earth's gravitational field is described by the geopotential V . At a point above
 160 the Earth's surface, with spherical coordinates radius r , co-latitude θ and longitude λ ,
 161 it can be expressed as a sum of Legendre functions:

$$V(r, \theta, \lambda) = \frac{GM}{a_e} \sum_{l=0}^{\infty} \left(\frac{a_e}{r} \right)^{l+1} \sum_{m=0}^l P_{lm}(\cos \theta) (C_{lm} \cos m\lambda + S_{lm} \sin m\lambda) \quad (1)$$

162 where G is the gravitational constant, M the mass of the Earth and a_e denotes
 163 its mean equatorial radius. P_{lm} are the Legendre polynomials of degree l and order m ,
 164 and C_{lm} and S_{lm} are the spherical harmonic coefficients. The higher the order l , the
 165 smaller the spatial scale [see, e.g., 23, for a good introduction]. Note that as l increases,
 166 $(a_e/r)^{l+1}$, and consequently also variations in V , become smaller. Thus, satellites at
 167 lower altitudes r can better resolve small wavelength features.

168 Equation 1 may be used to define equipotential surfaces, i.e. surfaces of constant
 169 potential V . The equipotential surface that would best fit the mean sea level at rest is
 170 referred to as the geoid, which in turn can be approximated by an ellipsoid of rotation.
 171 The height difference between such a 'reference ellipsoid' and the geoid is referred to as
 172 the geoid height and is approximated by Bruns formula:

$$N = \frac{V(R, \theta, \lambda) - U}{\gamma} \quad (2)$$

173 where U is the gravitational potential on the reference ellipsoid, equal to the constant
 potential of the geoid, and γ the normal gravity on the ellipsoid's surface. The latter
 can be further approximated by GM/a_e^2 , so that in turn the geoid height can be
 approximated by [23]:

$$N(\theta, \lambda) \approx a_e \sum_{l,m} P_{lm}(\cos \theta) (C_{lm} \cos m\lambda + S_{lm} \sin m\lambda) \quad (3)$$

174 From this it follows that variations in the geoid height can be fully described by
 175 the spherical harmonic coefficients C_{lm} and S_{lm} , referred to as *Stokes* coefficients in
 176 geodesy. It is this set of coefficients that is estimated from the satellite measurements and
 177 distributed by the GRACE science teams every month as Level-2 data. The maximum
 178 degree l of the monthly Stokes coefficients lies between 60–120, which corresponds to a
 179 spatial resolution of roughly 150–300 km (20,000 km/ l).

180 Geoid height is a commonly used unit in geodesy, but one more step is required to
 181 relate the Stokes coefficients to changes in (water) mass distribution, a more intuitive
 182 metric to most researchers studying the Earth's water cycle. On monthly to yearly time-
 183 scales, changes in the Earth's gravity field are primarily caused by redistribution of water
 184 in its fluid envelope, which all take place within a thin layer of a few kilometers near the
 185 Earth's surface. In this case, $(a_e/r)^{l+1}$ in Equation 1 reduces to 1 and the anomaly in
 186 surface density (i.e., mass per area) can then be obtained using the following equation
 187 [see 24, for a step-by-step derivation]:

$$188 \quad \Delta\sigma(\theta, \lambda) = \frac{\rho_e}{3} \sum_{l=0}^{\infty} \sum_{m=0}^l P_{lm}(\cos\theta) \frac{2l+1}{1+k_l^1} \times (\Delta C_{lm} \cos(m\lambda) + \Delta S_{lm} \sin(m\lambda)) \quad (4)$$

189 where we included the symbol Δ to indicate that we are dealing with time-variable
 190 quantities, and ρ_e is the average density of the Earth (5517 kg/m^3). The load Love
 191 numbers k_l^1 [e.g., 25] account for deformation of the solid Earth due to the loading of
 192 the mass anomaly on its surface, which will cause a small gravity perturbation as well.
 193 Units of $\Delta\sigma$ are typically kg/m^2 . Often, the surface density is divided by the density
 194 of water, which yields surface water height in *meters water equivalent*. An example of
 195 the surface height anomaly observed by GRACE for August 2005 is shown in Figure 3.
 196 When integrating $\Delta\sigma$ over an area, one obtains a volume estimate, usually expressed
 197 as km^3 of water, or, equivalently, gigatonnes (Gt). One gigatonne equals 10^{12} kg , a sea
 198 level rise of 1 mm requires approximately 360 Gt of water.

199 The monthly GRACE Stokes harmonics are publicly available and can be
 200 downloaded from <http://podaac.jpl.nasa.gov> and <http://isdc.gfz-potsdam.de>.
 201 While the availability of GRACE data only as unfamiliar spherical harmonics originally
 202 slowed its application toward wider use by non-geodesists, the data has more recently
 203 been made available in easier-to-use gridded format as well (<http://geoid.colorado.edu/grace/grace.php> or <http://grace.jpl.nasa.gov/data/>). Yet, as we will see
 204 later on, interpretation of these gridded maps is not always straightforward and requires
 205 some expertise.

207 Some researchers also derive regional mass anomalies directly from the Level-1
 208 range-rate data. In a method originally developed to study the gravity field of the
 209 moon, point masses or regional uniform mass concentrations ('mascons') are spread
 210 over the Earth's surface. The gravitation acceleration exerted by each mascon is then
 211 expressed as a sum of spherical harmonic functions so that the effect on the GRACE
 212 orbit can easily be computed. Each mascon is then given a scaling factor which is
 213 adjusted to give the best fit to the regional KBR observations [e.g., 26, 27]. Although
 214 this approach is computationally much more demanding, it has certain advantages,
 215 e.g., regional solutions can be obtained and certain constraints can be applied between
 216 neighbouring mascons to reduce the leakage problem, as discussed below.

1.2. Handling the GRACE data

The first GRACE science results were published about two years after the mission launch [28, 29]. Many geophysical features – such as the seasonal change in water storage in the Amazon river system – were readily recognizable, but surprisingly, the maps of surface water height showed distinctive North-South striping patterns (Figure 3a). Although it had been anticipated during the mission design phase that the higher degree Stokes coefficients (i.e., small spatial scale) would have larger errors than the lower degrees (large spatial scale), such – clearly unphysical – striping had not been foreseen. The origin of these stripes lies in the orbit geometry of the GRACE mission [e.g. 30, 31]. The gravity field is sampled using the variations in the along-track distance between the two satellites, which circle the Earth in a near-polar orbit. As a result, the observations bear a high sensitivity in the north-south direction, but little in the east-west direction. Errors in the instrument data, shortcomings in the background models used to remove high-frequency atmosphere and ocean signals, and other processing errors will consequently tend to end up in the east-west gravity gradients. Since the release of the first GRACE data, methods to process the satellite data have improved and new ocean and atmosphere models allow for a better removal of high-frequency variability signals from the observations. This has led to new, reprocessed GRACE solutions, which contain significantly less noise than earlier releases [32], as illustrated in Figure 3. Yet, although much reduced, the North-South striping problem persists.

Several methods have been developed to reduce the effect of noise in the GRACE data. One technique converts the global spherical harmonics into a local time series and then averages the observations over a larger, pre-determined region, such as river or drainage basins. If the area is sufficiently large – larger than the spatial decorrelation scale of the noise – the noise will tend to cancel out. Based on this concept, [33] formulated a ‘basin averaging approach’ which aims to isolate the signal of individual regions while minimizing the effects of the noise and contamination of signals from the exterior. The ‘basin averaged’ time series of the surface water anomalies can then be analyzed or compared to regional ground-based measurements. This has become a very common method of analysis with GRACE, especially in hydrological studies (see section 2).

Another straightforward and very commonly applied approach reduces the noise in the GRACE observations by smoothing the data. In the spectral domain, this means weighting the Stokes coefficients depending on the degree l , with a lower weight given to the noisier, higher degree Stokes coefficients. In the spatial domain, this is equivalent to convolving the GRACE maps with a smoothing kernel. A popular kernel is the Gaussian, bell-shaped, function, which decreases smoothly from unity at its center to zero at large angular distances (Figure 4) and is characterized by its *smoothing radius*, i.e., the distance on the Earth’s surface at which the kernel value has decreased to half the value at its center [34, 24]. As the smoothing radius increases, the higher degree Stokes coefficients are damped more strongly and the noise in the GRACE data

is reduced (Figure 5a-c). Unfortunately, using a large smoothing radius also means that the true, geophysical signals are damped and are smeared out over large regions, hindering a straightforward interpretation of the GRACE observations.

The Gaussian kernel has an isotropic character, i.e., it is independent of orientation, but as discussed above, the noise in the GRACE data has a strong non-isotropic North-South character. Non-isotropic filters have been developed [35, 36], but these generally still require a large smoothing radius to remove all stripes in the GRACE maps. A closer inspection of the GRACE Stokes coefficients by Swenson and Wahr [37] revealed that striping patterns could be traced back to correlated errors in the Stokes coefficients of even and odd degree l , respectively. This opened the door to more advanced post-processing methods which allowed a further increase of the spatial resolution of the GRACE data. To reduce the intercoefficient correlation, Swenson and Wahr [37] fit a quadratic polynomial in a moving window to the Stokes coefficients of even and odd degrees separately (for a fixed order m) and removed this from the original Stokes coefficients. Other methods apply principal component analysis on the Stokes coefficients [38] or use the full variance-covariance matrix of the Stokes coefficients [39, 40] to decorrelate the GRACE solutions. These advanced postprocessing methods have led to a reduction of noise in the GRACE data of 50% and more [Figure 6; 41].

Unfortunately, the limited resolution of the GRACE data and the required post-processing means that the observations do not represent point-measurements. Additionally, any type of post-processing filter or during-processing constraint which reduces GRACE errors can also reduce local signal amplitude [42, 43, 44, 45]. So, when studying a specific region, one cannot simply take the average of the GRACE observations over that region. Besides the signal attenuation, leakage effects will bias such a simple average: due to the low resolution, water mass variations in neighbouring areas will spill into the desired region, while part of the signal of interest will spread outside the region. Leakage is particularly problematic in regions of high spatial variability in surface water storage patterns, as well as along coastlines where smoothing with the ocean's far smaller signal notably damps the apparent hydrological signal. Rescaling is commonly used to remedy the signal loss caused by post-processing and the transformation of point-source signals to a finite number of spherical harmonics (e.g., up to degree and order 60). To compute a rescaling parameter, a model is made with higher spatial resolution than GRACE, then transformed to the limited set of spherical harmonics that GRACE uses and post-processed identically to GRACE. A ratio of the original model to the post-processed model signal amplitude is called the rescaling parameter. Assuming that the model reasonably represents the spatial pattern of the true signal, this ratio can act as a multiplier to upscale or downscale the actual post-processed GRACE data and counter the amplitude damping effect seen as leakage. Typically, the rescaling has been done on a basin scale [e.g., 46], though recently Landerer and Swenson [44] have tested and released a $1^\circ \times 1^\circ$ mapped version of GRACE with rescaling and rescaling errors included, specifically focused at hydrologists. Nonetheless, limitations and inaccuracies at short spatial scales remain a

300 problem, especially as the focus moves to smaller and smaller basins.

301 In addition to spatial limitations, GRACE's typical monthly sampling rate also
302 limits its ability to estimate signals that act at shorter than seasonal time scales, though
303 it handles annual and longer-term signals well. Recently, a few sub-monthly signals have
304 been produced [47, 48, 49, 50, 20, 26], but the remaining delay between observation
305 and data delivery makes real-time assessments (for which they would be most desired)
306 impossible. Typically, increasing the temporal resolution of the GRACE time series
307 means accepting an increased noise level in the signal, since the ground track coverage
308 becomes less dense. Various types of constraints can ameliorate the difficulty, but not
309 eliminate it entirely – and these constraints often alter the signal strength along with
310 that of the noise.

311 After these introductory sections, we will now give an overview of the Earth Science
312 applications of GRACE in the fields which have most benefited from this unique new
313 set of time-variable gravity observations (hydrology, solid Earth sciences, glaciology and
314 oceanography). Each section discusses the unknowns before GRACE was launched, the
315 major scientific advances the mission provided and its limitations.

2. GRACE and Hydrology: A bound on terrestrial water storage

GRACE's ability to accurately measure sub-yearly to decadal-trend mass changes on the global and regional scales has made it a unique data source for hydrology and hydrological modeling. Prior to the GRACE mission, total terrestrial water storage (TWS) changes over land could not be measured over significant spatial or temporal scales. Instead, the focus was on individual pieces of TWS: groundwater (GW), near-surface and deep soil moisture (SM), surface water (SW), snow-water equivalent (SWE) and ice, and water contained within biomass (BIO). These subsections of the terrestrial water storage were measured via *in situ* systems or other satellites, and/or were modeled from basic principles. However, the difficulty and expense of establishing and maintaining reliable *in situ* observation systems is significant, especially over large and remote areas and for long periods of time. Where observation coverage is good, *in situ* measurements have focused on particular sub-sections of the water signal, resulting in, for example, excellent coverage of near-surface soil moisture and groundwater, but no knowledge at all of surface water. Hydrological models also reflect this, often lacking one or more components of water storage in their computations. A growing selection of remote sensing hydrologic tools exist, but few have long data records and none besides GRACE see signals below a shallow subsurface layer.

GRACE's ability to measure the sum of all hydrologic components in the water column, over the entire planet, at monthly intervals has proven a bounty for large-scale hydrological researchers. Two parallel techniques exist when using GRACE for hydrologic purposes. The first, as suggested above, is to solve for changes in TWS directly, based on changes (Δ) in some or all of the individual components of water storage listed above:

$$\Delta TWS = \Delta GW + \Delta SM + \Delta SW + \Delta SWE + \Delta BIO \quad (5)$$

This technique is particularly valuable in combination with observed data for some of the terms on the right-hand side of equation 5, using GRACE to give the ΔTWS sum. The second common technique is to consider the processes which cause changes in terrestrial water storage, principally precipitation (P), evapotranspiration (E), and runoff/discharge (R):

$$\Delta TWS = P - E - R \quad (6)$$

This is often useful for modelers, who can use GRACE's estimate of terrestrial water storage changes to bound their estimates of P, E, and/or R, oftentimes in combination with other observations of those same variables. The combination of P-E can also be estimated based on atmospheric anomalies, if the change in water vapor and the divergence of the atmospheric moisture transport are known. Whether using equation 5 or 6, GRACE measurements present a mathematical bound which did not exist before.

Besides the main limitations of GRACE mentioned in the introduction, such as the need for smoothing and post-processing, the limited spatial resolution and leakage

of GRACE signal into and out of the desired region, a major complexity with using GRACE for hydrologic purposes is inherent in its definition: GRACE measures the entire water column as one measurement. This makes separation into hydrologic constituents complicated, requiring combination with other hydrologic products, all of which have their own limitations and errors. The differing spatial and temporal scales between GRACE (a global, monthly product) and *in situ* data such as river or well gauges (point-source measurements which are non-uniform in space and time) makes exact comparisons and combinations difficult. Complications can also arise if non-hydrologic mass signals, such as alterations of mass in the atmosphere or solid Earth or leakage from the nearby ocean, also occur in the region, a particular problem given that models to correct for such signals are not perfect. The lower noise levels of GRACE RL05 [32] are expected to reduce many of these problems, but the general design of the GRACE mission means that they cannot be completely eliminated.

The use of GRACE by hydrologists has gone through two historical stages: validation and full utilization. For several years after the 2002 launch of GRACE, the focus was on using hydrological models and observational data to determine the accuracy of GRACE itself. Many of the initial comparisons were qualitative and large-scale. Various researchers [27, 26, 51, 28] created side-by-side comparisons of GRACE with hydrological models, as in Figure 7a, or otherwise noted that the dynamically-active regions seen by GRACE matched where hydrological models and our previous understanding of weather and climate placed them. Others [52, 53, 29] compared GRACE results to hydrological models across large basins (Figure 7b) and noted that both amplitude and phase were typically close. Later, EOF analyses were used to better quantify the similarities [54, 55]. The images shown here use the most recent CSR RL05 GRACE series from February 2004 to January 2012, but even one or two years of RL01 GRACE were sufficient to verify the general accuracy of GRACE in large, hydrologically-active regions.

Once several years of GRACE data had been garnered, hydrological GRACE papers became more in-depth and quantitative, using models, *in situ* data, or both to verify the general accuracy of GRACE and estimate the combined error in GRACE and their other data sources. A fine early example is Swenson et al. [56], who made use of a widespread *in situ* well and soil moisture network in the US state of Illinois. Based on prior knowledge, they assumed that the dominant terms in equation 5 in Illinois were groundwater (GW) and near-surface soil moisture (SM), ignoring surface water, snow, and the effect of the biosphere. They smoothed and destriped three years (2003–2005) of GRACE RL01 data, took the significant gravitational signal associated with vertical land motion (see Section 3) into account, then used a basin average to compute the ΔTWS time series over the Illinois region. When they compared the GRACE ΔTWS to the sum of *in situ* ΔSM and ΔGW from wells, they found good agreement (Figure 8a). Seasonal amplitudes ranged between 5-10 cm depending on the year, while the RMS difference from the *in situ* $\Delta GW + \Delta SM$ was only 2 cm, much of which was likely caused by the 1.8 cm in estimated GRACE RMS errors. The three-year correlation between ΔTWS from

397 GRACE and $\Delta GW + \Delta SM$ from *in situ* measurements was 0.95. This was put forth
398 as early evidence that seasonal hydrological signals seen by GRACE are reasonable.
399 Additionally, Swenson et al. found that in Illinois, soil moisture and groundwater are of
400 approximately equal magnitude, with soil moisture sometimes lagging the groundwater
401 by a month or two (Figure 8b). This means that in order to compare with GRACE,
402 estimates of both groundwater and soil moisture are needed, not merely one or the other,
403 a finding which has been confirmed via terrestrial gravity measurements [e.g., 57]. Thus
404 a model which ignores either one would be unable to represent the true terrestrial water
405 storage well.

406 Unfortunately, groundwater is not predicted by several global hydrology models,
407 including one of the more commonly-used: the Global Land Data Assimilation
408 System (GLDAS, [58]). Moreover, it proved difficult to find other *in situ* systems of
409 measurement for both groundwater and soil moisture over large areas. Rodell et al.
410 [59] worked around this in the greater Mississippi basin by combining what they did
411 have: *in situ* well measurements for groundwater, and soil moisture and snow-water
412 equivalent estimates modeled by GLDAS. Rather than combining the *in situ* ΔGW
413 with the modeled $\Delta SM + \Delta SWE$ and comparing to GRACE's ΔTWS , they worked
414 equation 5 backwards, solving for the ΔGW which the GLDAS model could not provide.
415 They compared that to the *in situ* well measurements – which are not available in
416 many areas of the world – for verification that ΔGW can be estimated in such a
417 manner. Using two years of RL01 GRACE data (2002–2004), they demonstrated that
418 the seasonal groundwater signal in the wider Mississippi basin can be estimated using
419 GRACE terrestrial water storage and the $SM + SWE$ from a model. However, when they
420 repeated the same procedure for smaller subbasins of the Mississippi, they found that the
421 technique failed to properly determine the seasonal well signal in basins smaller than
422 about 900,000 km². While well undersampling in the spatial domain and inaccurate
423 assessments of well specific yields also provided serious concerns, the dominant error
424 source in these smaller subbasins was assumed to be the RL01 GRACE product.

425 A similar study was performed across the US state of Oklahoma [60], and another
426 over the High Plains Aquifer in the US [61]. The latter is particularly interesting in that
427 it investigated water storage changes in a semi-arid region which is heavily irrigated using
428 groundwater. It thereby touched on the socio-economic issue of water scarcity and large-
429 scale human pumping for groundwater, something not considered by most large-scale
430 hydrological models at the time. Strassberg et al. [61] averaged the RL01 GRACE fields
431 into three-month seasons to better reduce noise, then compared to *in situ* groundwater
432 data from 2719 intermittent wells in the area and modeled soil moisture estimates from
433 NLDAS (North American Land Data Assimilation System). The groundwater and soil
434 moisture signals were both large (5–7 cm maxima) and varied differently in time, with
435 a clear seasonal signal in the groundwater but not in the soil moisture. They found
436 a correlation of 0.82 between GRACE ΔTWS and the $\Delta GW + \Delta SM$ combination from
437 the wells and model (above the 95% confidence level). A 3.3 cm RMS difference existed
438 between the two series, largely caused by a greater estimated amplitude of $\Delta GW + \Delta SM$

439 compared to GRACE, which Strassberg et al. [61] posited may be due to overestimation
440 of ΔGW during local summer, when irrigation pumping is occurring. Despite the
441 imperfect matching, this paper provided firm evidence that GRACE could add value to
442 hydrological studies even in semi-arid regions where significant groundwater was being
443 pumped for irrigation.

444 Even before the launch of GRACE, hydrological modelers were aware of
445 imperfections in their models due to missing terrestrial water storage components.
446 However, these errors of omission came into sharp relief when presented with
447 independent GRACE results. For example, numerous researchers noted that while the
448 spatial pattern of GRACE ΔTWS matched with models, the amplitude of the models
449 was notably lower in many high-signal locations than what was seen with GRACE (the
450 Amazon basin in Figure 7, for example) and occasionally differed slightly in phase as
451 well (the Ganges basin in Figure 7). As the GRACE timespan lengthened, interannual
452 variations and long-term slopes (Figure 9) were also found to differ locally [62, 54, 63].
453 Based on comparisons like those listed above, modelers began to trust GRACE more
454 and started considering GRACE during their cycles of model improvements, to better
455 tune their parameters [64, 65] or directly assimilate GRACE TWS into their models
456 [66, 67].

457 Niu and Yang [68] wrote one of the earliest examples demonstrating GRACE's
458 use in improving hydrology models. They began with the standard NCAR CLM
459 hydrology model and, based on *in situ* information and basic principles, altered it
460 in five significant ways: (1) decreasing the canopy interception of precipitation, (2)
461 altering the percolation rate through the soil column, (3) decreasing surface runoff and
462 thus increasing infiltration of the surface, (4) reducing the rate of subsurface flow, and
463 (5) increasing the permeability of frozen soil. These modifications were made ahead of
464 time, then compared to GRACE, along with the original CLM model, as verification.
465 They found that the alterations resulted in ΔTWS maps which more closely matched
466 what GRACE saw than the original series did, demonstrably increasing the amplitude
467 of the hydrology signal in high-signal areas like the Amazon and Zambezi basins. When
468 looked at as basin-wide averages, the RMS difference between the modified model time
469 series and GRACE was half or less the size of the RMS difference between the original
470 model and GRACE over large cold basins (Ob), classic monsoon basins (Yangtze), and
471 tropical rainforest basins (Amazon). The improvement continued to hold for basins on
472 the order of 300,000 km², as well. This demonstrated not simply an improvement of
473 one model over another, but also a method with which the independent GRACE data
474 set could help determine the precise features of a model which cause improvement. In
475 a later paper, Niu et al. [69] used similar techniques to determine an appropriate runoff
476 decay factor for use with modeled snow.

477 Werth and Güntner [65] used GRACE to tune the WaterGAP Global Hydrology
478 Model (WGHM) in a more statistically rigorous fashion. As they had only six years
479 of GRACE data (2003–2008), they removed all long-term trends and focused only on
480 seasonal and interannual variability. They performed sensitivity analysis on 21 model

481 parameters having to do with soil moisture, groundwater, surface water, snow-water
482 equivalent, and biomass over 28 large river basins. After choosing the 6-8 most sensitive
483 parameters in each separate basin, they used a Pareto-based multi-objective calibration
484 scheme to balance the fit to GRACE's Δ TWS and a secondary independent data set,
485 river discharge. Their optimized results were then compared to the original model and
486 explanations given for the differences seen. Overall, the calibrated model increased the
487 variability of terrestrial water storage throughout the tropical and temperate regions
488 while decreasing it in colder areas, making the calibrated model better match what is
489 seen with GRACE. The parameters causing the changes depended largely on the basin.
490 In tropical and temperate basins, a deeper rooting depth allowed for greater seasonal
491 storage as soil moisture. In basins with widespread rivers, lower river flow velocities
492 and larger runoff coefficients kept water in the rivers for longer, thus increasing and
493 delaying the seasonal maxima in terrestrial water storage. In colder basins, raising the
494 temperature of snow melt drove the snow to melt later, changing the phase of the signal
495 more than the amplitude. Groundwater variability decreased in many arid and semi-arid
496 regions due to increased evapotranspiration. The optimization findings also suggested a
497 route forward to more improvements, such as using more than one soil moisture layer to
498 prevent excessive drying from evaporation, decorrelating the soil moisture from GW in
499 some areas, and testing to optimize parameters which set GW timing and river volume.
500 Werth and Güntner [65] noted that while a few basins were relatively insensitive to this
501 optimization scheme, in general, the use of GRACE in combination with river discharge
502 rates improved the tuning of the WGHM.

503 A similar combined optimization scheme using river discharge and GRACE TWS
504 was also used by Lo et al. [64] to tune their CLM model, and Zaitchik et al. [67]
505 assimilated the two data sets along with groundwater observations into their GLDAS
506 model for testing as well. Houborg et al. [70] assimilated GRACE into the Catchment
507 Land Surface Model (CLSM), then applied that model to the specific problem of drought
508 monitoring in North America. They first determined that the GRACE-assimilated
509 model better matched *in situ* GW+SM data than did the original, un-assimilated
510 CLSM model in most areas of the US. The addition of GRACE helped overcome
511 various weaknesses in the CLSM, while the assimilation technique allowed the individual
512 terrestrial water storage components of surface soil moisture, root-zone soil moisture,
513 and GW to be separated (Figure 10), as they cannot be in GRACE alone. This
514 combination of GRACE plus model could help improve the US and North American
515 Drought Monitors in the future.

516 By around 2008, reductions in GRACE errors via release RL04, a longer time
517 series, and increasing confidence with the data began allowing research into more varied
518 subjects. (Güntner [71] is an excellent survey paper describing the state of GRACE
519 hydrology at that time.) Local analyses of a wide selection of hydrological basins around
520 the world have since been completed: in North America [72, 73, 74, 75], South America
521 [76, 62, 77, 78, 79], Africa [80, 81, 82, 83, 84], Europe [85], Australia [86, 87, 88],
522 Asia [89, 90, 91, 92, 93], and the Arctic [94, 95]. Several studies revolved around

523 the transference of water between the land and the ocean, particularly concerning the
524 teleconnections of El Niño/La Niña [81, 62, 96, 97, 98, 99].

525 GRACE has also begun to be used in combination with GPS to estimate the short-
526 term solid-earth deformations caused by variations in local hydrologic loading. Van
527 Dam et al. [100] compared the vertical surface displacements derived from GRACE
528 to GPS data from stations in Europe and found substantial differences in amplitude
529 and phase for most sites. They attributed these differences to tidal aliasing in the GPS
530 data, since the differences were largest at coastal sites. Steckler et al. [101] used GRACE
531 along with river gauge data to estimate Young's Modulus for the elastic loading of the
532 lithosphere caused by monsoon flooding in Bangladesh. Kusche and Schrama [102]
533 demonstrated how to combine GPS and GRACE into a single J2 series as well as a
534 low-resolution (degrees 2-7 only) time series. Tregoning et al. [103] compared 10-day-
535 averaged GPS measurements of crustal deformation with 10-day-averaged estimates of
536 elastic deformation from GRACE. This demonstrated that a significant part of the non-
537 linear GPS motions, particularly in the vertical direction, are caused by hydrological
538 changes picked up by GRACE. After taking the monthly deformations from GRACE
539 into account, Tesmer et al. [104] found a 0-20% reduction in GPS weighted RMS at
540 43% of their GPS stations and more than a 20% improvement at an additional 34%,
541 percentages which improve if only the annual signal is considered. They noted that the
542 GPS stations most likely to be harmed or not improve by the addition of GRACE were
543 all located on islands or peninsulas – places where the deformational signal estimated
544 from GRACE is likely smaller than the noise and leakage in GRACE, and thus where
545 GRACE should not be expected to provide assistance. Valtý et al. [105] computed the
546 vertical displacement from loading at European GPS sites by combining GRACE with
547 GPS and global circulation models, then used the "three-cornered hat" technique to
548 compute the errors from each contributing data source, assuming the errors in each
549 data set are independent. They determined that, over large areas, GRACE's precision
550 was about twice that of GPS, and that such combined solutions for loading vertical
551 displacement are not very sensitive to the specific choice of GRACE or GPS processing
552 center.

553 Additionally, topics directly impacting people fell under study. A primary man-
554 caused signal visible by GRACE is the depletion of freshwater via the pumping of
555 underground aquifers, mainly for irrigation of farmland. This research is of considerable
556 importance to regional planners, as groundwater is often slow to recharge, and extensive
557 overdrawing of reservoirs could lead to costly land subsidence and future water shortages.
558 Unfortunately, monitoring of groundwater use is limited and withdrawals for personal
559 use and irrigation typically unrestricted. Additionally, most hydrological models
560 (including GLDAS) do not model groundwater at all, or else model it without including
561 anthropogenic withdrawal effects, or else (as WGHM) have yet to perfect their model
562 of both natural and anthropogenic groundwater changes. Model estimates of trends,
563 therefore, are often wrong in areas with significant groundwater reduction. Improving
564 the modeled estimates of groundwater depletion by humans is thus a subject of

565 current effort by some hydrological modelers [106, 107, 108, 109]. GRACE's estimate
566 of variations in total terrestrial water storage is perhaps the only independent tool able
567 to estimate the actual amount of water being withdrawn in comparison to the recharge
568 by precipitation and flow each year.

569 Two dominant examples of this sort of research consider the highly-irrigated regions
570 of northern India and interior California. Rodell et al. [91] focused on the depletion of
571 GW in arid and semi-arid northern India, which is suspected to be larger than the rate
572 of recharge. The Indus River plain aquifer is heavily drawn on to support agriculture
573 and straddles the border between India and Pakistan, making land-based monitoring
574 systems politically problematic as well as expensive. The use of GRACE for monitoring
575 this region is made more complicated by the proximity of the Himalayas only about
576 100km to the northwest [110]. Rodell et al. [91] use the GLDAS hydrology model to
577 estimate soil moisture in the region, then estimate ΔGW from the difference between
578 GRACE ΔTWS and the modeled ΔSM from 2002–2008. Groundwater was shown to
579 have a negative trend of about 4 cm/yr (Figure 11), which would cause a 0.33 m/yr
580 fall in the local water table, on average. As precipitation was normal or even slightly
581 greater than normal during the time period, and as measurable drops in *in situ* water
582 levels have also been noticed, the mass loss is presumed to come predominantly from the
583 drawing of groundwater for irrigation, rather than from natural causes. Additionally,
584 they note that much of the water used from irrigation must be either evaporating or
585 running off into rivers, rather than seeping through the soil back into the aquifer, which
586 would be invisible to GRACE. In only six years, this region of India lost 109 km³ of its
587 freshwater. If its consumption continues unabated, serious water shortages will cause
588 hardship in future years. Several other studies have since confirmed these basic findings
589 [110, 92].

590 A similar set of studies has been conducted by Famiglietti et al. [111] in the Central
591 Valley of California. As with the Indus River aquifer, the aquifers underlying the
592 Sacramento and San Joaquin river basins are heavily pumped for agricultural irrigation.
593 The southern San Joaquin basin, in particular, is a relatively dry area with little available
594 surface water. Famiglietti et al. [111] first checked GRACE's accuracy over this region
595 by collecting *in situ* measurements of precipitation, evaporation, and streamflow runoff
596 and comparing them to GRACE's ΔTWS through the use of equation 5. They found
597 excellent agreement at the seasonal scale, which gives confidence behind the ability of
598 GRACE to measure accurate mass changes in this area. It also verified that the known
599 wintertime droughts in 2006/07 and 2008/09 were large enough to be visible. Then,
600 using *in situ* measurements of surface water, a local model of snow-water equivalent
601 which is constrained by *in situ* measurements, and modeled soil moisture, they solved
602 for groundwater using GRACE and equation 5. Over six years (2004–2010), local
603 terrestrial water storage dropped by about 31 cm/yr with groundwater estimated to
604 make up about 20 cm/yr of that loss. Over 80% of this occurred in the drier San
605 Joaquin basin. However, Famiglietti et al. [111] note that prior to the drought beginning
606 in winter of 2006/07, groundwater storage was roughly balanced, with neither large

607 gains nor decreases. Only after the onset of the drought did a clear negative trend set
608 in. They note that, historically, this seems typical: regional farmers draw more GW
609 for irrigation during dry times, but their non-drought-time withdrawals approximately
610 balance with the natural recharge rate, leading to significant depletion of the aquifer
611 over the long-term. GRACE could be used in such a manner, in combination with other
612 measurements, to help create a long-term plan for sustainable water use in this sensitive
613 and valuable region.

614 In addition to man-caused water storage change, more recent studies have focused
615 on natural changes which could have profound impacts on human life. Extended floods
616 and droughts, in particular, have been measured with GRACE. In areas with few *in*
617 *situ* measurement systems in place, such as the Amazon [62, 77], GRACE is one of
618 only a few remote systems capable of estimating the magnitude and duration of such
619 weather events. While other remote systems like MODIS (Moderate Resolution Imaging
620 Spectroradiometer) or Landsat measure surface water extent (but not depth), and
621 TRMM (Tropical Rainfall Measuring Mission) observes rainfall in the tropics, none but
622 GRACE give us information on what is happening under the surface over time. Even
623 in places where effort has gone in to installing regular *in situ* measurement devices,
624 GRACE provides assistance and a wide-view image of the situation. Leblanc et al. [87]
625 used GRACE to measure a decade-long drought in southeastern Australia, for example.
626 Australia has a good, though spatially limited, *in situ* measurement system for surface
627 water and GW, but is dependent on models for estimates of soil moisture. Leblanc et al.
628 [87] used equation 5 to verify that the yearly-averaged combination of their model and
629 *in situ* data approximately summed to the Δ TWS seen by GRACE, with correlations of
630 0.92-0.94 for the 2003–2007 period. Groundwater was shown to account for the majority
631 (86%) of the 13 cm Δ TWS loss seen by GRACE from 2002–2006, with soil moisture
632 losing most of its available water during the early part of the drought. GRACE also
633 measured the increase in mass associated with the precipitation increase in 2007, most of
634 which is believed to have gone into replenishing the soil moisture rather than increasing
635 surface flow. Leblanc et al. (2009) then used GRACE to calculate the severity of
636 the drought in a quantitative way, relative to a 2001 threshold (Figure 12). Without
637 requiring the use of any modeled data, they estimated the average total deficit volume
638 during 2002–2007 to be about 140 km³, with a maximum severity of approximately 240
639 km³ during early 2007.

640 To summarize, GRACE has been demonstrated to be useful for measuring
641 hydrological signals hard to estimate in other ways, including estimates of water storage
642 change in poorly monitored regions; annual and longer-term GW change due to human
643 activity; the relation of groundwater, surface water, and soil moisture to droughts and
644 floods; the short-term elastic deformation of the Earth to hydrologic loading; and
645 the teleconnections between land hydrology and oceanography. Limited spatial and
646 temporal resolution make GRACE an imperfect product for some investigations, but
647 overall, it has added to the body of hydrological understanding and will surely continue
648 to do so for years to come.

3. GRACE and the solid Earth: an attractive look into the Earth's interior

Most studies using GRACE data focus on processes occurring in the ocean, cryosphere or hydrosphere, which represent redistribution of water within a thin layer at the Earth's surface. However, since the mean density of the Earth is about five times as large as that of water, GRACE measurements are especially sensitive to mass redistribution in the Earth's interior. Given that GRACE cannot distinguish the source of the mass change (*on* or *within* the Earth), a correction for such solid Earth signals is critical if one wants to interpret the surface mass redistribution from GRACE correctly, in particular when one looks at long-term trends. However, these processes in the Earth's interior are not just a source of noise: conversely, GRACE has also been used to improve our understanding of the solid Earth. Most processes in the Earth, like mantle convection and plate subduction, occur on long enough time scales to be considered as static over the GRACE period. Other processes, such as glacial-isostatic adjustment (GIA) lead to a long-term trend in the GRACE time series, whereas very large earthquakes, like the Sumatra-Andaman Earthquake, will typically show up as abrupt jumps in the gravity field. These two processes will be discussed next.

Glacial Isostatic Adjustment

The Earth's interior responds to changes of the load on its surface, for example, the retreat and re-advance of ice sheets, with viscoelastic deformation seeking to gain a new equilibrium state. This process, glacial-isostatic adjustment, induces changes in the Earth's gravity field, the rotation of the Earth, surface geometry and sea-level height. On long time scales, the most important redistribution of ice mass is associated with the glacial cycles. Paleoclimatic records indicate that over the last 800,000 years – that is the period most relevant for GIA – glacial and interglacial epochs alternated with a period of about 100,000 years. This period coincides with the variation of the Earth's orbital eccentricity, the Milankovich cycle of 95,800 yr, and several theories have been proposed about orbital forcing of the glacial cycles [e.g., 112, 113], yet their role in triggering internal feedbacks in the climate system are still far from understood [114].

Recent glacial cycles exhibit a glaciation phase, marked by a steady growth of ice during about 90–100 thousand years, followed by a rapid deglaciation phase that lasts only about 10–20 thousand years, with the Last-Glacial Maximum (LGM) about 21,000 years before present (BP). During the LGM, the Laurentide Ice Sheet, for example, covered large parts of the North American continent with ice of several km in thickness, depressing the Earth surface by hundreds of meters (schematically shown in Figure 13). The response of the Earth can be described by the flexure of an elastic plate, the lithosphere, with a thickness of about 100 km covering the viscoelastic mantle. Due to the high viscosity of the displaced mantle material, the adjustment to the ice retreat following the LGM is delayed, leading to surface displacement and gravity changes of the Earth on time scales of 10,000 years – a process still ongoing today. In the 18th century, Celsius [115] was among the first to collect evidence of falling sea-level and changing

689 coastlines related to GIA. Today, an imprint of GIA is clearly visible in the temporal
690 trends of GRACE gravity-fields, for example in Fennoscandia and North America (as
691 illustrated in Figure 14). GIA is also strongly present in Antarctica, but is less clearly
692 visible in GRACE due to superposition with recent changes in continental ice, due to
693 variations in glacier flow and snow accumulation.

694 GIA not only leads to deformation of the Earth's surface, it also has a dominant
695 impact on the sea-level relative to the Earth surface. As an ice sheet retreats, its
696 gravitational attraction decreases and the sea level drops in its vicinity. In contrast, in
697 regions with a GIA-induced increase of mass, the gravitational attraction increases and
698 sea level tends to rise. In addition, the water volume changes – as ice is redistributed
699 between the ocean and the continent – as well as the geometry of the ocean basin
700 through deformation and flooding/falling dry of land in response to changing surface
701 loads. These interactions between changes in the gravity field, deformation of the solid
702 Earth and also disturbances in the Earth's rotation vector will yield regional variations
703 in relative sea level which are much more complicated than a uniform rise or fall of
704 the ocean's surface. This concept was already acknowledged in 1835 by Lyell [116],
705 who studied rock formations formerly submerged in the ocean along the Baltic coast
706 and concluded that, in this region, the relative sea-level "is very different in different
707 places". Figure 15 shows geological evidence recording the viscoelastic, exponential-
708 type fall of relative sea-level typical for GIA in the near-field of a former ice sheet, here
709 the Fennoscandian ice sheet. Clearly, these regional variations needs to be considered
710 in the interpretation of geomorphological indicators of past sea-level change, as well
711 as in future projections. A unified theory describing the effects of sea-level changes
712 on a Maxwell-viscoelastic, self-gravitating Earth was put forward by Farrell and Clark
713 [117], building on the work of Woodward [118]; the related integral equation describing
714 gravitationally consistent the mass redistribution between ice and ocean has become
715 known as the *sea-level equation (SLE)* and it is now implemented in all state-of-the-art
716 numerical models of GIA [e.g., 119, 120].

717 Modeling of GIA requires two main ingredients: an ice model and knowledge of
718 the Earth's structure. The former describes the loading and unloading of the Earth's
719 surface by the waxing and waning of the ice sheets. Constraints for extent and timing are
720 typically taken from glacial trim lines, dating of moraines pushed forward by advancing
721 glaciers and paleo-indicators of sea level far from GIA regions. For the Earth structure,
722 the distribution of density and elasticity are taken from models based on seismological
723 screening of the Earth, like the Preliminary Reference Earth Model (PREM) [121]. The
724 Earth's rheology can only be obtained from creep experiments of mantle rocks [122],
725 but it was the investigation of GIA that first provided constraints on the Earth's mantle
726 viscosity [e.g., 123]. The ice model and Earth structure used in GIA models are strongly
727 coupled: present-day uplift in a certain region can be due to a strong loss of ice after
728 the LGM, but also by a moderate loss combined with a slow response of the solid Earth.
729 The situation becomes even more complicated when a re-advance of the ice occurred.
730 Ice and Earth models are therefore often iteratively adjusted until an optimal match is

731 found with present-day crustal deformation, e.g. from relative sea level indicators, and
732 nowadays also GPS measurements and GRACE observations.

733 Theory and numerical models solving GIA, as well as the first model-based
734 interpretations of observations in terms of the Earth's viscoelastic structure, date back to
735 the mid-1970s [e.g., 124, 125]. Since then, theoretical descriptions and their numerical
736 implementation have continuously been advanced [e.g., 126, 127, 128, 129]. Current
737 models now not only include the solution of the sea-level equation [130, 131], but also
738 GIA-induced variations of the Earth's rotation [e.g., 132, 133, 134, 135], two- and three-
739 dimensional distributions of mantle viscosities [e.g., 136, 137, 138, 139, 140, 141, 142] and
740 may allow for non-Newtonian [e.g., 143], composite rheologies [144] and compressible
741 viscoelasticity [e.g., 145].

742 Over the instrumental period of about 100 yrs, the temporal behavior of GIA
743 is well approximated by a linear trend, an exception being young and tectonically
744 active provinces with a very low-viscous upper mantle, such as Alaska, Patagonia or the
745 Antarctic Peninsula. This means that GIA is present in trend estimates from geodetic
746 time series of surface deformation from GPS, tide-gauge and alimetry measurements of
747 sea level, as well as measurements of the Earth's rotational variations, classical leveling,
748 surface-gravity and geocenter motion and in particular the gravity field changes from
749 GRACE. Because of the long time scales associated with GIA, seasonal variations in
750 the GRACE data related to e.g. the global hydrological cycle are hardly affected. But
751 for the study of interannual and long-term mass trends, a correction for GIA needs
752 to be subtracted from the GRACE observations. This is in particular the case for
753 estimates of the integrated ocean mass change from GRACE where the GIA correction
754 is of the same order of magnitude as the signal (see section 5) and for monitoring the
755 mass balance of the ice sheets. As mentioned above, GIA models are often iteratively
756 adjusted until an optimal agreement is reached with crustal uplift data. Unfortunately,
757 uplift data is scarce for the polar ice sheets, due to the remote, hostile environment
758 and the fact that much of the region is still covered by ice. Particularly, the poorly
759 defined ice loading history and Earth rheology of the Antarctic region has been a key
760 limitation in estimating the Antarctic ice-mass balance from GRACE [146, 147]. Since
761 the uncorrected GRACE data over Antarctica show a trend close to zero, it is the
762 GIA model that determines the contribution of the ice sheet to sea level change. Early
763 GIA models showed widely varying GIA corrections, ranging from 113 to 271 Gt/yr
764 [148], equivalent to a sea-level rise of 0.30–0.75 mm/yr. In the course of the 2000s, an
765 increasing number of GPS stations have been installed in the interior of Antarctica as
766 part of the POLENET project (www.polenet.org), complementing near-coastal GPS
767 stations available since mid-1990s. Thomas et al. [149] re-assessed the ground motion
768 at the available Antarctic GPS stations and found that the GIA models systematically
769 overestimate the uplift recorded by GPS. These GPS data, together with new evidence
770 from glacial geology that the West-Antarctic ice sheet lost significantly less ice since the
771 LGM than previously thought, have lead to a revision of the GIA predictions. The most
772 recent GIA corrections for the Antarctic continent are now in the range of 6 to 103 Gt/yr,

773 with a preferred value of $\sim 40\text{--}60$ Gt/yr. This is about half the magnitude of earlier
774 estimates, with the consequence of attributing substantially weaker mass loss to the
775 Antarctic Ice Sheet [150, 146, 151, 147]. A substantial uncertainty remains concerning
776 the GIA signal underlying the East-Antarctic ice sheet, and regional to local patterns
777 of the solid Earth response.

778 For North America, however, GRACE has provided new insights into GIA. It has
779 been argued that, at some stage, the Laurentide Ice Sheet consisted of two distinct ice
780 domes located south-east and west of Hudson Bay [e.g., 152]. Tamisiea et al. [153] first
781 analyzed the spatial GIA pattern in the GRACE trends for 2002 to 2005, and interpreted
782 its signature in favour of such a glaciation scenario (Figure 14). Later van der Wal et al.
783 [154] showed that part of these 5-year GRACE trend must be attributed to water storage
784 variations south-east of Hudson Bay from summer 2003 to summer 2006, which can, for
785 short time series, produce a gravity rate comparable to GIA. With two more years of
786 GRACE data (August 2002 to August 2009), Sasgen et al. [155] confirmed that the
787 pronounced two-dome GIA pattern is much reduced, yet a kidney-shaped anomaly is
788 retained. These low positive GIA amplitudes may suggest early ice disintegrating within
789 the Hudson Bay area, leading to comparably early floating of ice and hence de-loading
790 of the continent. The problem of contamination by hydrological signals and noise in the
791 GRACE data remains, currently hampering secure conclusions, although a combination
792 of GRACE with other data sets, such as GPS [156] and terrestrial gravity data [157],
793 may help to remedy this problem [63].

794 Paulson et al. [158] was the first to invert the GIA signal in the GRACE data
795 over North America for the mantle viscosity using numerical modelling. Although the
796 authors had to conclude that the GRACE and relative sea level data are insensitive
797 to mantle viscosity below 1800 km depth, and that data can distinguish at most two
798 layers of different viscosity, they demonstrated consistency between the inversion of
799 GRACE and relative sea-level data. A new aspect GRACE brought into the study is
800 the analysis of spatial patterns ('fingerprints') of GIA associated with specific mantle
801 viscosities. The inversion of the GIA signal magnitude remains somewhat ambiguous
802 due to the trade-off between mantle viscosity and load as discussed earlier. Although
803 this ambiguity is inherent also in the GRACE inversion, Paulson et al. [158] treat the
804 (unknown) magnitude of the load as a free parameter that is adjusted to optimize the
805 fit to the GRACE data. Then, the residual misfit depends mainly on the modelled and
806 observed spatial pattern of the GIA that is mainly governed by the mantle viscosity.
807 In this sense, GRACE represents a valuable new data set in addition to point-wise
808 measurements like GPS, tide-gauges or sea-level indicators [122].

809 For the region of Fennoscandia, the ongoing adjustment has been monitored by
810 GPS studies, most important the Baseline Inferences for Fennoscandian Rebound
811 Observations, Sea Level and Tectonics (BIFROST) project [159, 160]. The results
812 indicate a GIA-induced land-uplift at rates of up to 8 mm/yr close to the former load
813 centre. Agreement between GRACE and the terrestrial data in terms of the spatial
814 pattern and magnitude could be achieved after a robust multi-year GRACE trend was

815 available. Since the Fennoscandian GIA pattern is well recovered by GPS, the signal
816 could be used to verify GRACE post-processing methods [e.g., 161]. As for North
817 America, the separation of the GIA signal and that of hydrological mass variations
818 remains the largest challenge and source of uncertainty. The first joint inversion of
819 GRACE, GPS and tide gauge data was performed by Hill et al. [162], obtaining results
820 that are consistent with previous models, but with an improvement in the spatial
821 pattern, which again demonstrates the power of combining GRACE with other data
822 sets.

823 *Seismology*

824 A second area of solid Earth research where the time-variable measurements from
825 GRACE have provided new insights is seismology. For the first time, widespread
826 gravity changes induced by earthquakes can be observed directly [163]. Since the
827 signal generated by most earthquakes is small in comparison with the background noise,
828 only the largest seismic events, those with moment magnitudes $M_w > 8$ [164], can be
829 successfully observed.

830 Such giant earthquakes are characterized by a displacement at the fault interface
831 of several tens of meters, distributed over a surface of 300–1000 km along fault by
832 100–200 km across fault. They generate seismic waves that are detected around
833 the globe, deform the earth's surface by several meters close to the fault and at
834 the centimeter-level a few thousand kilometers from the epicenter, and can generate
835 significant tsunamis. Observations of those processes, such as seismic waves, surface
836 deformation and tsunamis, are available within hours to days after each seismic event
837 and can be used to constrain the earthquake kinematics and dynamics. However, most
838 major seismic events occur at the boundaries of oceanic regions, so that the availability
839 of direct observations of surface deformation (mainly by GPS) is spatially highly
840 heterogeneous and mostly limited to one side of the fault (over neighbouring continental
841 areas). Furthermore, seismic observations, which can be used to determine the locations
842 and magnitudes of coseismic events beneath either the continents or oceans, are not
843 sensitive to long-period postseismic motion. Since space-based gravity observations
844 provide homogeneous coverage of the earth's surface, and because they detect mass
845 redistribution at scales of months and longer, they can reveal seismic information that
846 would otherwise go unnoticed.

847 GRACE observations have improved our understanding of the largest earthquakes
848 of the last decade, for two time-frames: the occurrence of a seismic event (coseismic
849 phase) and the period after that (postseismic phase). There are three main postseismic
850 processes: afterslip, poroelastic relaxation and viscoelastic relaxation. Afterslip is
851 equivalent to an earthquake which occurs so slowly that it does not produce seismic
852 waves, at time scales from a few hours to several weeks. This additional slip is usually
853 located either on the same fault activated by the earthquake, or on deeper segments that
854 have not released seismic energy. Poroelastic relaxation is related to the fact that the

855 sudden pore-pressure change induced by an earthquake can displace fluids contained in
856 rocks, and the same fluids slowly return to their original location during a few months
857 to years after the seismic event [165, 166]. Viscoelastic relaxation, which also plays a
858 major role in the process of GIA discussed earlier, occurs in deeper parts of the Earth,
859 where temperatures and pressures are so high that rocks behave as high-viscosity fluids
860 (viscosities in the range 10^{18} – 10^{21} Pa s). In seismically active areas, this is typically
861 the case below depths of 25-40 km. After an earthquake, the fault displacement (slip)
862 causes an increase in stress at the bottom of the top brittle layer, and this stress is
863 slowly released through viscous flow that can last for decades [167, 168].

864 In one of the first GRACE earthquake studies, Han et al. [169] used raw
865 measurements of the inter-satellite distance changes (Level-1 data) to determine the
866 co-seismic gravity signal from the 2004 Sumatra-Andaman event. Level-1 data are
867 available relatively quickly, and allow for the isolation of sudden gravity changes from
868 sub-monthly time series. Han et al. [169] concluded that among the major factors
869 contributing to the gravity signal were density changes within the earth's upper layers.
870 Density changes have often been included in deformation models [170, 171], but they
871 had not previously received much attention because dilatation effects play only a limited
872 role in determining changes in the earth's geometry, such as those observed by GPS and
873 InSAR. However, when modelling the gravity changes observed by GRACE, the role of
874 density variations is found to be as large as that of the displacement of rock material
875 [169, 172]. This surprising result was later discussed in more detail by Cambiotti et al.
876 [173] and Broerse et al. [174], who showed that the crucial effects of dilatation result
877 from a combination of the large-scale sensitivity of GRACE and the presence of an
878 ocean. The effects of dilatation on the deformation are small compared to the peak
879 value, and so have little impact on geometrical observations, which tend to focus on
880 the peak displacements. But those effects are spread over a large area, particularly for
881 an earthquake with a large focal plane such as the Sumatra-Andaman event, and so
882 can have a significant impact on large-scale measurements. The presence of an ocean is
883 important because it dramatically reduces the density discontinuity at the solid earth's
884 surface (from about 2600 kg/m^3 to 1600 kg/m^3), and consequently reduces the gravity
885 signal due to topographic changes (the Bouguer effect). This causes a further increase
886 of the relative contribution of dilatation to the total gravity change. Other studies
887 followed in 2007, showing that coseismic signals could be detected in pre-processed
888 (Level 2) data, as well [175, 176, 177]. These studies opened the way to a broader use
889 of GRACE measurements by the solid Earth community, since Level 2 data are freely
890 distributed by the official GRACE processing centres. Mega-thrusts later became the
891 object of intensive research, with the first results often published within only a few
892 months after each event. This was the case, for example, for the 2010 Maule [178, 179]
893 and the 2011 Tohoku-Oki [180, 181] earthquakes.

894 Apart from modelling issues (i.e., determining which processes need to be accounted
895 for to reproduce GRACE observations), the main objective of using GRACE data
896 to study coseismic deformation is to improve fault-reconstruction models. This is

897 important because more accurate fault models can help in understanding the relation
898 between recent and past earthquakes in the same region [182], and to help isolate
899 postseismic signals. This line of study has been addressed in several ways: first of
900 all, existing fault models obtained from seismic and GPS data have been corroborated
901 by GRACE data for the Sumatra-Andaman [e.g., 169, 177, 183], Maule [178, 179] and
902 Tohoku-Oki [180, 184] events; secondly, GRACE data have been used to obtain Centroid
903 Moment Tensor (CMT) solutions for the Sumatra-Andaman [173, 172], Maule [172],
904 Tohoku-Oki [181, 185, 172] and the east Indian Ocean [172] earthquakes; finally, a few
905 studies have used GRACE data to constrain a finite-fault model for the Maule [186] and
906 Tohoku-Oki [187, 188] events.

907 As suggested by the number of studies listed above, perhaps the most interesting
908 application of GRACE data in coseismic studies has been the inversion for CMT
909 solutions. In a CMT description, a seismic source is represented by a point-like double-
910 couple and characterized by a few fundamental parameters: seismic energy, fault plane
911 orientation, and slip direction. Those parameters are enough to completely define
912 the earthquake, as long as the point-source approximation is valid, i.e., as long as
913 observations are taken far enough from the location of the seismic event. Because
914 of the large-scale sensitivity of GRACE, CMT parameters are particularly well suited
915 for an inversion of GRACE data, in what could be called 'GRACE seismology'.

916 This approach has been recently formalized by Han et al. [172], who applied it to
917 all seismic events observable by GRACE up to that time (with the exception of the
918 2005 Nias earthquake, which can not be clearly separated from the co- and postseismic
919 effects of the 2004 Sumatra-Andaman earthquake). Forward models of earthquake-
920 induced gravity changes computed using the GRACE-inferred CMT parameters, are
921 shown in Figure 16. Han et al.'s study has highlighted how the depth of a seismic event
922 is crucial for establishing the importance of density changes, and hence for characterizing
923 the pattern and amplitude of its gravity signature. It also showed that large trade-offs
924 are present in the determination of seismic energy vs. dip angle, which is the inclination
925 of the fault plane in the vertical direction, and of the direction of slip vs. strike angle,
926 which is the orientation of the fault plane in the horizontal direction. An example of the
927 energy-dip angle trade-off as a function of depth is shown in Figure 17. The implication is
928 that GRACE data should best be viewed as supporting traditional seismic and geodetic
929 data when inverting for earthquake mechanisms. Nonetheless, a CMT solution based on
930 GRACE observations alone does provide an estimate of the total energy released during
931 the first few weeks after the seismic event, including contributions from slow post-seismic
932 processes. Those are hard to measure using other techniques and are therefore rarely
933 observed. Results from Han et al. [172] support the presence of a slow slip for the Sumatra-
934 Andaman earthquake, as had been suggested earlier on the basis of seismic inversions
935 of ultra-long periodic motion [189, 190]. A slow component has not been detected by
936 GRACE for any other event.

937 The fact that GRACE provides large-scale spatial coverage of an earthquake area,
938 raises the possibility of providing better constraints on postseismic processes than can

939 be obtained with sparse and unevenly distributed GPS measurements. This should
940 be particularly true for viscoelastic relaxation, which is more widespread and longer-
941 lasting than the effects of other processes, and therefore better suited to the spatial and
942 temporal resolution of GRACE data. In addition, GRACE observations of postseismic
943 deformation following large earthquakes can provide information about the mechanical
944 properties (the rheology) of the entire upper mantle in the vicinity of the earthquake, and
945 improvement over what can be learned from smaller events, since the depth sensitivity
946 is roughly proportional to the earthquake size.

947 The first paper to address postseismic processes with GRACE data was Ogawa and
948 Heki [175]'s study of the Sumatra-Andaman earthquake. After analyzing monthly data
949 spanning 4 years (including 16 months after the event), they came to the conclusion
950 that the observed recovery of the initial geoid depression could best be explained by
951 the diffusion of water. In contrast to previous studies of poroelastic relaxation in the
952 upper crust [e.g., 166], in this case the flow was predicted to have taken place in the
953 upper mantle, where pressure and temperature conditions are so high that water is in a
954 supercritical state. This study remains the only study, to date, to have addressed this
955 process, in spite of the important role of water in the dynamics of the earth's interior
956 [191].

957 A few papers [183, 192, 193] have modelled the observed postseismic signal after
958 the Sumatra-Andaman event as the result of viscoelastic relaxation. All studies agree
959 that relaxation is characterized by a transient phase with fast flow followed by a slower
960 steady-state phase. The simplest model that can represent such a process is a Burgers
961 body, which has a mechanical analogue of a spring and dash-pot in parallel (Kelvin
962 element), combined in series with a spring and dash-pot in series (Maxwell element). The
963 Kelvin element accounts for most of the transient signal, usually localized in the shallow
964 part of the upper mantle (the top 100–200 km), while the Maxwell element represents
965 the steady-state deformation throughout the entire mantle, as is also assumed in GIA
966 studies (discussed earlier in this section). Though such a mechanical model had already
967 been suggested on the basis of GPS data alone [194], the availability of GRACE data
968 made it possible to better discriminate viscoelastic effects from the effects of afterslip,
969 which had also been proposed as a candidate explanation for the early postseismic phase
970 [e.g., 195]. Since afterslip causes a deformation pattern similar to the coseismic signal,
971 but with much smaller amplitudes, its identification requires the availability of accurate
972 near-field measurements, which in the Sumatra-Andaman region were limited to a few
973 GPS sites. Based on GRACE data alone, Han and Simons [183] strongly favoured
974 viscoelastic relaxation as the primary postseismic mechanism for this event, with the
975 possibility of a small role of afterslip in the first few days after the earthquake. Panet
976 et al. [192], however, invoked the presence of a small amount of afterslip, on the basis
977 of GRACE data and a few GPS sites at about 500–1000 km from the fault. Following a
978 different approach, Hoechner et al. [193] started from GPS data to refine the coseismic
979 model and to reduce the number of candidate postseismic models, and to estimate the
980 optimal crustal thickness. Then, they used GRACE data to discriminate between two

981 alternatives, the combination of a Maxwell model and afterslip vs. a Burgers model,
982 and found that the Burgers model provides a much better fit to gravity observations
983 (Figure 18). Interestingly, this distinction was made possible by the fact that the two
984 processes caused different patterns in the oceanic areas west of the Andaman islands,
985 where no observations except those from GRACE were available.

986 When summarizing the role of GRACE data in improving our knowledge of the
987 seismic cycle around the major subduction zones, we can safely say that results so
988 far have already exceeded expectations. The accurate isolation of the coseismic signal
989 has provided interesting information about slip occurring outside the classical seismic
990 spectrum. However, the most important insights will likely originate from the study
991 of postseismic deformation, which promises to highlight how stress evolves at scales
992 of years to centuries, and how it is related to the recurrence of large earthquakes
993 [196]. Since several years of observations are required to discriminate between different
994 postseismic processes, there is still much to be learned by continuing to monitor the
995 regions encompassing recent mega-thrusts events.

4. GRACE and the cryosphere: weighing the ice

Until not too long ago, ice sheets and, to a lesser extent, glaciers were considered to be rather inert systems, reacting only slowly to climate changes. The mass balance (MB) of an ice body – the temporal change of its mass M – can be expressed as:

$$\frac{dM}{dt} = MB = SMB - D \quad (7)$$

where SMB stands for surface mass balance (SMB), the sum of processes that deposit mass on the surface (precipitation) and remove mass from the surface (runoff, drifting snow sublimation and erosion and surface sublimation), and D is the ice discharge across the grounding line, where we neglect the small basal melting of grounded ice and changes in the grounding line position [197]. In the vast, hostile polar environment, collecting sufficient *in situ* observations to constrain the MB of the ice sheets would be a gargantuan task and until about 20 years ago, estimates of the contribution of the ice sheets to sea level changes were necessarily based on extrapolation of sparse set of samples.

A giant leap forward in our understanding of the cryosphere was made by the advent of satellite remote sensing. Despite the lack of missions specifically dedicated at observing the mass balance of the cryosphere, estimates of volume and mass changes were already made in the 1990s using satellite radar altimetry. These missions were typically designed to measure height changes over the ocean, which is relatively smooth compared to the outlet glaciers at the ice sheet's edges. The rugged topography in these locations introduces an ambiguity in the determination of the echo position of the emitted radar beam: over flat surfaces the first returned radar pulse will be associated with the point beneath the satellite, but along-track variations in the ice surface will move this point away from nadir, so that the exact location of the measurement is unknown. This becomes especially problematic in the coastal regions, where outlet glaciers are located in narrow fjords with a cross section smaller than the radar footprint, typically a few km. Furthermore, depending on the properties of the surface snowpack, the radar pulse penetrates in the snow adding further ambiguity to the observed height variations [e.g., 198]. A dedicated ice altimetry mission, ICESat, launched in 2003 and decommissioned in 2010, countered these limitations by using a laser beam with a footprint of ~ 70 m, sufficiently small to resolve narrow glaciers features and with minimal surface penetration. Unfortunately, due to degradation of the laser system, measurements were coarse in time (~ 3 campaigns/yr) and space. The ESA Cryosat-2 mission, launched in 2010 and currently in orbit, uses a Synthetic Aperture Interferometric Radar Altimeter to accurately determine the angle of arrival of its radar pulse, which allows measurements even in very irregular terrain. Yet, a major problem, associated with all geometric measurements, remains: to relate surface elevation changes to mass changes, the observations need to be multiplied with the local surface density. This is less trivial than one would assume. In regions dominated by ice dynamics, the density used should be close to that of ice. In contrast, in areas where melt or

1036 accumulation changes at the surface dominate, it should be roughly that of snow. In
1037 many regions, both mechanisms operate and an intermediate value is to be used. Snow
1038 and ice density vary by a factor 2-3, ranging from 100–200 kg/m³ for freshly fallen
1039 snow to 800–917 kg/m³ for ice, thus introducing a significant uncertainty in the mass
1040 change estimates from altimetry. Furthermore, spurious trends may be observed due
1041 to firn compaction (compaction of the top snow layer under its own weight), which
1042 are unrelated to mass changes and difficult to correct for as they depend on the snow
1043 properties, temperature variations and accumulation rate.

1044 Another satellite-based method, the input-output method (IOM) combines
1045 measurements of the influx of surface mass with the outflux at the boundaries of the ice
1046 field. Surface mass balance (SMB) is taken from (regional) climate models which are
1047 driven by meteorological re-analysis data [e.g., 199]. The outflux by glacier discharge (D)
1048 is obtained by multiplying ice thickness with ice flow velocities at the glacier's grounding
1049 line. These glacier velocities can be either obtained from in situ flow measurements
1050 or from space, e.g., using Interferometric Synthetic Aperture Radar (InSAR). This
1051 technique has a high spatial resolution and can map individual glacier systems, but
1052 combines two large quantities which both have large uncertainties. Furthermore,
1053 observations of ice flow are made typically only once a year, which does not allow
1054 the interpretation of rapid, month-to-month discharge events, and do not always cover
1055 all glacier systems.

1056 Although GRACE has its own limitations (in particular its low resolution and
1057 sensitivity to glacial isostatic adjustment – see section 3), it measures mass changes
1058 directly with global coverage at monthly intervals and thus provides an excellent tool to
1059 monitor the cryosphere. Whereas seasonal changes in the GRACE maps are dominated
1060 by hydrology, the strongest interannual changes and trends are found in glaciated areas
1061 (Figure 19). Relatively soon after the mission's launch, the first mass balance estimates
1062 of the two major ice sheets became available. For the Greenland Ice Sheet (GrIS),
1063 most pre-GRACE studies suggested that the ice sheet had shifted from being in near-
1064 balance to losing mass in the mid-1990s [e.g., 200]. One of the first GRACE studies
1065 focusing on Greenland did indeed suggest a mass loss of 75 ± 26 Gt/yr for Apr. 2002–
1066 Jul. 2004 [46], although the time series of just two years was still too short to draw
1067 any firm conclusions. Indeed, interannual variability in the GrIS system lead to a
1068 wide band of mass balance estimates in the first few years of the GRACE mission.
1069 Extending the time series by two years, Velicogna and Wahr [201] found a radically
1070 different mass loss of -227 ± 33 Gt/yr for Apr. 2002–Apr. 2006, with a 250% increase
1071 between the first and second half of the observation period. These estimates were based
1072 on the *averaging-kernel* method which calculates the average signal over a large area
1073 from the monthly spherical harmonic gravity fields [33] and did not allow a regional
1074 separation of the mass changes. Luthcke et al. [27] used the mascon approach to
1075 estimate mass changes directly from the intersatellite K-band range and range rate,
1076 which allowed the first interpretation at a drainage-system scale. A strong mass loss in
1077 the coastal regions was observed, which was only partly compensated by mass gain in

1078 the interior of the ice sheet. Interestingly, this pattern mirrored the responses to climate
1079 warming as predicted by climate models, with increased precipitation at high altitudes
1080 and thinning at the margins due to warmer temperatures. The overall mass loss of
1081 Luthcke et al. [27] added up to 101 ± 16 Gt/yr (2003–2005), mainly concentrated in the
1082 southeast and to a lesser extent in the northwest. The difference with the estimates
1083 of Velicogna and Wahr [201] likely arose from interannual variability and the relatively
1084 low signal-to-noise ratio of the first release of the GRACE spherical harmonic solutions.
1085 Indeed, when improved GRACE solutions became available, and with the help of post-
1086 processing filtering, Wouters et al. [202] showed that regional partitioning of the mass
1087 loss is feasible with the standard global spherical harmonics as well. For the entire study
1088 period (2003–2008) a mass loss of 179 ± 25 Gt/yr was reported, but when considering
1089 the same observation period, results were consistent with Luthcke et al. [27]. This also
1090 implies that the mass loss in the last few years was comparatively larger, which was
1091 attributed to increased melt in the summer months. Again, the inland growth and
1092 coastal ablation was observed, with an epicenter in the southeast and increasing mass
1093 losses in the northwest. This spreading of the mass loss to the northwest (illustrated in
1094 Figure 20) was later confirmed in other studies [e.g., 203, 204, 205] and independently
1095 by GPS stations which recorded uplift of the Earth surface in response to the diminished
1096 ice load. In the same study, Khan et al. [206] also reported moderate deceleration of
1097 the southeast ice loss in 2006 based on GRACE and GPS observations.

1098 As discussed earlier, GRACE only observes integral mass changes and cannot
1099 separate the individual components contributing to these changes. Van den Broeke et al.
1100 [197] successfully compared GRACE time series to IOM mass balance for the GrIS and
1101 found a good agreement between the two fully independent data sets. This validation
1102 of the IOM data allowed a further partitioning of the individual components (equation
1103 7) contributing to the mass loss observed by GRACE. Roughly half of the mass loss was
1104 attributed to an increase in discharge (D), the other half to changes in SMB processes. In
1105 particular, it was shown that in the pre-GRACE era, a large positive anomaly in surface
1106 melt (and consequently runoff) had developed, balanced by an increase in precipitation.
1107 After 2004, precipitation levelled off, but runoff remained high, resulting in a negative
1108 SMB for the GrIS. The model also showed that approximately 30% of the meltwater
1109 refroze in the top firn layer of the ice sheet, thereby partly reducing the total mass loss,
1110 but also leading to a release of a significant amount of energy to the snowpack. Locally,
1111 temperatures of the firn layer were estimated to have increased by as much as 5 to 10 K.
1112 Sasgen et al. [203] continued along this path and found that the GRACE observations
1113 also agree with the IOM results at a regional scale. They revealed that the accelerating
1114 ice-mass loss along the west-coast of the ice sheet was a consequence of reduced SMB
1115 compared to the first few years of the GRACE observations, combined with an increase
1116 in glacier discharge. Furthermore, a good agreement was found between the regional
1117 GRACE mass balances and surface height changes from ICESat.

1118 As the GRACE observational record lengthened, studies started to focus on
1119 interannual variations in the mass balance of the GrIS. A good example is the work

of Tedesco et al. [207] who compared various observations of the record melt which occurred in summer 2012. GRACE showed a mass loss of approximately 550 Gt during the summer months, equivalent to about 1.5 mm sea level rise. Although noise in the GRACE data makes it hard to exactly determine month-to-month variations, this signal clearly exceeded the mean ice-mass loss of previous summers (about 350 Gt/yr for 2002-2011). Similarly, all other data sets used in the comparison (surface temperature, albedo and melting, modelled SMB and runoff) showed new records compared to the long-term observations. These record events were attributed to a highly negative North Atlantic Oscillation, an index related to large-scale pressure patterns in the northern hemisphere, which has been in a negative state since summer 2006, leading to advection of warm air to Greenland.

Estimating mass changes of the Antarctic Ice Sheet has been proven to be slightly more challenging. Whereas GIA is small and fairly well constrained for the GrIS, it poses a much larger problem in Antarctica (see section 3). Also, the interannual variability of the AIS is large compared to the trend so that the choice of the observation window is important. A third complication is the fact that the AIS covers a much larger area, which makes the total mass balance much more sensitive to how the GRACE data is treated (e.g., the choice of the degree-1 or C_{20} correction as mentioned in section 1). As in the GrIS, initial estimates of the AIS mass balance showed quite some disagreement. Velicogna and Wahr [148] reported the first trends for Antarctica at -139 ± 73 Gt/yr for 2002-2005, where the large uncertainty mainly resulted from disagreement between GIA models. The majority of the ice loss was found to originate in West Antarctica, while East Antarctica was roughly in balance. Chen et al. [208] localized the mass loss in West Antarctica to the Amundsen Sea Embayment region and the mass gain in the East to the Enderby Land region, but added that it was unclear whether the latter represents actual ice accumulation or should be attributed to an incorrect GIA correction. However, comparing GRACE data to altimeter observations, Gunter et al. [209] and Horwath et al. [210] found a similar positive signal in the altimetry surface elevation data, which are much less sensitive to GIA, suggesting that the mass gain is real. In a follow-up investigation using GRACE, Chen et al. [211] also identified the Antarctic Peninsula as a region of significant mass loss, which was later confirmed by Horwath and Dietrich [212] and Sasgen et al. [213]. The former reported a trend of -109 ± 48 Gt/yr for Antarctica as a whole (Aug. 2002–Jan. 2008).

Whereas most studies up to 2009 had found the East AIS to be gaining mass or to be in near-balance, Chen et al. [214] reported the EAIS to be losing mass at a rate of -57 ± 52 Gt/yr and a total AIS ice-mass loss of -190 ± 77 Gt/yr. However, SMB is highly variable over the eastern part of the AIS, making the statistics sensitive to the observation window chosen. Horwath et al. [210] identified a sequence of alternating periods of mass gain and loss in the region in both GRACE data and independent surface height observations from the ENVISAT altimetry satellite. Using GRACE, Boening et al. [215] observed an increase of approximately 350 Gt between 2009 and 2011 along the coast of Dronning Maud Land in East Antarctica. Further inspection

1162 of atmospheric reanalysis data attributed this mass gain to anomalously high snowfall
1163 in just two months, May 2009 and June 2010, due to atmospheric blocking events
1164 advecting moist ocean air towards the East Antarctic coast. The El Niño Southern
1165 Oscillation has also been linked to interannual variations in the mass balance of the
1166 AIS, in particular at the Antarctic Peninsula and in the Amundsen Sea sector, where
1167 the transport of atmospheric moisture from the ocean towards the continent is regulated
1168 by the Amundsen Low pressure system. Maximum correlation between the Southern
1169 Oscillation and interannual mass variations ($\sim \pm 30$ Gt) in these regions from GRACE
1170 were observed at a lag of 10 months [213].

1171 Overall, when uncorrected for GIA, the apparent mass change in the GRACE
1172 time series is close to zero for Antarctica, so that the final result strongly depends
1173 on the method used to correct for GIA. Riva et al. [216] published a first AIS trend
1174 estimate which did not rely on GIA modelling, but separated ice-mass loss from GIA
1175 by combining the GRACE gravity data with ICESat surface elevation changes. This
1176 concept, based on earlier theoretical work of Velicogna and Wahr [217], relies on the
1177 fact that GRACE mass and ICESat elevation observations bear different sensitivities
1178 to GIA and ice-mass loss, respectively. Their GIA correction of 100 ± 67 Gt/yr was
1179 considerably smaller than the correction used in Velicogna and Wahr [148] (176 ± 72
1180 Gt/yr). A wide uncertainty range remained, due to noise in the observations and the
1181 fact that firn compaction was neglected in the surface height trends, but this result
1182 suggested that the AIS GIA correction and consequently also the mass loss may have
1183 been overestimated so far. Indeed, as discussed in Section 3, a comparison of crustal
1184 uplift predicted by GIA models to vertical motion recorded by GPS stations indicated
1185 that the models systematically overestimated the GIA signal [149]. Recently developed
1186 GIA models suggest a GIA signal in the range of 6 to 103 Gt/yr, with a preferred
1187 value of ~ 40 – 60 Gt/yr [218, 150, 151]. King et al. [146] applied the regional approach
1188 of Wouters et al. [202] to Antarctica, and, using the GIA correction of Whitehouse
1189 et al. [150], estimated an ice-mass change significantly lower than previous estimates
1190 (-69 ± 18 Gt/yr for Aug. 2002–Dec. 2010), again concentrated along the coastal zone of
1191 the Amundsen Sea sector.

1192 As is evident from the above overview, initially, mass loss trends reported in early
1193 GRACE studies disagreed by a factor of almost 2 for both ice sheets due to the different
1194 processing methods and, in particular, the time spans used. These early studies were
1195 based on only a few years of data, and surface mass balance for the GrIS and AIS may
1196 vary from one year to another by several hundred gigatonnes [219, 220], so adding just
1197 one year of measurements may change a trend substantially. Nowadays, as researchers
1198 have become more aware of the unique character of the GRACE data and the longer
1199 observations makes the statistics less susceptible to the choice of the time window,
1200 more recent estimates have converged. The Ice sheet Mass Balance Inter-comparison
1201 Exercise [221] compared GRACE mass balance estimates from six different research
1202 groups. A common time span was used (2003–2010) and all groups used the same GIA
1203 models, so that the differences between the estimates can be attributed to the data

1204 source (the global Level-2 spherical harmonics provided by the GRACE science teams,
1205 or the 'mascons' estimated directly from the Level-1 range-rate data) and the analysis
1206 scheme used to estimate the mass changes from the GRACE data. This showed that
1207 all estimates agree within their respective uncertainties, for both ice sheets. Trends
1208 differed by approximately ± 10 Gt/yr between the six groups, which can be taken as
1209 the approximate current methodological uncertainty. For the GrIS, this is comparable
1210 to the uncertainty in the GIA correction, for the AIS, GIA remains the main source of
1211 uncertainty (see Section 3 for a discussion). At time of writing, mass loss of the GrIS
1212 stands at approximately -251 ± 20 Gt/yr (Jan. 2003–Dec. 2012; update of Wouters et al.
1213 [222]). For the AIS, the numbers still depends on the approach used to correct for GIA
1214 and mass loss is nowadays in the range of -67 ± 18 Gt/yr (Mar. 2003–Jul. 2012; update
1215 of King et al. [146]) to -114 ± 23 Gt/yr (Jan. 2003–Sep. 2012; [151]). As is evident from
1216 Figure 21, the rate of mass loss of both ice sheets appears to have been steadily increasing
1217 since the launch of the GRACE satellites. Velicogna [223] found that the GrIS and AIS
1218 time series are indeed better characterized by a quadratic rather than a linear fit. This
1219 study reported an acceleration of -26 ± 14 Gt/yr² and -30 ± 11 Gt/yr² for Antarctica and
1220 Greenland, respectively, for 2002–2009 (fitting a $\alpha_0 + \alpha_1 t + 0.5\alpha_2 t^2$ function, where
1221 α_1 symbolises the trend and α_2 the acceleration). Rignot et al. [224] extended the
1222 GRACE time series by one year and reported acceleration which were approximately
1223 50% smaller (-13.2 ± 10 Gt/yr² for AIS and -17.0 ± 8 Gt/yr² for GrIS). These two studies
1224 used a slightly different approach to estimate the accelerations: fitting a quadratic to the
1225 GRACE mass anomalies (cumulative mass balance, $M(t)$) in Velicogna [223] versus
1226 fitting a linear trend to the monthly mass balance values (dM/dt) in Rignot et al.
1227 [224], but this explains only a few Gt/yr² of the differences. Adding another two years
1228 of data, Wouters et al. [222] found -21 ± 13 Gt/yr² and -25 ± 9 Gt/yr², respectively. Since
1229 acceleration estimates are unaffected by GIA (this slow phenomenon can be assumed to
1230 be approximately linear over the time period considered), this indicates that, again, the
1231 statistics are sensitive to the choice of the observation window and, to some degree, to
1232 the choice of data and processing [146, 225]. The high interannual variability in SMB
1233 makes the current GRACE record too short to robustly separate long-term accelerations
1234 from internal ice sheet variability. About 20 years of observations would be required
1235 to obtain an acceptable signal-to-noise ratio [222], highlighting the need for a follow-up
1236 GRACE mission.

1237 GRACE has also provided important new insights in the mass balance of smaller
1238 ice caps and glaciers systems. Direct observations of glaciers are sparse, both in space
1239 and in time, because of the labour intensive nature and tend to be biased toward glaciers
1240 systems in accessible, mostly maritime, climate conditions. Approximately 60% of the
1241 *in situ* glacier mass balance records are from the smaller European Alps, Scandinavia
1242 and northwestern America [226]. Very large and less accessible glaciers, in contrast, are
1243 undersampled and lack continuous and uninterrupted observation series. Both problems
1244 can be overcome by GRACE, which provides global and continuous observations. Yet,
1245 as the spatial scale becomes smaller, the effect of noise in the GRACE data becomes

1246 larger and validation of the GRACE observations of glaciers by independent methods
1247 becomes often desirable.

1248 Much of the attention has focused on the glaciers in the (sub)Arctic region. In the
1249 Gulf of Alaska (GoA), airborne altimetry observations in the 1990s and early 2000s
1250 suggested a glacier mass loss of -96 ± 35 Gt/yr for 1995–2001 [227]. This number
1251 was based on extrapolation of 28 profiled glaciers and the observations did not allow
1252 to resolve interannual variations. The first GRACE-based estimates confirmed the
1253 altimetry results, with trends of typically 100–110 Gt/yr in the first few years of the
1254 GRACE mission [\sim 2003–2005; 228, 229, 230]. However, the GRACE time series revealed
1255 substantial interannual variability in the mass budget of the GoA glaciers (see Figure 22):
1256 anomalously high snowfall in the winter of 2007 [230] was followed by high mass loss in
1257 2009, which Arendt et al. [231] linked to the Mount Redoubt eruption in March of that
1258 year. The ash fall of the volcanic plume caused a decrease in the ice surface albedo in the
1259 GoA region, leading to a greater absorption of solar radiation and hence surface melt.
1260 They report a mass trend of -61 ± 11 Gt/yr for 2004–2010, somewhat more negative
1261 than the -46 ± 7 Gt/yr of Jacob et al. [110] for a slightly longer period (2003–2010).
1262 Interestingly, GRACE suggests that the neighbouring glaciers in Western Canada and
1263 USA are gaining mass at a moderate rate of a few Gt/yr (Fig. 22; [110, 232]), although
1264 the uncertainty due to GIA and leakage of hydrological signals is large for this region
1265 and *in situ* measurements indicate that these glaciers are actually losing mass [232].

1266 Located northwest of the GrIS, the glaciers and ice caps of the Canadian Arctic
1267 Archipelago (CAA) hold about one-third of the global volume of land ice outside the
1268 ice sheets. Mass loss in the northern CAA was reported in the study of Wouters et al.
1269 [202]. A few years later, Gardner et al. [233] compared data from ICESat, GRACE
1270 and a regional climate model for 2004–2009 and found that all three data sets indicated
1271 a sharp acceleration of the mass loss occurring around 2007 (Fig. 22), mainly due
1272 to increased melt in response to higher air temperatures. About two-third of the ice
1273 loss (39 ± 9 Gt/yr) was attributed to the northern part of the archipelago, while in the
1274 southern part, the melt (24 ± 7 Gt/yr) was found to have doubled compared to its long-
1275 term value (11.1 ± 1.8 Gt/yr for 1963–2008 [234]). Recently, GRACE data was also used
1276 to validate climate projections of a more advanced regional climate model in the CAA
1277 region, which indicates that the accelerated ice-mass loss will be sustained in the 21st
1278 century [235].

1279 Another region where glaciology has much benefited from the GRACE mission is
1280 the Russian High Arctic. *In-situ* measurements are extremely sparse in this region, for
1281 example, Severnaya Zemlya has been surveyed only three times (1957, 1958 and 1969)
1282 and no *in situ* surface mass balance measurements at all are available for Franz Josef
1283 Land [236]. Moholdt et al. [237] assessed the regional glacier mass budget for 2003–
1284 2009 using ICESat and GRACE and found a small imbalance of 9.1 ± 2.0 Gt/yr for this
1285 period, mainly due to ice loss in Novaya Zemlya. Comparable ice loss has been observed
1286 with GRACE in Iceland [\sim -11 Gt/yr; e.g., 202, 110, 232] and Svalbard [-3 to -9 Gt/yr,
1287 depending on the observation window e.g., 202, 110, 232].

1288 In the Southern Hemisphere, the main glaciated areas outside Antarctica are the
1289 Patagonia Icefields in the Southern Andes. Based on comparison of topographic data
1290 obtained between 1968 and 2000, the glaciers in the region have been estimated to
1291 have lost ~ 15 Gt/yr during this period, with an increase in the late 1990s [238]. The
1292 acceleration was confirmed by the first GRACE study of the area, which reported a
1293 mass loss of -25 ± 10 Gt/yr [239]. This rate appears to have remained relatively constant
1294 within the GRACE era (Fig. 22), with values in later studies ranging from 23 to 29
1295 Gt/yr [110, 232] and compares well to independent estimates based on differencing of
1296 digital elevation models [240]. The Patagonia Icefields are located in a zone of low mantle
1297 viscosity (see section 3), so that the solid earth reacts relatively rapidly to changes in ice
1298 load, such as those since the Little Ice Age (LIA). Ivins et al. [241] combined GRACE
1299 observations with GPS data to simultaneously invert for ice loss and solid earth (both
1300 LIA and GIA) effects, yielding an ice-mass loss of -26 ± 6 Gt/yr.

1301 Arguably the most challenging region to estimate glacier mass balances using
1302 GRACE is the High Mountain Asia region, which encompasses the Himalayas,
1303 Karakoram, Pamir and Tianshan mountain ranges and the Tibetan Plateau. Complex
1304 hydrological processes, such as highly variable monsoon precipitation and groundwater
1305 extraction in the neighbouring India Plains (see Section 2), seismological activity and
1306 poorly constrained GIA and LIA, make the GRACE estimates very dependent on the
1307 corrections used to isolate the glacier signal. Matsuo and Heki [242] obtained an
1308 average mass loss of -47 ± 12 Gt/yr for 2003–2009, but did not include a correction
1309 for hydrological processes. Gardner et al. [232] did include a correction for this (with a
1310 large uncertainty) and reported a lower loss of -19 ± 20 Gt/yr for the same period. Both
1311 estimates are within the error bounds of the -29 ± 13 Gt/yr estimated from ICESat
1312 altimetry [232]. As is evident from figure 22, the signal shows large year-to-year
1313 variability which is reflected in the even lower estimate of Jacob et al. [110] of -4 ± 20
1314 Gt/yr for 2003–2010 due to a positive mass balance in the last few years of the time
1315 series.

1316 To date, two studies have been published which provide a global mass balance
1317 estimate of the world's glaciers and ice caps (excluding peripheral glaciers on Greenland
1318 and Antarctica). Summing up all regions, Jacob et al. [110] reported an average mass
1319 loss of -148 ± 30 Gt/yr for 2003–2010. For a slightly shorter period (2003–2009), the
1320 GRACE-based estimate of Gardner et al. [232] resulted in a total of -168 ± 35 Gt/yr.
1321 Both numbers are considerably smaller than estimates based on interpolation of *in*
1322 *situ* observations [-335 ± 124 Gt/yr for 2003–2009; 232], which for a large part may be
1323 attributable to undersampling problems in the latter method, but also to the limitations
1324 of GRACE in separating glacier signals from other sources of mass variation.

5. GRACE and the Ocean: More than sea level rise

Oceanography benefits from both the time-mean and time-variable components of satellite gravity. The mean component (the geoid) can be combined with sea surface height (SSH) from satellite altimetry to determine the dynamic ocean topography, the spatial gradients of which are directly proportional to surface geostrophic currents [243]. Although this has been theoretically known for over 30 years, it has only recently been possible to realize it. Early gravity models were too inaccurate to be useful except at the very longest wavelengths, much larger than the width of major current systems [244, 245]. Although methods were developed to include finer scale gravity information based on gradients of SSH [e.g., 246], these mean gravity models were found to have absorbed much of the gradients of dynamic topography as well, making them useless for determining the surface geostrophic currents [247].

Even a very early gravity model from GRACE, based on less than 90 days of observations, demonstrated dramatic improvement [247]. The mean surface geostrophic currents are now capable of being resolved for all regions at an unprecedented resolution (Figure 23). With more data available from GRACE, along with improved terrestrial and airborne gravity data and higher-resolution gravimetry from the GOCE mission after 2009, the global surface geostrophic currents can now be resolved over widths of less than 100 km [248, 249, 250].

The earliest use of the time-variable gravity data from GRACE over the ocean was for validation purposes, by assuming the residual variations over the ocean relative to a model represented noise [29, 251]. These early studies concluded that the signal-to-noise ratio in the GRACE time-variable data was likely too small to make them useful for ocean applications, except in small regions where extreme ocean bottom pressure variations were likely to exist. However, Chambers et al. [252] demonstrated that by averaging over the entire ocean basin, GRACE was capable of measuring global ocean mass variability to an accuracy of a few mm of equivalent sea level. Although the magnitude of global mean ocean mass fluctuations (~ 1 cm amplitude) is small compared to local sea level variations (>20 cm in some regions) the signal has a very large-scale coherent pattern that is very nearly uniform across the world's oceans. This is because the ocean adjusts via fast barotropic waves to water mass fluxes, either from changes in precipitation and/or evaporation [253] or melting of ice sheets [254]. The response time to reach equilibrium is less than a week. Considering the size of this mass being lost from the ice sheets, presumably with most going into the oceans and staying there (Section 4), GRACE is perfectly suited to measure the mass component of sea level rise.

However, GRACE will also measure the GIA signal over the ocean (Section 3). In order to accurately determine the effect of current ocean mass increase, one needs to remove the GIA signal from the GRACE observations. There has been considerable controversy in the literature regarding the appropriate correction recently, with two groups arguing for corrections that differed by 1 mm yr^{-1} of equivalent sea level rise [255, 256], which is the size of the expected signal. Chambers et al. [256] concluded that

1366 the correction suggested by Peltier [255] suffered from two significant errors – applying
1367 a non-zero global mean mass trend to the GIA model and an apparent error in the
1368 application of the polar wander rates. Subsequently, Peltier et al. [257] have found an
1369 error in their code that created the second artefact, and have admitted that for GRACE
1370 applications, the GIA global mean mass rate should be zero. The two groups now agree
1371 on the correction rate to within the estimated uncertainty of 20-30% [258, 257], which
1372 is still limited by our current knowledge of mantle viscosity and ice histories.

1373 Global mean sea level (GMSL) is the sum of the mass component and the
1374 thermosteric component. Seasonal variations in the mass component are roughly two
1375 times larger than the seasonal variation in total GMSL and 180° out of phase, but the
1376 mechanisms for this are well understood [259, 260, 261]. It is caused by the timing and
1377 size of land-ocean water mass exchange compared to that of the global ocean thermal
1378 expansion (thermosteric sea level). Global mean thermosteric variations peak in the
1379 Austral Summer (due to the larger ocean area in the Southern Hemisphere), whereas
1380 ocean mass peaks in the Boreal Summer (due to larger land area in the Northern
1381 Hemisphere which stores more water during Boreal Winter). Moreover, the amplitude
1382 of the seasonal thermosteric variation is half the size of the amplitude of ocean mass
1383 change.

1384 The longer-term trends and interannual variations in the mass component of GMSL
1385 have been less well understood than the seasonal variations, and measurements from
1386 GRACE have significantly improved our understanding. Many efforts have focused
1387 on closing the 'sea level budget' of trends and estimating the relative size of different
1388 contributions. Early efforts had no direct measurement of the mass component, and
1389 so either used estimates of mass loss from ice sheets and glaciers to infer a trend [e.g.,
1390 262] or used the residual between GMSL and thermosteric trends [263, 264]. Initial
1391 results attempting to close the sea level budget with global measurements from altimetry
1392 (total GMSL), GRACE (mass component), and temperature profiles from the Argo
1393 floats (thermosteric component) suffered from pressure bias errors with the Argo data,
1394 changing sampling of Argo as the number of floats increased, biases in the radiometer
1395 correction to altimetry, and the aforementioned GIA correction [264, 261, 265, 266, 267].

1396 However, after correcting altimetry for known biases, removing Argo floats with
1397 pressure biases and using only floats after 2005 when data are relatively well distributed
1398 globally, all studies now find closure of the sea level budget within the uncertainty
1399 [256, 268, 269, 270]. Between 2002 and 2012, the trend in the mass component of
1400 GMSL explains 60–80% of the observed rise of GMSL over the same period (Figure 24).
1401 The residual 20%–40% is caused by thermosteric sea level rise. Roughly 70% of the
1402 mass increase is coming from the Greenland and Antarctica ice sheets (Section 4).

1403 In addition to the longer-term trend in ocean mass, it is clear that many interannual
1404 variations in GMSL correspond to changes in the mass component and not the
1405 thermosteric sea level. This is most apparent between 2010-2012, when the large
1406 oscillation from low anomalies to high anomalies in global mean sea level is found
1407 mainly in ocean mass (Figure 24). Previous studies using land hydrology models and

1408 combinations of altimetry and steric data had suggested that interannual mass variations
1409 related to cycling of water between the continents and oceans could be responsible for
1410 observed El Niño variations in GMSL [272, 263, 273]. Willis et al. [261] confirmed
1411 the existence of relatively large interannual changes in ocean mass that was directly
1412 reflected in sea level, and Chambers and Schröter [274] found that mass variations
1413 dominated the interannual GMSL fluctuations between 2005 and 2007. Boening et al.
1414 [270] suggested the much larger fluctuations between 2010 and 2012 were caused by
1415 the 2011 La Niña, which changed evaporation and precipitation patterns so much that
1416 a large amount of water was transferred from the ocean to land for a short period of
1417 time. In a subsequent study, Fasullo et al. [271] demonstrated that it was much more
1418 complicated, and involved a very unique combination of a strong negative phase of the
1419 Indian Ocean Dipole, a positive phase of the Southern Annual Mode, and the strong La
1420 Niña, all of which led to an anomalously high amount of precipitation over the interior
1421 of Australia. The patterns converged to dump up to more than 400% more rainfall
1422 than average between 1 September and 30 November 2010, according to analysis by the
1423 Australian Bureau of Meteorology. Since there is no direct drainage from this region to
1424 the ocean, the water filled a large, normally dry lake called Lake Eyre, where it stayed
1425 until it evaporated. It is estimated that these events occur roughly every forty to fifty
1426 years in Australia. These studies have shown without a doubt that large interannual
1427 variations in GMSL are more likely due to changes in water cycling between the oceans
1428 and continents than due to changes in the heat storage.

1429 The time-variable mass measured by GRACE has also been used to quantify certain
1430 aspects of regional ocean dynamics. Low-frequency variations in ocean bottom pressure
1431 caused by changes in the circulation and transport are particularly difficult to measure
1432 or model. Bottom pressure recorders (BPRs) are expensive and difficult to deploy.
1433 Moreover, they have significant drifts in the recorded pressure over time, making them
1434 useless for measuring variations with periods longer than about 1-year. Models can
1435 simulate low-frequency ocean bottom pressure, but results are often suspect due to
1436 the time-scale needed to update the state in the deep ocean – of order 100 years
1437 or longer. Since the deep density structure of the ocean is still poorly known and
1438 most ocean models have been run to simulate less than thirty years of the ocean state,
1439 deep ocean state parameters are still adjusting and can cause spurious drift and low-
1440 frequency signals in ocean bottom pressure. One of the earliest studies demonstrating
1441 the usefulness of GRACE for regional ocean dynamics was by Morison et al. [275], who
1442 used the observations to measure a shift in the gyre circulation in the Arctic Ocean.
1443 Although BPRs saw a dramatic drop in pressure in the center of the Arctic Ocean
1444 from 2005 to 2006 (Figure 25), it was unclear if this was a real signal or drift in the
1445 instrument. GRACE measurements confirmed this was not a drift in the BPRs and that
1446 the trend had in fact started earlier. Moreover, maps of ocean bottom pressure (OBP;
1447 1 mbar \approx 1 cm of water) from the GRACE mission clearly showed that the drop was
1448 associated with increasing OBP in the coastal regions, consistent with a change in the
1449 gyre circulation. Morison et al. [276] have continued to rely on these observations to

1450 document low-frequency variability of the Arctic Ocean circulation and have combined
1451 the GRACE data with altimetry sea surface height and *in situ* measurements to infer
1452 the regional distribution of freshwater content in the Arctic ocean, which they link to
1453 Arctic Oscillation.

1454 Another oceanic region where GRACE has been used to better understand low-
1455 frequency mass variations is the North Pacific. This region has large variations in OBP.
1456 Previous studies showed this was mainly caused by large sub-monthly and seasonal
1457 variations driven by changing wind curl over the region, but also intensified by the
1458 bottom topography [e.g., 277], which traps mass moving into the region instead of
1459 allowing readjustments to propagate as free Rossby waves. Bingham and Hughes [278]
1460 compared the seasonal cycle in the GRACE observations to the output of a numerical
1461 ocean model and showed that the satellites can detect large-scale OBP variations at
1462 these time scales in the region. Song and Zlotnicki [279] found a significant interannual
1463 fluctuation in the OBP from 2003 to 2005, and suggested that the timing was consistent
1464 with OBP variations simulated in a model, but only for that brief 2-year period.
1465 Chambers and Willis [280] examined a longer time-span of data in the area and found
1466 a significantly longer-lasting increase in OBP lasting until 2007, which they verified
1467 as real by comparing with steric-corrected altimetry in the region. Further study by
1468 Chambers [281] confirmed the increasing trend in OBP lasted until at least 2009 in both
1469 GRACE and steric-corrected sea level before beginning to level off somewhat (Figure
1470 26). Two different ocean models failed to reproduce the event. Chambers and Willis
1471 [280] demonstrated that the first model did not accurately reproduce the observed steric
1472 signal or sea surface height in 2003 and 2006, even though these data were assimilated
1473 into the model. Chambers [281] demonstrated that the ECMWF winds driving the
1474 second model were inconsistent with satellite observed winds; changes in the satellite
1475 winds, however, were consistent with increasing ocean bottom pressure in the region.

1476 GRACE measurements have also been used to track exchanges of mass between
1477 ocean basins. Although previous studies based on models demonstrated there are
1478 large-scale redistributions of mass within the ocean at periods of a year or shorter
1479 [282, 277, 283], interannual variations were considered suspect due to potential drift in
1480 the models. Chambers and Willis [284], however, demonstrated large, coherent mass
1481 exchanges between the Indo-Atlantic and Pacific oceans, on time-scales longer than 1-
1482 year (Figure 27). These were observed in GRACE observations, which verified model
1483 simulations, although the GRACE data indicated larger amplitudes. Although the size
1484 of the total mass being moved around is quite large (± 1500 Gt including seasonal terms,
1485 ± 800 Gt removing seasonal), the equivalent sea level change is small (a few mm) as the
1486 mass is distributed more or less uniformly over the entire basin. The change in volume
1487 transport required to support this mass exchange is of the order of 0.001 Sv (1 Sv =
1488 10^6 m³/sec). For comparison, the size of month-to-month variability of transport in
1489 the Antarctic Circumpolar Current (ACC), which has the largest volume transports of
1490 any ocean current is about ± 10 Sv (one standard deviation) about the mean of 125 Sv
1491 [285]. The capability to measure the variability of the net transport into and out of

1492 a basin using in situ instrumentation is therefore limited to a precision of about ± 10
1493 Sv. Thus, by using basin-scale averages of ocean mass variability with satellite gravity,
1494 one can detect otherwise unmeasurable changes in oceanic transports, at least the net
1495 transport into a large region.

1496 In some areas, GRACE may be able to detect transport variation for a specific
1497 current system. One such current is the ACC, which has measureable currents to the
1498 sea floor. When the geostrophic transport varies, it has to be balanced by changing
1499 pressure across the current, which should be observable by GRACE. This is important,
1500 as measuring the transport of the ACC and especially its low-frequency variability is
1501 difficult. This can only be done directly by measuring temperature and salinity along
1502 a north-south transect of the ACC, such as along the Drake Passage, then estimating
1503 geostrophic current shear. However, this is only precise if the measurements are made to
1504 the bottom, and a current reading is also made at some depth as a reference, neither of
1505 which has been done more than a handful of times due to the expense [285]. Errors by not
1506 measuring to depth and assuming a reference velocity of zero can be of the order of 25 Sv
1507 or more. Other estimates have been made using bottom pressure gauges based on some
1508 assumptions that simplify the problem [e.g. 286]. However, since these sensors drift,
1509 it is difficult to determine long-term changes in transport with any certainty. Climate
1510 models have predicted a poleward movement and strengthening of the Southern Ocean
1511 winds and the ACC in the in a warming world [e.g., 287], so there is a need to measure
1512 whether the transport is increasing to confirm the models

1513 While there have been attempts to measure the transport of the Antarctic
1514 Circumpolar Current with GRACE, all have focused on seasonal and shorter period
1515 fluctuations, and for averages over large areas, generally the size of the Pacific sector
1516 of the ACC, and have included portions of the transport that does not pass through
1517 the Drake Passage [288, 289, 290]. Results show generally good agreement with the
1518 seasonal and higher frequency variability predicted by models, with differences of about
1519 3 Sv RMS. Little work has been done to evaluate low-frequency variations, however,
1520 except for some evaluation of correlations between GRACE derived transport for the
1521 ACC averaged over the Pacific sector and the Southern Annual Mode (SAM) [290]. The
1522 SAM is often used as an index of wind variability over the Southern Ocean, and has
1523 variations from a few weeks to many decades. Although correlations between GRACE-
1524 derived transport and SAM have been shown to be high [290], the results are likely
1525 biased by the high-frequency and seasonal variability. No analysis was done for the
1526 longer than annual period. However, assuming monthly errors of 3 Sv with a random
1527 autocorrelation, a change in transport of less than 0.3 Sv/year should be detectable by
1528 GRACE with 90% confidence using the current 10-year record.

1529 Most oceanographic studies using GRACE focus on large-scale phenomena, occurring
1530 in the open ocean. This is partly due to the fact that locally, the amplitude of OBP
1531 signals generally falls below the noise level of GRACE. Near the coast, the comparably
1532 weak OBP variations are obscured by signal leakage from nearby land hydrology, due to
1533 the limited spatial resolution of GRACE. An exception are shallow semi-enclosed shelf

1534 zones, where the water column is generally well mixed and wind stress is distributed
1535 over a relatively thin column, leading to predominantly barotropic variability. GRACE
1536 has been used to identify large OBP variations in the Gulf of Carpentaria (Australia)
1537 [291] and the Gulf of Thailand [292], with a seasonal amplitude of 20 cm and more.
1538 Interestingly, the hydrological signals over land captured by GRACE can also be used
1539 to infer OBP variations in the oceans. As explained in Section 3, changes in mass
1540 loading on land will alter the gravitational pull on the ocean, so that water moving from
1541 land to ocean will not be distributed as a uniform layer in the ocean. Continental mass
1542 anomalies from GRACE have been used as input in the sea-level equation to show that
1543 meltwater from land ice will lead to an above-average sea level rise between 40°N/S [293]
1544 and that seasonal water exchange between land and ocean leads to non-uniform relative
1545 sea-level variations of ~ 2 to 17 mm, with a distinct North-South gradient [294, 295].
1546 Another oceanographic application where GRACE has led to advancement is modelling
1547 of ocean tides. Tidal models rely heavily on sea surface height observations from satellite
1548 altimetry. These observations do not always cover the high latitudes, so that empirical
1549 tidal models are relatively poorly constrained in polar areas. Various studies have used
1550 the GRACE intersatellite range-rate observations to invert local tidal mass variations
1551 and revealed tidal variations not predicted by tidal models, in particular in the Arctic
1552 [296] and Antarctic [e.g., 36, 297] regions.

6. Conclusions and Perspectives

Over the past decade, GRACE has gone from being an experimental measurement needing to be verified by more trusted *in situ* data, to a respected tool for Earth scientists representing a fixed bound on the total change in water storage over medium to large regions. Terrestrial water storage can now be measured at large scales and in remote areas, the mass balance of the ice sheet and larger ice caps and glaciers can be monitored at an unprecedented temporal resolution, and the exchange of water masses between ocean regions can be tracked directly. Whereas with the original RL01 data, only large seasonal signals were confidently visible above the processing errors, the newest release (RL05) brings with it lower errors and a far larger selection of possible uses. Due to the improved data quality, the expertise in handling and interpreting this new data product gained since the mission launch, and the increasing interaction between GRACE-processors and researchers from other fields, the focus of GRACE-related research has moved from simply observing variations in water storage to explaining and interpreting these observations. Earth system modellers and GRACE processors are now engaged in an iterative cycle of mutual improvement for their products and GRACE has become a popular tool to validate and tune Earth system models, especially in hydrology [e.g., 64, 65] and glaciology [e.g., 197, 298, 235]. GRACE data are nowadays being directly assimilated into ocean [299] and hydrology [67, 70] models and are also fed into model simulations to assess the impacts of climate change, such as the potential weakening of the Atlantic meridional overturning due to increased meltwater input from the Greenland Ice Sheet [300]. Furthermore, the mission has already lead to a successful spin-off, the Gravity Recovery and Interior Laboratory (GRAIL), which mapped the Moon's gravity field in 2012, using basically the same concept as GRACE.

With a mission length of more than 11 years and counting, the nominal 5-yr mission lifetime has long been exceeded. Both satellites still operate nominally, and with the current low solar activity (leading to less atmospheric drag), the cold gas reserves of the satellites' attitude and orbit control system are expected to last until 2018–2019. The batteries, however, are starting to feel their age. Over the years, the capacity of the battery cells has degraded and one of the two satellites has suffered two cell failures. Measures have been taken to extend the battery lifetime, which involves that, since 2011, no scientific data are collected when the sun is positioned unfavourably with respect to the satellites' orbit and the solar arrays cannot collect sufficient energy. This occurs about every 161 days, but, if a third battery cell would fail, there would be a data gap every 30–50 days. A follow-on mission has been approved and funded and is planned to be launched in 2017. This will be almost a carbon-copy of the current GRACE mission, but with evolved versions of some of the components (such as the KBR, GPS and accelerometer systems) and include an experimental laser link between the two satellites to prove the feasibility of the much more precise laser inter-satellite ranging for future gravity missions.

1594 The fact that the GRACE satellites sense mass redistribution as one measurement
1595 can either be seen as an advantage (e.g., in hydrology, where total terrestrial water
1596 storage can be measured directly), or as a limitation (e.g., when studying the cryosphere,
1597 where trends in ice mass are difficult to separate from GIA). This is inherent in
1598 the mission principle and is very unlikely to change in future GRACE-like missions.
1599 However, for other characteristics of the GRACE observations, there is room for
1600 improvement. A reduction of the North-South striping, and the noise level in general,
1601 would lead to a more accurate estimation of the mass redistribution. Since this
1602 reduces the need for smoothing and post-processing, this would also allow a higher
1603 spatial resolution, and thus a better separation of individual signals (e.g., between
1604 hydrological and oceanographic signals in coastal regions). The quality of submonthly
1605 gravity solutions may also improve, although there will always be a trade-off to be made
1606 between an acceptable noise level and spatial resolution, and the temporal resolution,
1607 since a sufficiently dense groundtrack coverage is required. Several conceptual studies
1608 for a redesigned GRACE successor are being carried out, funded nationally and by
1609 space agencies such as ESA and NASA, with input from the broad international user
1610 community. Various new mission architectures are being considered, such as two pairs
1611 of satellites in different orbital planes, which would substantially increase the spatial
1612 resolution and reduce the North-South striping problem [e.g., 301, 302, 303]. Such a
1613 GRACE II mission is expected to be launched in the 2020s, which would ensure the
1614 long-term availability of time-variable gravity and allow the scientific community to
1615 continue to monitor changes in, and improve our understanding of, the Earth's water
1616 cycle and large scale mass redistribution in its interior.

1617 **Acknowledgments**

1618 The authors would like to thank the anonymous reviewer and editor for their helpful and
1619 constructive comments, and Volker Klemann and Srinivas Bettadpur for commenting
1620 on parts of the manuscript. Shin-Chan Han, Andreas Hoechner, Rasmus Houborg,
1621 Volker Klemann, Marc Leblanc, Matthew Rodell, Holger Steffen and Sean Swenson
1622 are acknowledged for sharing their figures, and M. King, R. Bingham and P. Moore
1623 for updating and sharing their Antarctica trend numbers. B. Wouters is funded by a
1624 Marie Curie International Outgoing Fellowship within the 7th European Community
1625 Framework Programme (FP7-PEOPLE-2011-IOF-301260). I. Sasgen acknowledges
1626 support from the DFG priority program SPP1158 'Antarctic Research' through grant
1627 SA 1734/4-1. J. A. Bonin and D. P. Chambers were both supported under NASA Grant
1628 NNX12AL28G from the GRACE Science Team.

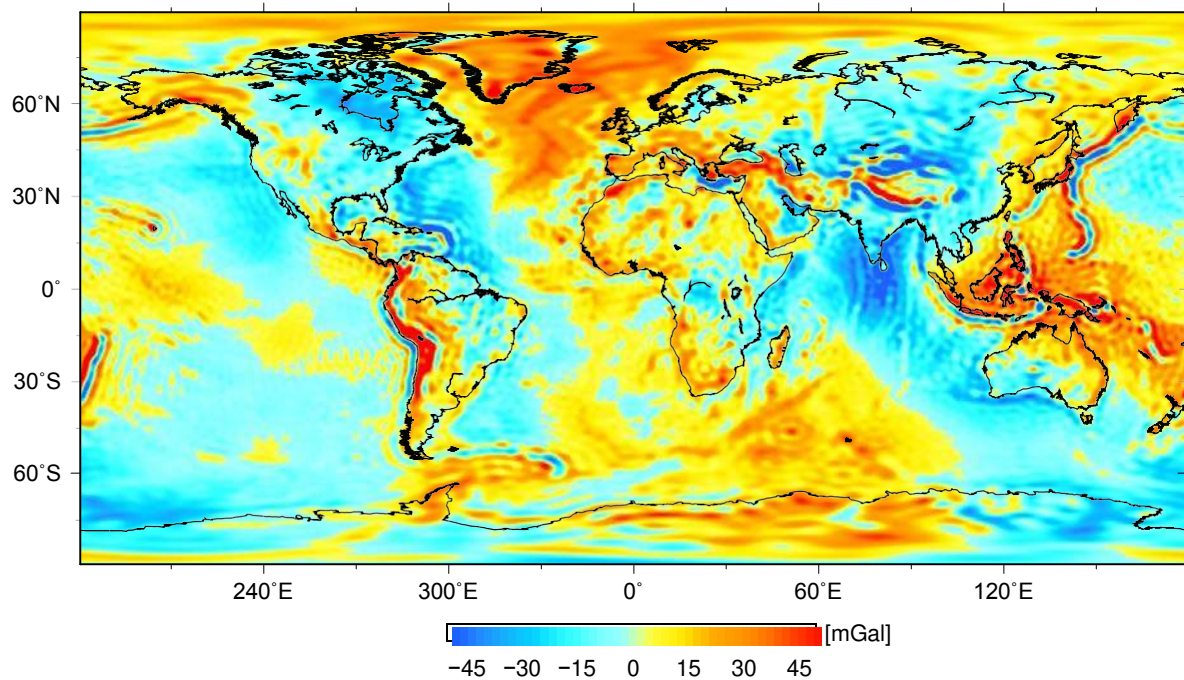
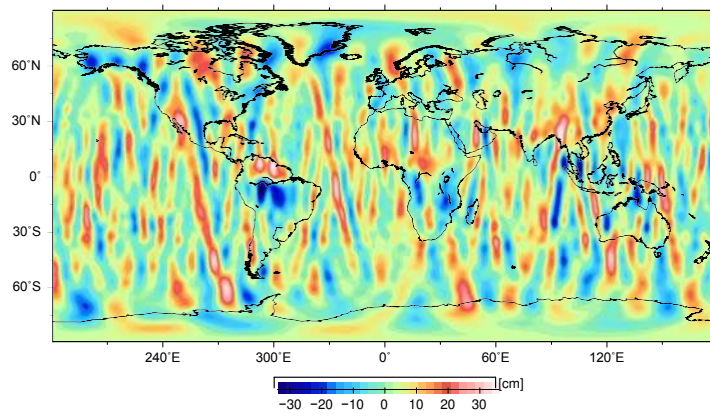


Figure 1. Static gravity anomalies based on 4 years of GRACE observations, illustrating the regional variations in the gravity field due to topography and variations in the Earth's density. The anomalies are computed as the difference between gravity on the geoid and the normal gravity on a reference ellipsoid. Units are milligal ($1 \text{ mGal} = 10^{-5} \text{ m/s}^2$).

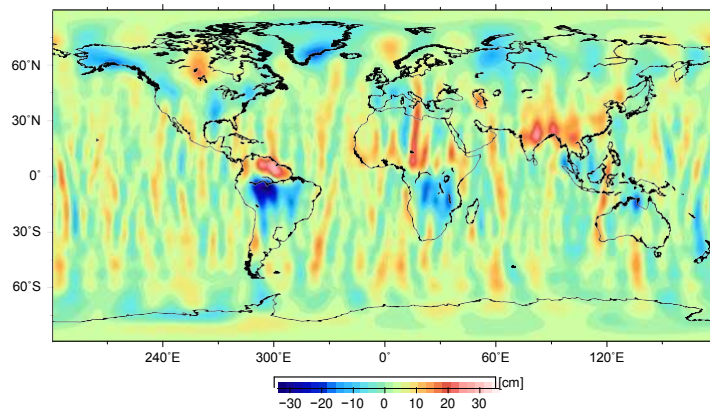


Figure 2. Artist's impression of the GRACE satellites (credit: NASA).'

a)



b)



c)

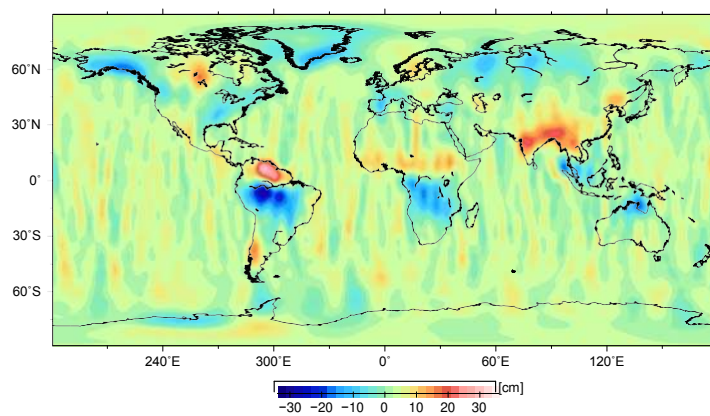


Figure 3. Maps of the observed surface water height anomaly for August 2005, based on three GRACE releases: a) the original first release (CSR RL01); b) the fourth release (CSR RL04) and c) fifth release (RL05). The data are smoothed with a 350 km Gaussian kernel.

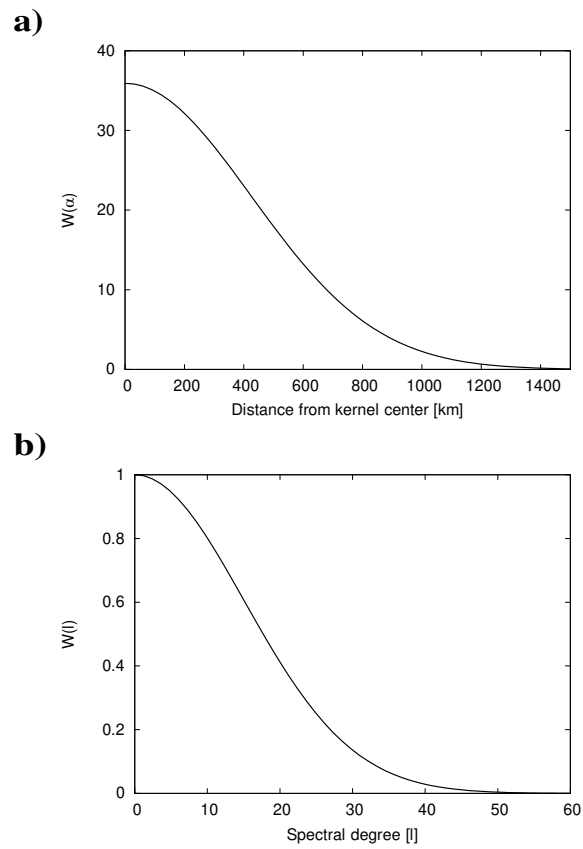
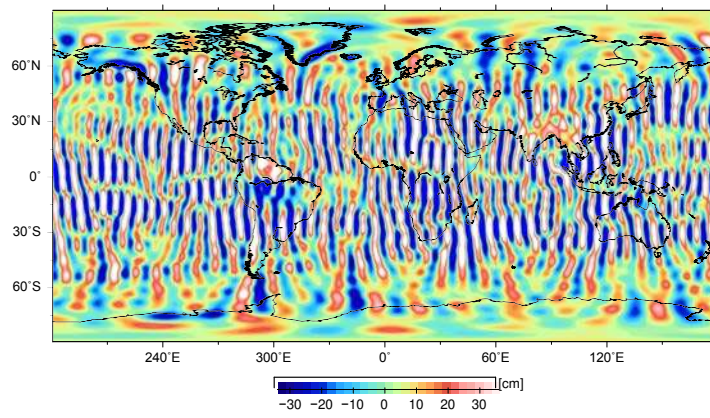
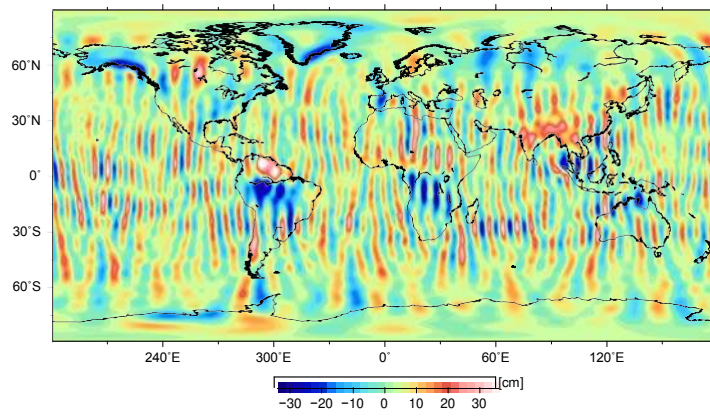


Figure 4. Value of a Gaussian smoothing kernel W for a smoothing radius of 500 km, a) as a function of the distance from the center point and b) as a function of the spherical harmonic degree l .

a)



b)



c)

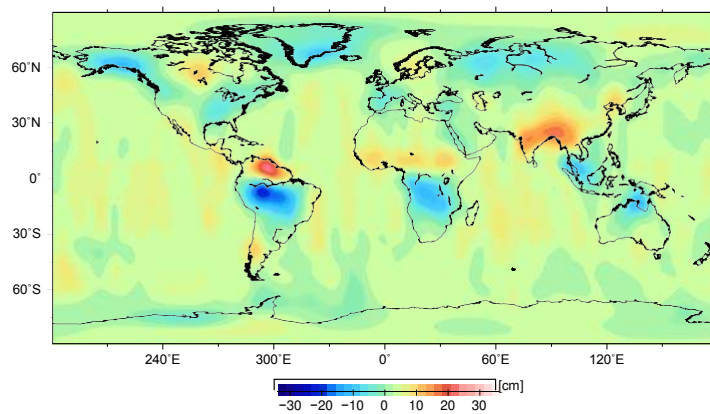


Figure 5. Surface water height anomaly for August 2005 observed by GRACE (based on CSR RL05 data), smoothed with a Gaussian kernel with three different smoothing radii: a) 0 km; b) 200 km and c) 500 km. An animation showing the 500 km monthly surface water height anomalies for 2003–2012 is available from stacks.iop.org/...

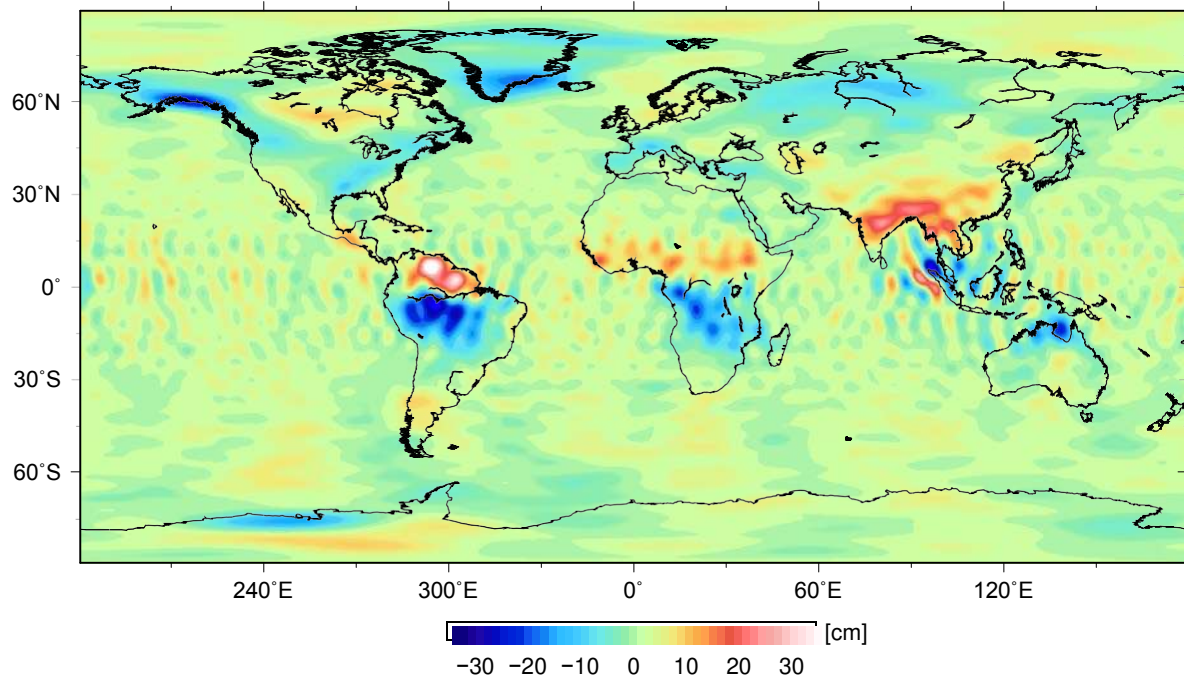


Figure 6. Surface water height anomaly for August 2005, smoothed with a 200 km Gaussian kernel as in Figure 5b, but now with the destriping algorithm of Swenson and Wahr [37] applied.

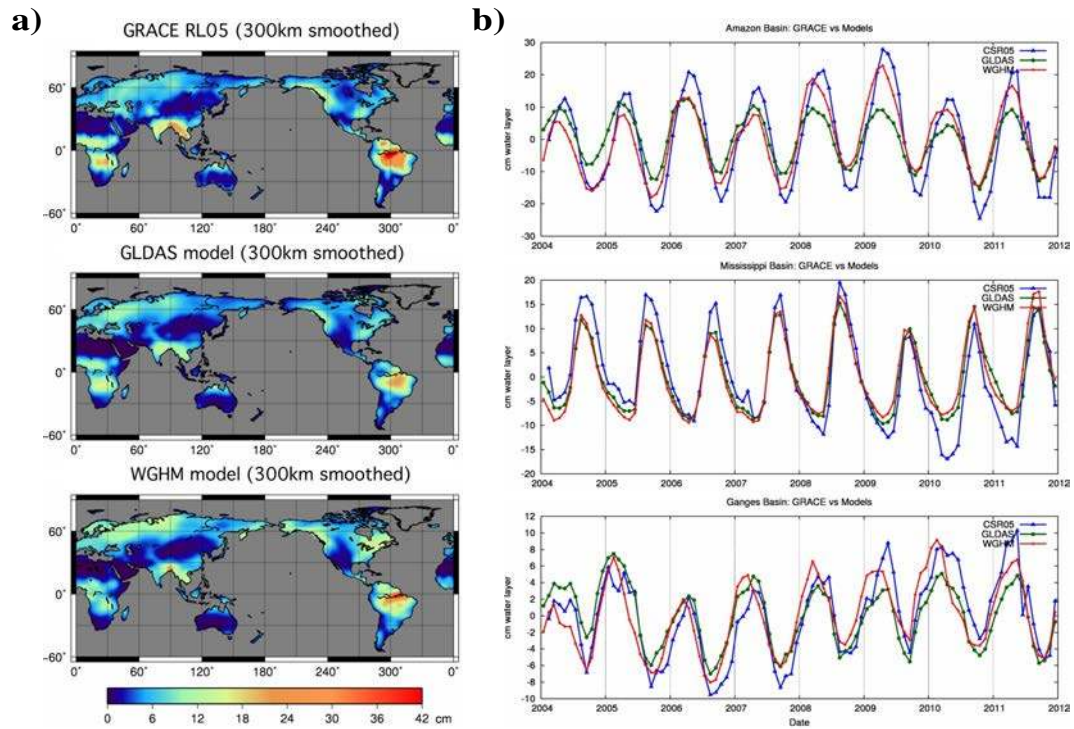


Figure 7. Comparison of a) annual signal amplitude and b) signals across three large basins for CSR RL05 GRACE and the hydrology models GLDAS and WGHM. Data is from 2004–2011, 300 km Gaussian smoothing applied to all series.

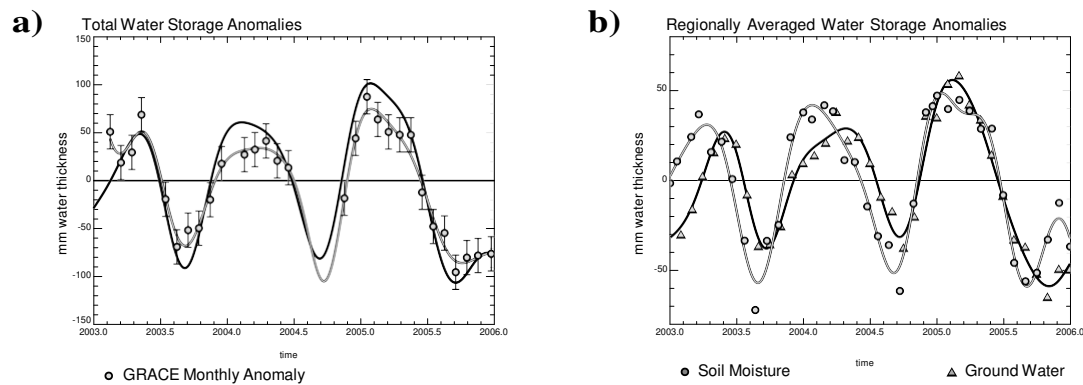


Figure 8. a) Total water storage anomalies from GRACE in the Illinois region (circles are monthly anomalies, gray line is the data smoothed to accentuate the seasonal variations [56]), and combined *in situ* soil moisture and groundwater measurements (black line is the smoothed time series). X-axis is time in years, and Y-axis is storage change in mm. b) *In situ* soil moisture and groundwater storage anomalies. Circles are monthly anomalies of soil moisture to 1 meter depth, triangles are groundwater anomalies below 1 meter depth; gray/black lines are smoothed soil moisture/ groundwater smoothed time series respectively. Adapted from Figures 3 and 4 from Swenson et al. [56] (copyright AGU 2006, this material is reproduced with permission of John Wiley & Sons, Inc.).

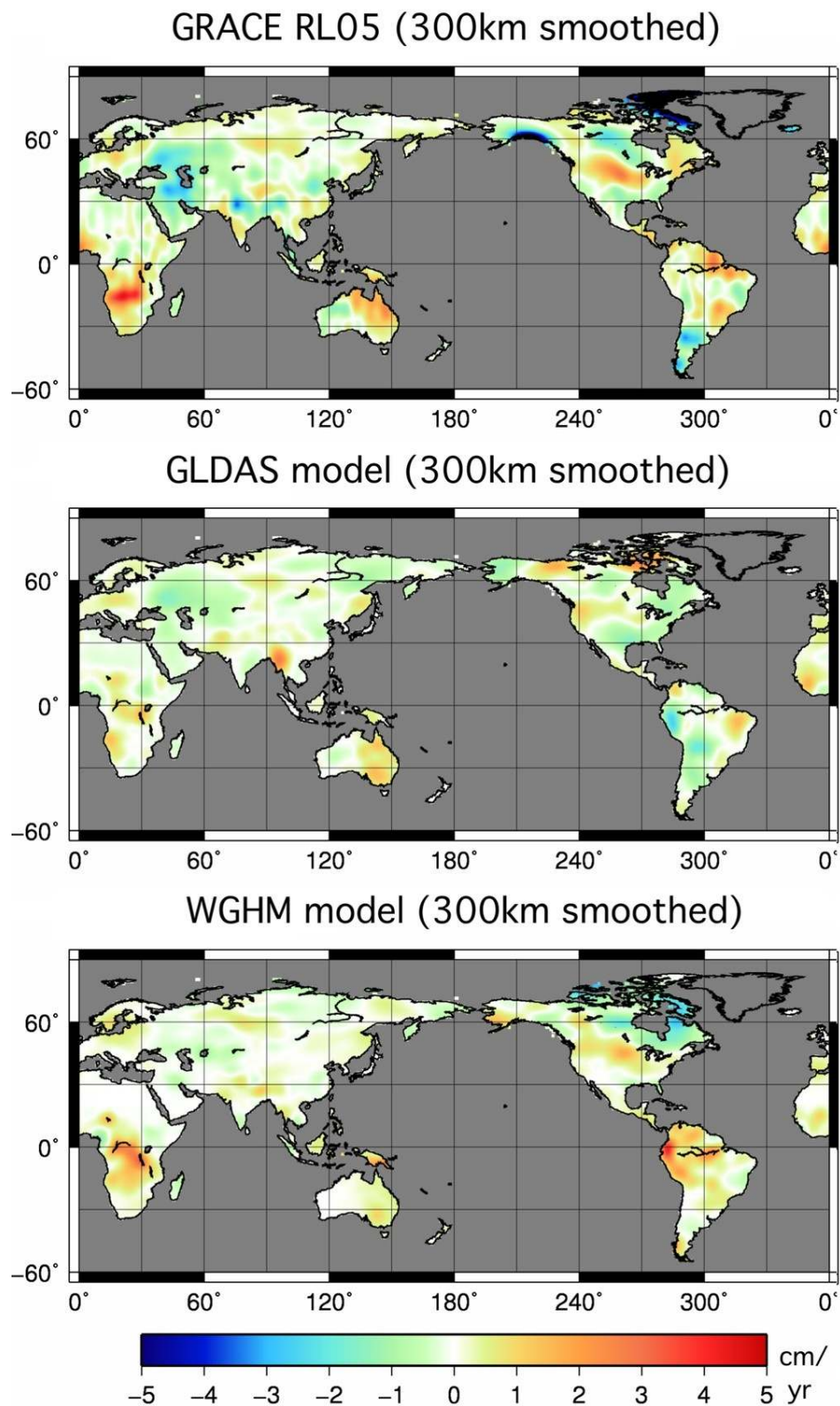


Figure 9. Comparison of trends in surface water height for CSR RL05 GRACE(top) and the hydrology models GLDAS (middle) and WGHM (bottom). Data is from 2004–2011, 300 km Gaussiann smoothing applied to all series.

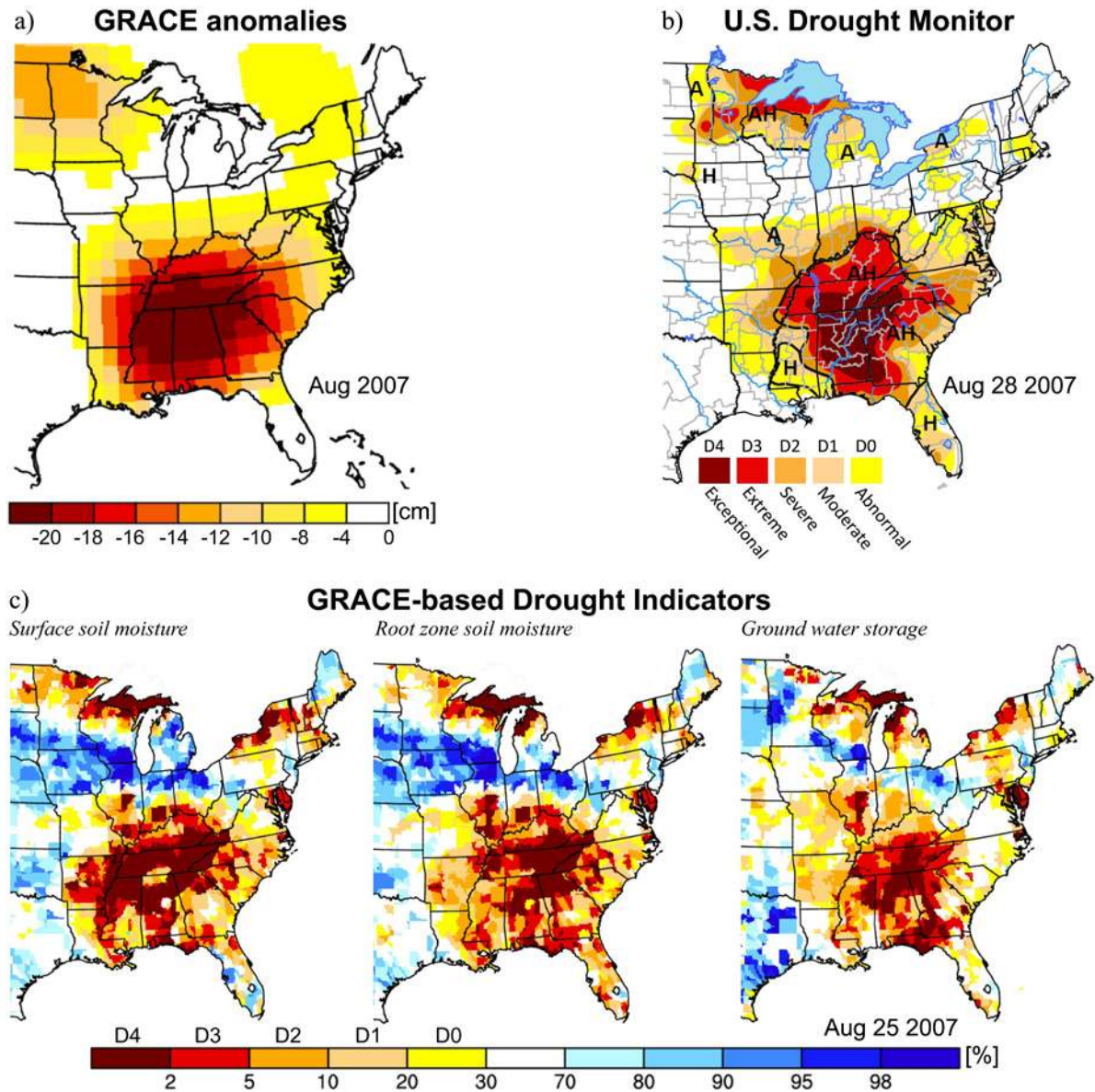


Figure 10. Correspondence between (a) the GRACE monthly water storage anomalies, (b) the U.S. Drought Monitor product, and (c) drought indicators based on model-assimilated GRACE terrestrial water storage observations during the drought in the southeastern United States in August 2007. In Figure 10b A, H, and AH define agricultural drought, hydrological drought, and a mix of A and H, respectively. From Houborg et al. [70] (copyright AGU 2012, this material is reproduced with permission of John Wiley & Sons, Inc.).

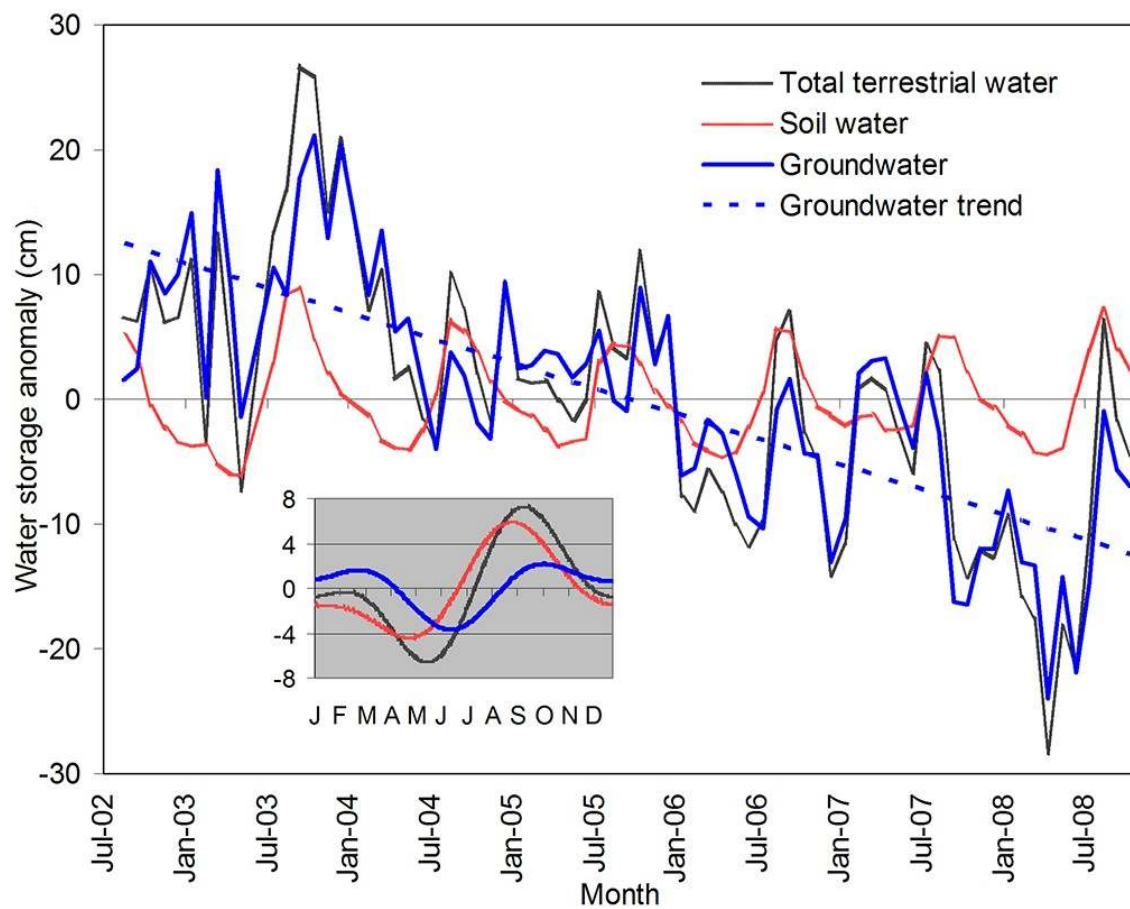


Figure 11. Monthly time series of anomalies of GRACE-derived total terrestrial water storage, modelled soil-water storage and estimated groundwater storage, averaged over Rajasthan, Punjab and Haryana, plotted as equivalent heights of water in centimetres. Also shown is the best-fit linear groundwater trend. Inset, mean seasonal cycle of each variable. From Rodell et al. [91] (copyright Macmillan Publishers Limited, 2009, this material is reproduced with permission of Nature Publishing Group.).

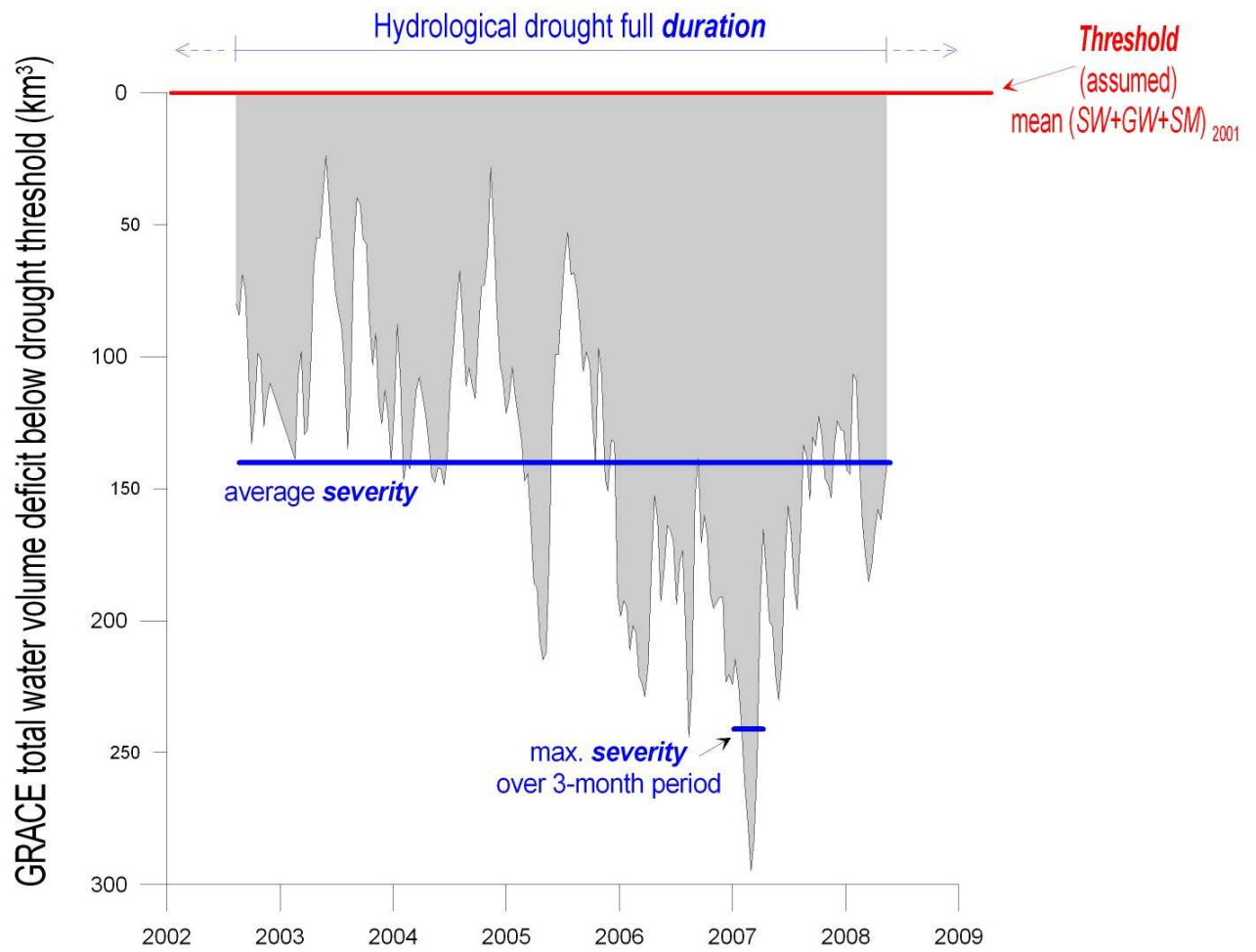


Figure 12. Severity of the multiyear drought derived from GRACE total water deficit across the Murray-Darling Basin. From Leblanc et al. [87] (copyright AGU 2009, this material is reproduced with permission of John Wiley & Sons, Inc.).

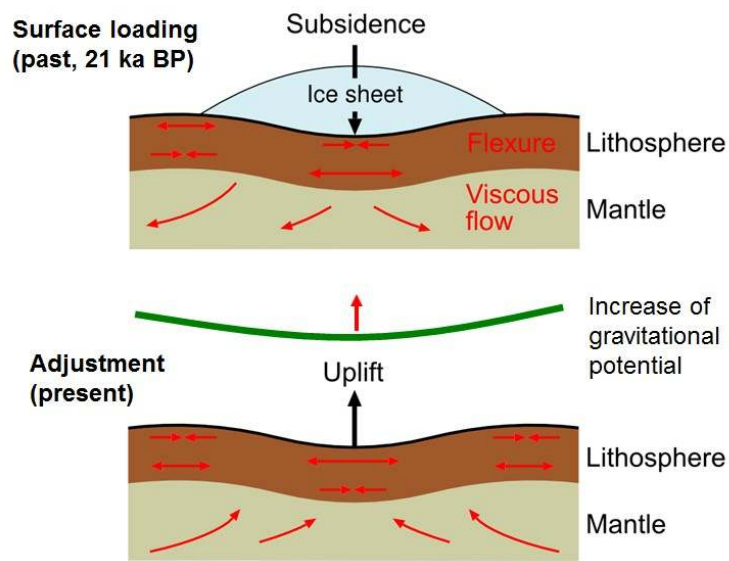


Figure 13. Illustration of the glacial-isostatic adjustment process (courtesy of Volker Klemann).

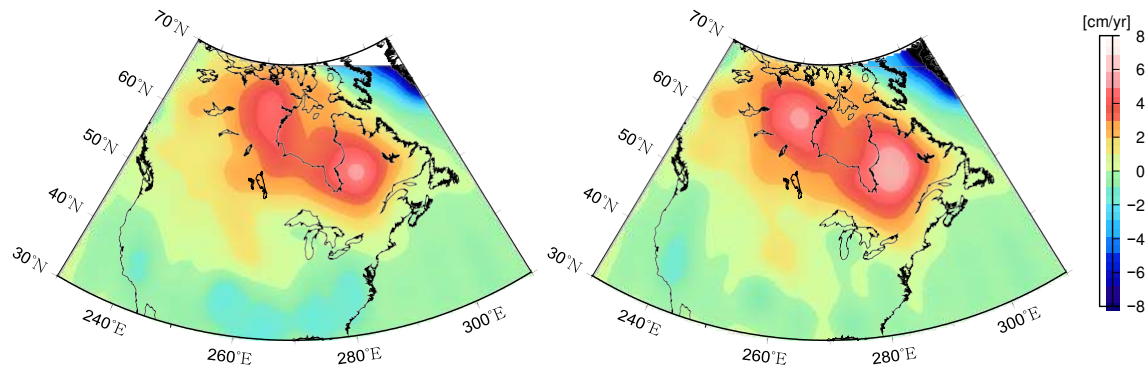


Figure 14. Apparent trend in surface mass loading from GRACE over North America for 2003-2012, without (left) and with (right) correction for hydrological mass variations (after Tamisiea et al. [153]). Two distinct anomalies left and right of the Hudson Bay are visible, which could be related to the presence of an ice sheet with two domes during the Last Glacial Maximum.

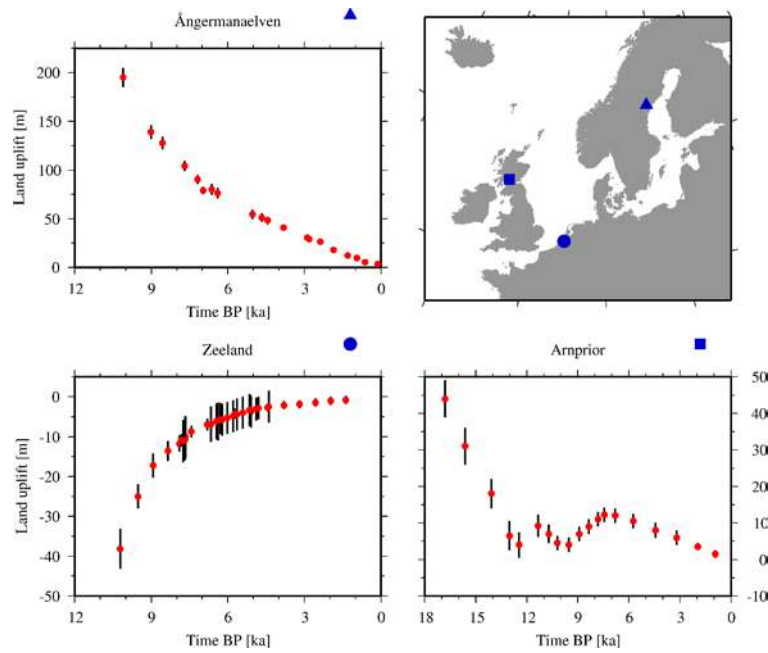


Figure 15. Examples of sea-level data (red dots with error bars) in Europe showing the different regional changes in relative sea level in response to the desintegration of the Fennoscandian ice sheet after the LGM. From Steffen and Wu [122] (copyright Elsevier Ltd. 2011, this material is reproduced with permission of Elsevier).

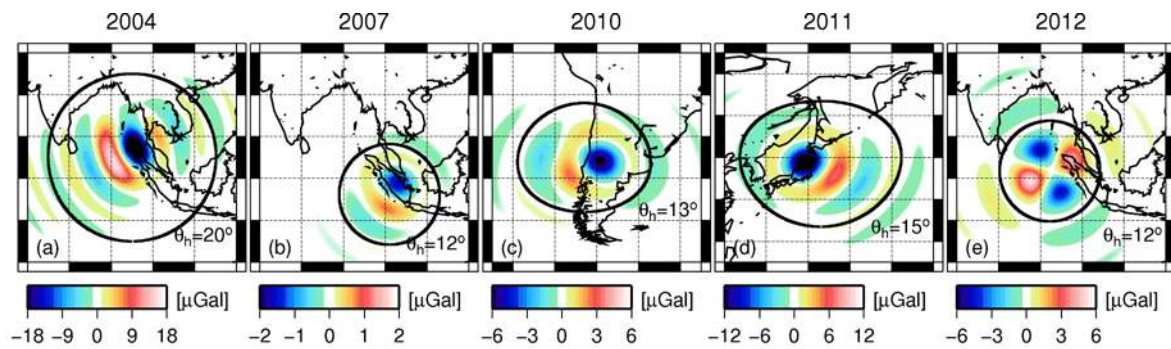


Figure 16. Synthetic gravity changes computed from centroid moment tensor (CMT) solutions for the 2004 Sumatra-Andaman earthquake, 2007 Bengkulu, 2010 Maule, 2011 Tohoku-Oki, and 2012 Indian Ocean earthquakes, respectively. The black circle delineates the spherical cap of radius θ_h defining the region of localization used in GRACE data post-processing (adapted from Figure 6 of Han et al. [172] (copyright AGU 2013, this material is reproduced with permission of John Wiley & Sons, Inc.)).

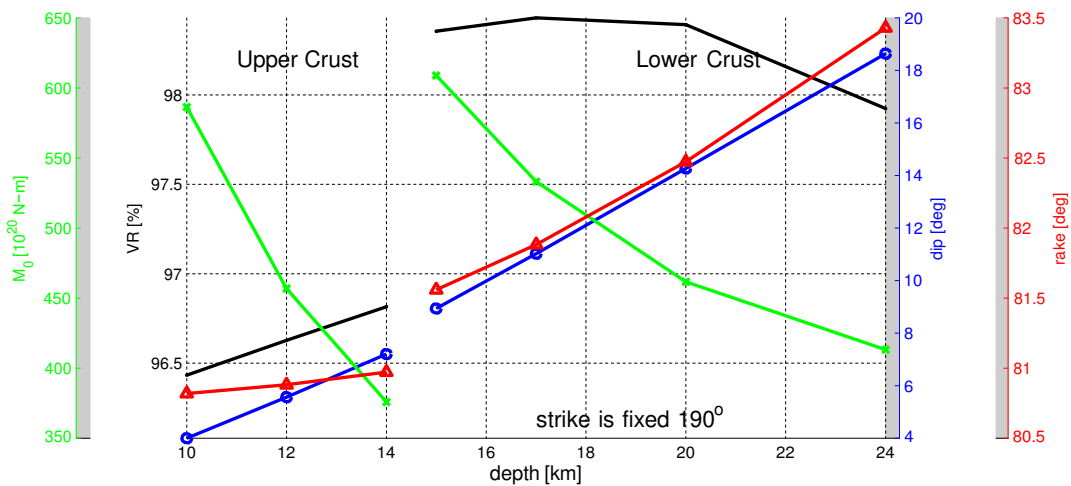


Figure 17. Examples of trade-offs in the determination of moment magnitude (M_0 , green), relative slip direction (rake, red) and vertical fault inclination (dip, blue) as a function of depth, for the 2011 Tohoku-Oki earthquake. A black line indicates the variance reduction (VR). The trade-off can be seen from the fact that the VR is almost flat for depths of 15–20 km, while large changes in M_0 are compensated by changes in dip angle. From Han et al. [172] (copyright AGU 2013, this material is reproduced with permission of John Wiley & Sons, Inc.).

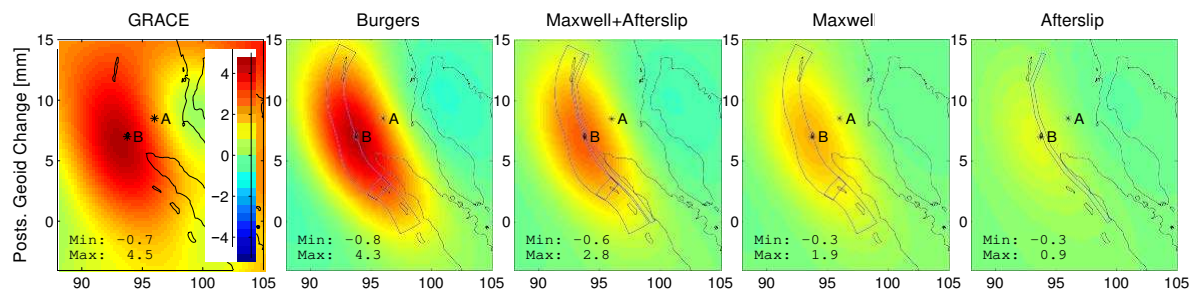


Figure 18. Postseismic geoid change, shown as average of fourth year minus first year after the 2004 Sumatra-Andama earthquake. Burgers rheology is in accordance with GRACE, and Maxwell rheology plus afterslip model underpredicts the observed effect. From Hoechner et al. [193] (copyright AGU 2011, this material is reproduced with permission of John Wiley & Sons, Inc.).

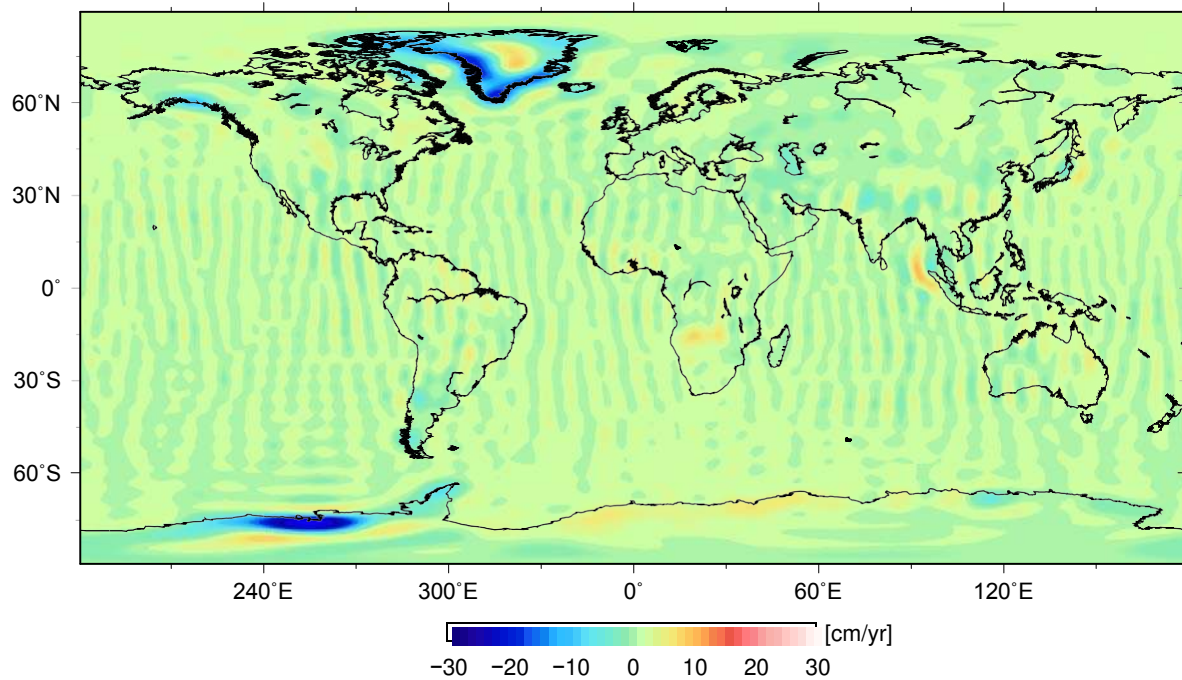


Figure 19. Trends in surface water mass height observed by GRACE for 2003–2013, based on GRACE CSR RL05 data and smoothed with a 100 km Gaussian kernel. The strongest trends are found in glaciated areas such as Greenland and the Arctic, Antarctica and Alaska, but the imprint of the Sumatra-Andaman earthquake can also be distinguished near 5°N 95°E.

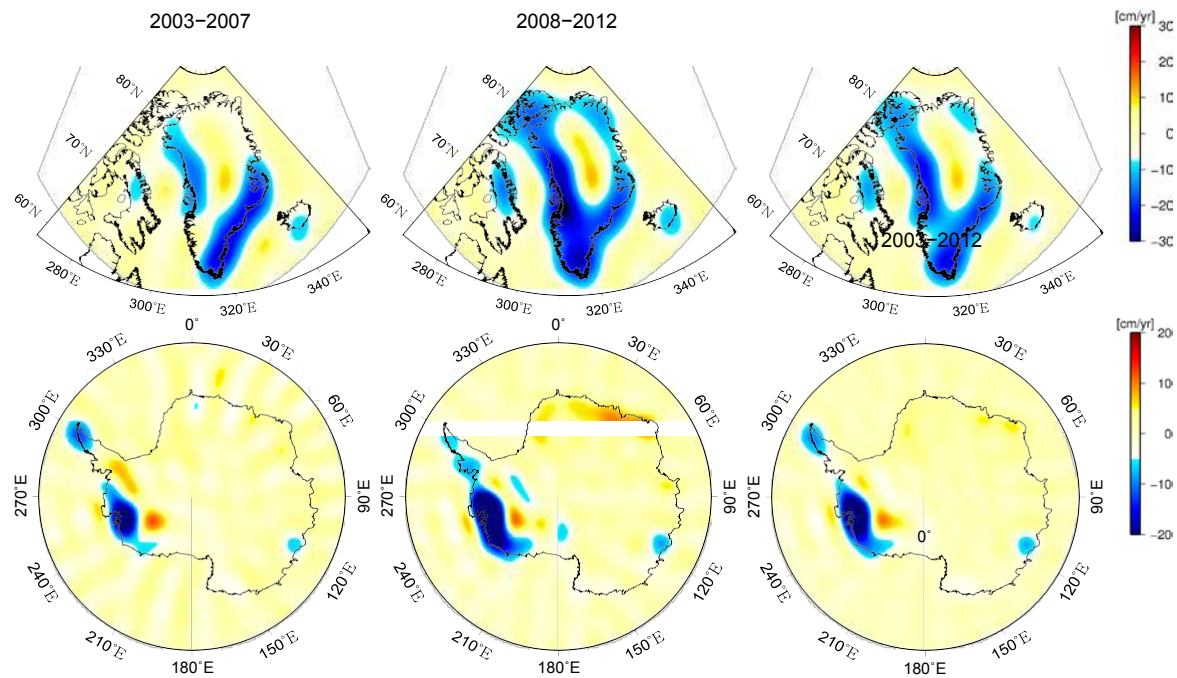


Figure 20. Mean annual mass trends for 2003-2007, 2008-2012 and 2003-2012 (based on CSR RL05 data), after correcting for GIA [304] and expressed as cm/yr equivalent water height for the Greenland (top) and Antarctic (bottom) Ice Sheet, illustrating the interannual variations in the observations. Animations showing the monthly evolution of the mass changes is available from stacks.iop.org/... (Greenland region) and stacks.iop.org/... (Antarctica).

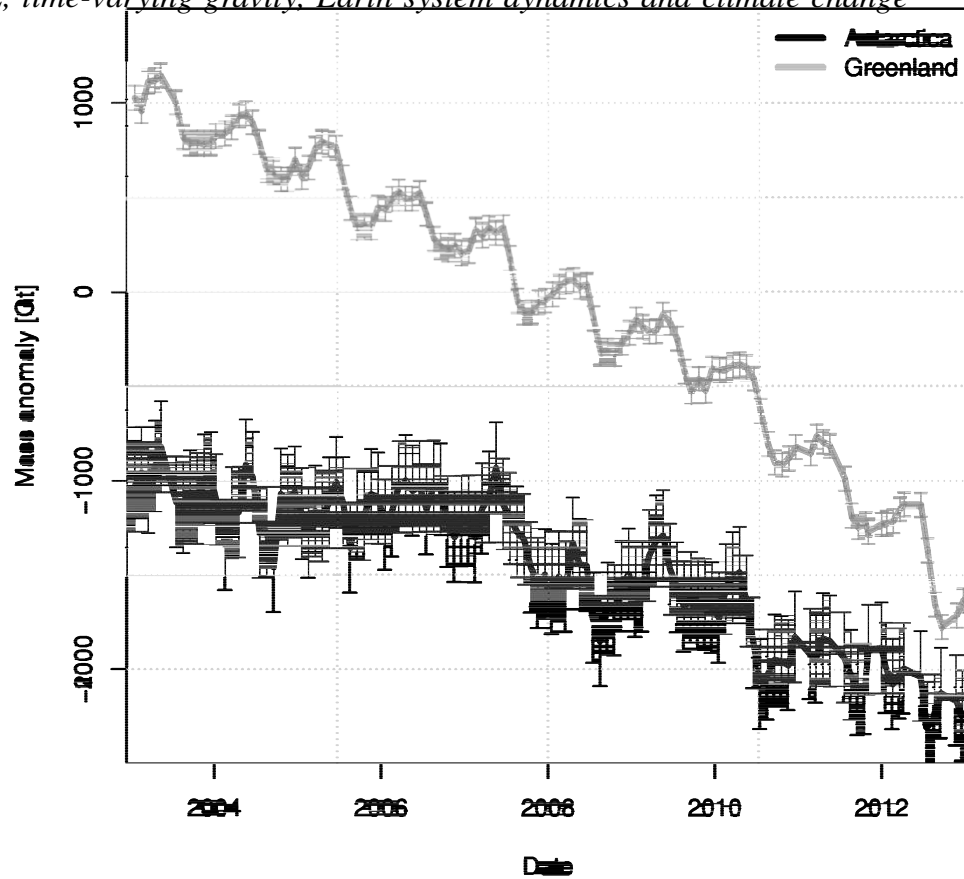


Figure 21. Cumulative mass balance of the Greenland and Antarctic Ice Sheet for Jan. 2003–Dec. 2012 (update of Wouters et al. [222]) and Sasgen et al. [151]). As discussed in Section 4, the trends depend to a certain degree on the correction for GIA effects, in particular for Antarctica. The two time series represent anomalies and have been vertically shifted with respect to each other for clarity.

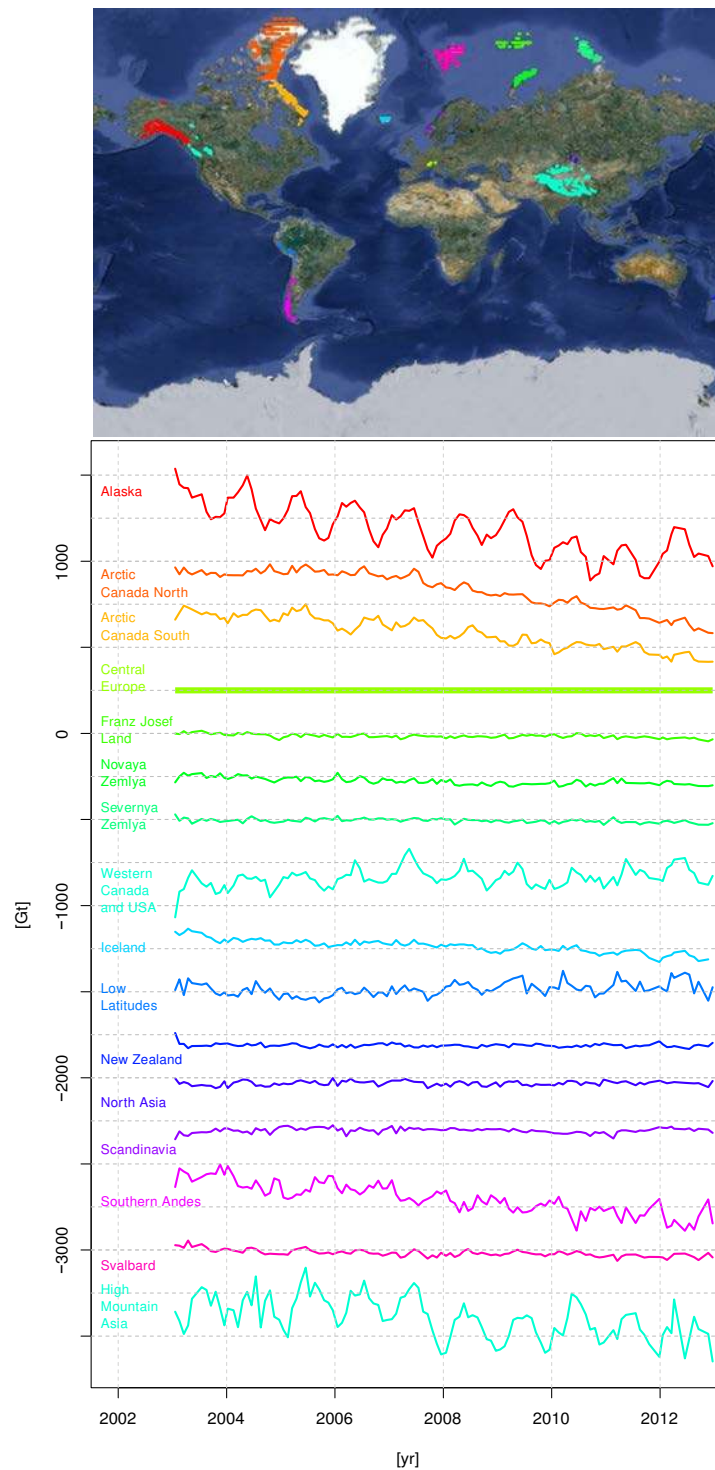


Figure 22. Cumulative mass balance for Jan. 2003–Dec. 2012 for glaciers and ice caps, based on GRACE CSR RL05 data and estimated using the method of Gardner et al. [232]. A correction for hydrology (using GLDAS-NOAH025) and GIA (using the model of A et al. [304]) has been applied. The time series represent anomalies and have been vertically shifted with respect to each other for clarity. The regions are shown in the top figure.

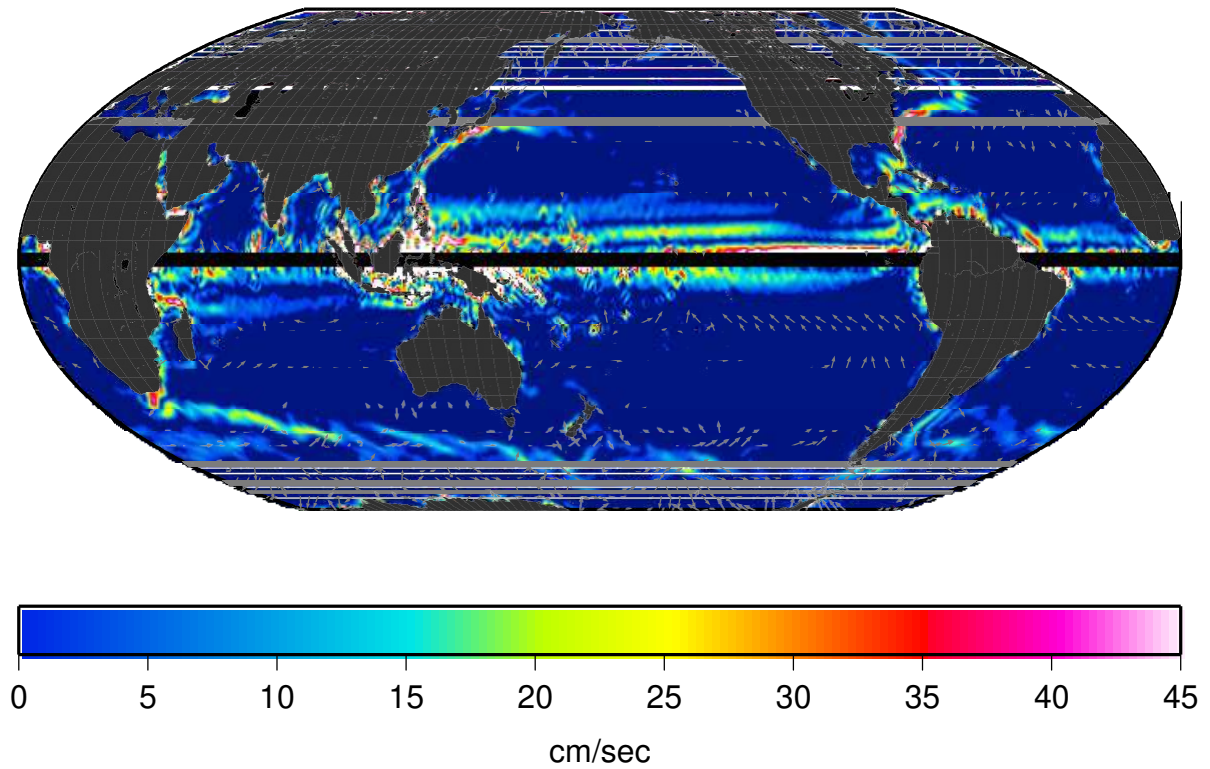


Figure 23. Surface geostrophic currents determined from a mean ocean dynamic topography calculated from altimetry sea surface height [305] and a geoid based on GRACE and other in situ gravity measurements [250]. Colours denote the magnitude of the velocity, and the arrows denote the direction. The length of the arrows is unrelated to the size of the current. Updated from Tapley et al. [247].

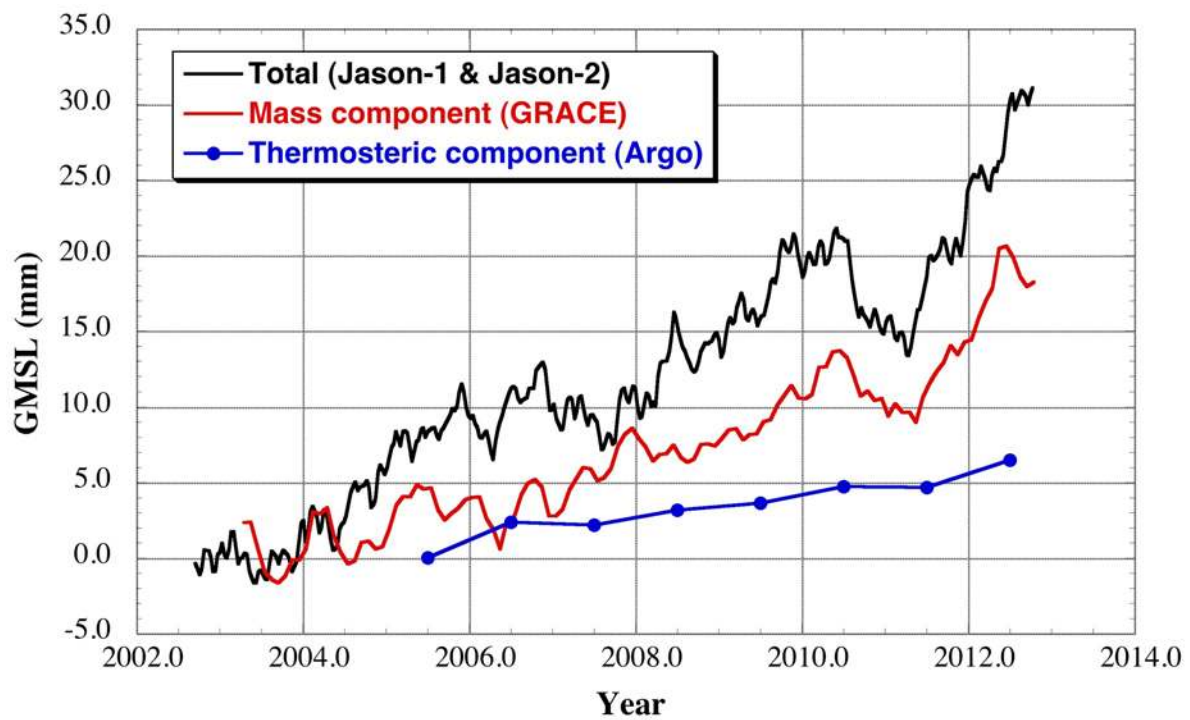


Figure 24. Non-seasonal GMSL change since 2003 (black line), including the mass component from GRACE (red line), and the thermosteric component for the upper 2000 m from Argo (blue line). The GMSL and mass component have had a 2-month running mean applied, while the thermosteric component is yearly averages. Total GMSL data are updated from Nerem et al. [267], mass component is updated from Chambers et al. [256], and thermosteric component is updated from Levitus et al. [306].

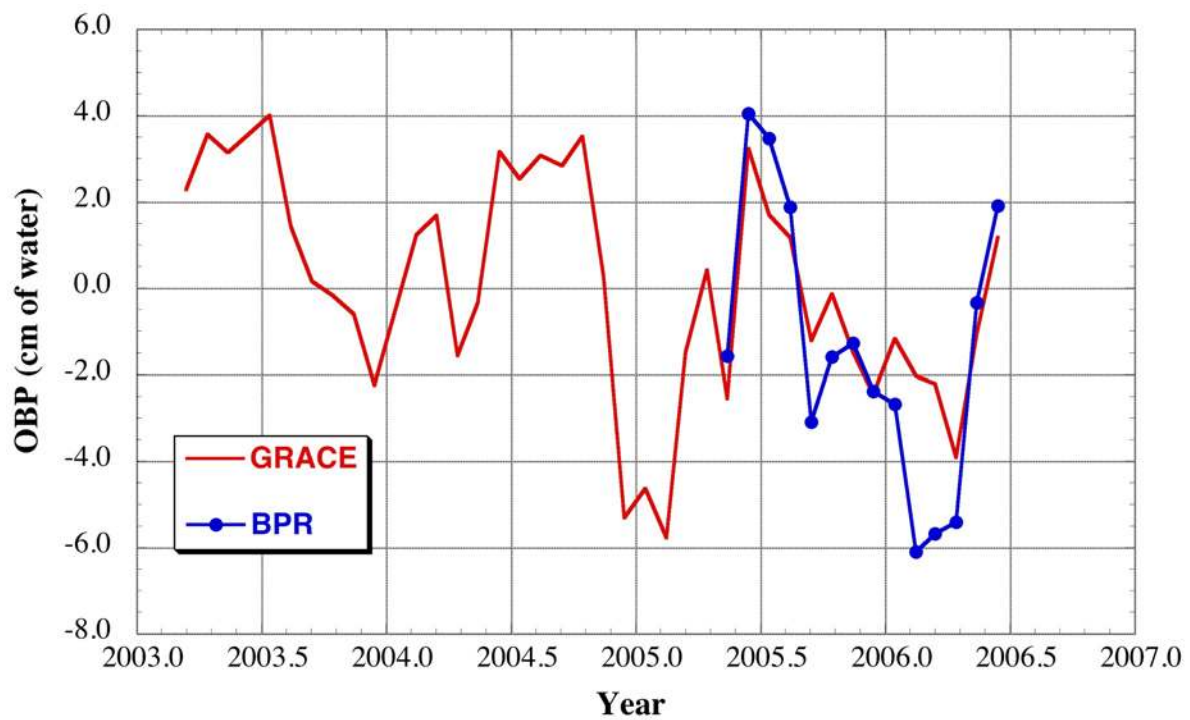


Figure 25. Ocean bottom pressure (in cm of equivalent water) measured by GRACE (red line), and a bottom pressure recorder (blue line) near the North Pole, after Morison et al. [275]. The GRACE data have been updated from Morison et al. [275] and are based on CSR RL05 data [32].

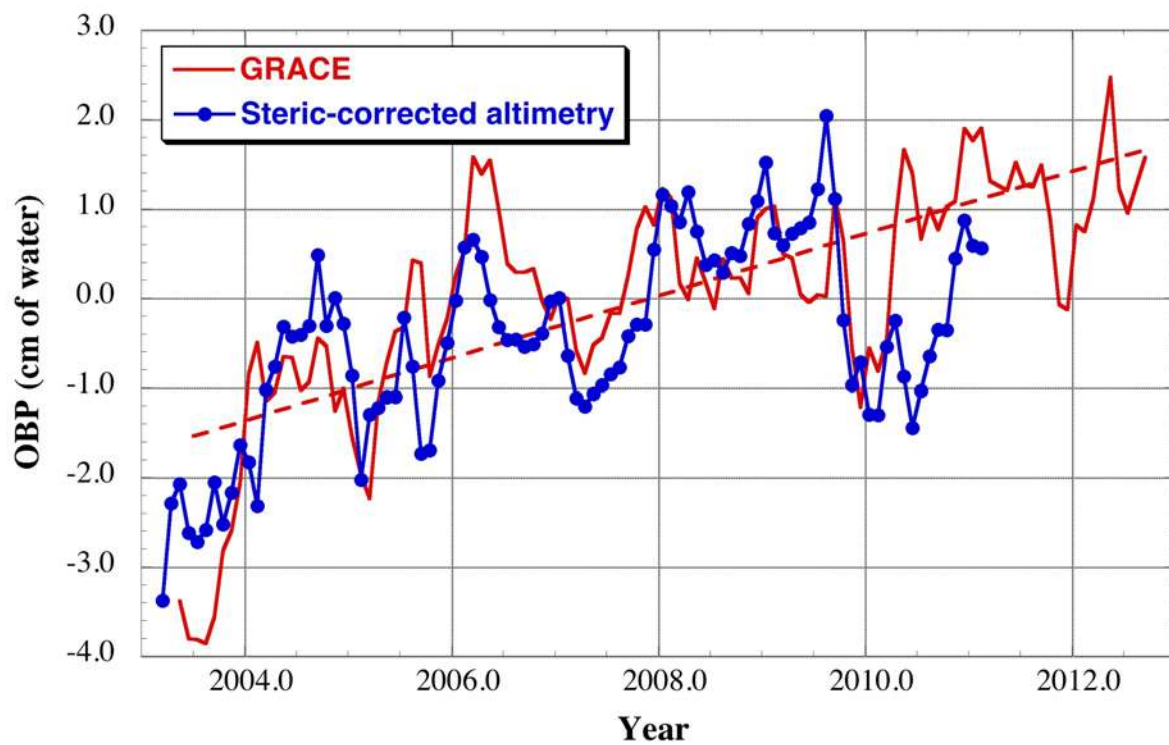


Figure 26. Monthly, non-seasonal OBP averaged over the North Pacific region 35°N–45°N, 160°E–185°E for (a) GRACE and steric-corrected altimetry (updated from Chambers and Willis [280], Chambers [281]). Both time series have been smoothed with a 5-month running mean. The dashed line represents the best-fit linear trend to the longer GRACE observations.

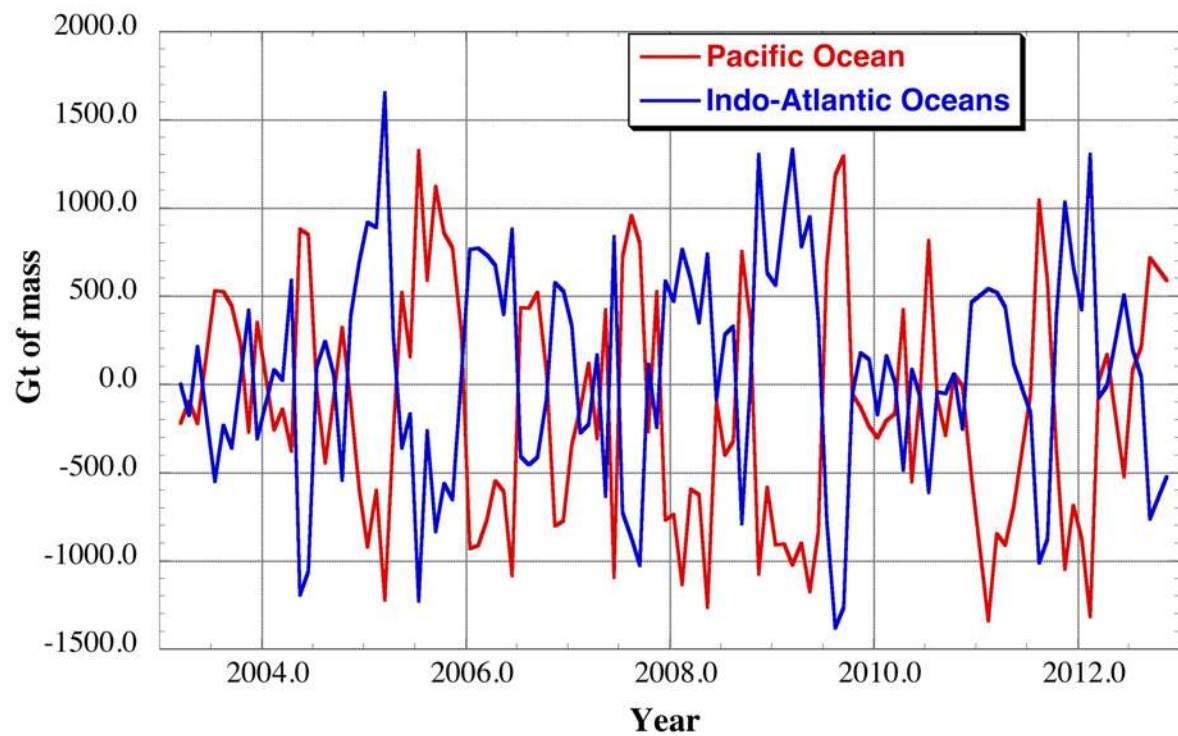


Figure 27. Monthly total mass anomaly (global mean variation removed) for the Indo-Atlantic Oceans (blue) and Pacific Ocean (red) observed by GRACE (CSR RL05), updated from Chambers and Willis [284]. The correlation between the two is -0.94, representing an exchange of mass between the Pacific and Indo-Atlantic Oceans.

References

- [1] D. Crossley, J. Hinderer, and U. Riccardi. The measurement of surface gravity. *Reports on Progress in Physics*, 76(4):046101, 2013.
- [2] LAGEOS-I (Laser Geodynamics Satellite-I)/LAGEOS-II. URL <https://directory.eoportal.org/web/eoportal/satellite-missions/l/lageos>.
- [3] M. K. Cheng, R. J. Eanes, C. K. Shum, B. E. Schutz, and B. D. Tapley. Temporal variations in low degree zonal harmonics from Starlette orbit analysis. *Geophys. Res. Lett.*, 16:393–396, May 1989. doi: 10.1029/GL016i005p00393.
- [4] C. Reigber, H. Lühr, and P. Schwintzer. CHAMP mission status. *Adv. Spac. Res.*, 30:129–134, July 2002. doi: 10.1016/S0273-1177(02)00276-4.
- [5] R. S. Nerem, C. Jekeli, and W. M. Kaula. Gravity field determination and characteristics: Retrospective and prospective. *J. Geophys. Res.*, 100:15053–15074, 1995. doi: 10.1029/94JB03257.
- [6] NASA. *Geophysical and Geodetic Requirements for Global Gravity Field Measurements, 1987-2000: Report of a Gravity Workshop, Colorado Springs, CO*. NASA geodyn. Branch, Division of Earth Science and Applications, Washington, D.C., 1987.
- [7] NRC. *Applications of a Dedicated Gravitational Satellite Mission*. National Academy Press, Washington, D.C., 1979.
- [8] NRC. *A Strategy for Earth Science from Space in the 1980's: Part I: Solid Earth and Oceans*. National Academy Press, Washington, D.C., 1982.
- [9] J. O. Dickey, C. R. Bentley, R. Bilham, J. A. Carton, R. J. Eanes, T. A. Herring, W. M. Kaula, G. S. E. Lagerloef, S. Rojstaczer, W. H. F. Smith, H. M. van den Dool, J. M. Wahr, and M. T. Zuber. *Satellite Gravity and the Geosphere*. National Research Council Report. National Academy Press, 1997.
- [10] I. Ciufolini, A. Paolozzi, E. Pavlis, J. Ries, R. Koenig, R. Matzner, G. Sindoni, and H. Neumayer. Towards a one percent measurement of frame dragging by spin with satellite laser ranging to LAGEOS, LAGEOS 2 and LARES and grace gravity models. *Space Science Reviews*, 148(1-4):71–104, 2009. ISSN 0038-6308. doi: 10.1007/s11214-009-9585-7.
- [11] R. R. B. von Frese, L. V. Potts, S. B. Wells, T. E. Leftwich, H. R. Kim, J. W. Kim, A. V. Golynsky, O. Hernandez, and L. R. Gaya-Piqué. GRACE gravity evidence for an impact basin in Wilkes Land, Antarctica. *Geochem. Geophys. Geosy.*, 10: 2014–+, February 2009. doi: 10.1029/2008GC002149.
- [12] S. L. Bruinsma and J. M. Forbes. Storm-Time Equatorial Density Enhancements Observed by CHAMP and GRACE. *J. Spacecraft Rockets*, 44:1154–1159, November 2007. doi: 10.2514/1.28134.
- [13] A. Cazenave and J. Chen. Time-variable gravity from space and present-day mass

- 1667 redistribution in the Earth system. *Earth and Planetary Science Letters*, 298:
1668 263–274, 10/2010 2010. doi: 10.1016/j.epsl.2010.07.035.
- 1669 [14] V. Zlotnicki, S. Bettadpur, F. W. Landerer, and M. M. Watkins. Gravity Recovery
1670 and Climate Experiment (GRACE): Detection of Ice Mass Loss, Terrestrial Mass
1671 Changes, and Ocean Mass Gains *Earth System Monitoring* ed J. Orcutt (New
1672 York: Springer), pp. 123–152, 2013 doi: 10.1007/978-1-4614-5684-1_7.
- 1673 [15] C. Reigber, R. Schmidt, F. Flechtner, R. König, U. Meyer, K.-H. Neumayer,
1674 P. Schwintzer, and S. Y. Zhu. An Earth gravity field model complete to degree
1675 and order 150 from GRACE: EIGEN-GRACE02S. *J. geodyn.*, 39:1–10, January
1676 2005. doi: 10.1016/j.jog.2004.07.001.
- 1677 [16] B. Tapley, J. Ries, S. Bettadpur, D. Chambers, M. Cheng, F. Condi, B. Gunter,
1678 Z. Kang, P. Nagel, R. Pastor, T. Pekker, S. Poole, and F. Wang. GGM02
1679 An improved Earth gravity field model from GRACE. *J. Geodesy*, 79:467–478,
1680 November 2005. doi: 10.1007/s00190-005-0480-z.
- 1681 [17] S. V. Bettadpur. UTCSR level-2 processing standards document for level-2
1682 product release 0004. Technical Report GRACE 327-742, CSR, Austin, TX, USA,
1683 2007.
- 1684 [18] F. Flechtner. GFZ level-2 processing standards document for level-2 product
1685 release 0004. Technical Report GRACE 327-743, GFZ, Potsdam, Germany, 2007.
- 1686 [19] M. Watkins and D.-N. Yuan. JPL level-2 processing standards document for
1687 level-2 product release 04. Technical Report GRACE 327-744, JPL, Pasadena,
1688 CA, USA, 2007.
- 1689 [20] J.-M. Lemoine, S. Bruinsma, S. Loyer, R. Biancale, J.-C. Marty, F. Perosanz, and
1690 G. Balmino. Temporal gravity field models inferred from GRACE data. *Adv.
1691 Spac. Res.*, 39:1620–1629, 2007. doi: 10.1016/j.asr.2007.03.062.
- 1692 [21] X. Liu. *Global gravity field recovery from satellite-to-satellite tracking data with
1693 the acceleration approach*. PhD. thesis, Netherlands Geodetic Commission,
1694 Publication on Geodesy 68, TU Delft, Delft, The Netherlands, 2008.
- 1695 [22] T. Mayer-Gürr, A. Eicker, E. Kurtenbach, and K.-H. Ilk. ITG-GRACE: Global
1696 Static and Temporal Gravity Field Models from GRACE Data. In F. Flechtner,
1697 T. Gruber, A. Güntner, M. Manda, M. Rothacher, T. Schöne, and J. Wickert,
1698 editors, *System Earth via Geodetic-Geophysical Space Techniques*, pages 159–
1699 168. Springer, Berlin, Heidelberg, 2010. ISBN ISBN 978-3-642-10227-1. doi:
1700 10.1007/978-3-642-10228-8_13.
- 1701 [23] W. A. Heiskanen and H. Moritz. *Physical geodesy*. San Francisco, W. H. Freeman
1702 [1967], 1967.
- 1703 [24] J. Wahr, M. Molenaar, and F. Bryan. Time variability of the earth’s gravity field:
1704 Hydrological and oceanic effects and their possible detection using GRACE. *J.
1705 Geophys. Res. (Solid Earth)*, 103(B12):30305–30229, 1998.

- 1706 [25] W. E. Farrell. Deformation of the Earth by surface loads. *Rev. Geophys. and*
1707 *Space Phys.*, 10:761–797, August 1972.
- 1708 [26] D. D. Rowlands, S. B. Luthcke, S. M. Klosko, F. G. R. Lemoine, D. S. Chinn, J. J.
1709 McCarthy, C. M. Cox, and O. B. Anderson. Resolving mass flux at high spatial
1710 and temporal resolution using GRACE intersatellite measurements. *Geophys. Res.*
1711 *Lett.*, 32:4310–+, February 2005. doi: 10.1029/2004GL021908.
- 1712 [27] S. B. Luthcke, H. J. Zwally, W. Abdalati, D. D. Rowlands, R. D. Ray, R. S.
1713 Nerem, F. G. Lemoine, J. J. McCarthy, and D. S. Chinn. Recent Greenland ice
1714 mass loss by drainage system from satellite gravity observations. *Science*, 314:
1715 1286–1289, December 2006. doi: 10.1126/Science.1130776.
- 1716 [28] B.D. Tapley, S. Bettadpur, J.C. Ries, P.F. Thompson, and M.M. Watkins.
1717 GRACE measurements of mass variability in the earth system. *Science*, 305,
1718 2004.
- 1719 [29] J. Wahr, S. Swenson, V. Zlotnicki, and I. Velicogna. Time variable gravity from
1720 GRACE: First results. *Geophys. Res. Lett.*, 31:L11501, 2004. doi: 10.1029/
1721 2004GL019779.
- 1722 [30] R. D. Ray and S. B. Luthcke. Tide model errors and GRACE gravimetry: towards
1723 a more realistic assessment. *Geophys. J. Int.*, 167:1055–1059, December 2006. doi:
1724 10.1111/j.1365-246X.2006.03229.x.
- 1725 [31] E. J. O. Schrama and P. N. A. M. Visser. Accuracy assessment of the monthly
1726 GRACE geoids based upon a simulation. *J. Geodesy*, 81:67–80, January 2007.
1727 doi: 10.1007/s00190-006-0085-1.
- 1728 [32] D. P. Chambers and J. A. Bonin. Evaluation of Release-05 GRACE time-variable
1729 gravity coefficients over the ocean. *Ocean Science*, 8:859–868, October 2012. doi:
1730 10.5194/os-8-859-2012.
- 1731 [33] S. Swenson and J. Wahr. Methods for inferring regional surface-mass anomalies
1732 from gravity recovery and climate experiment (GRACE) measurements of time-
1733 variable gravity. *J. Geophys. Res.*, 107(B9):219, 2002. doi: 10.1029/2001JB000576.
- 1734 [34] C. Jekeli. Alternative methods to smooth the Earth’s gravity field. Technical
1735 Report Report 327, Department of Geodetic Science and Surveying, Ohio State
1736 University, December 1981.
- 1737 [35] J. L. Chen, C. R. Wilson, and K.-W. Seo. Optimized smoothing of Gravity
1738 Recovery and Climate Experiment (GRACE) time-variable gravity observations.
1739 *J. Geophys. Res.*, 111:6408–+, June 2006. doi: 10.1029/2005JB004064.
- 1740 [36] S.-C. Han, C. K. Shum, and K. Matsumoto. GRACE observations of M_2 and S_2
1741 ocean tides underneath the Filchner-Ronne and Larsen ice shelves, Antarctica.
1742 *Geophys. Res. Lett.*, 32:20311–+, October 2005. doi: 10.1029/2005GL024296.
- 1743 [37] S. Swenson and J. Wahr. Post-processing removal of correlated errors in GRACE
1744 data. *Geophys. Res. Lett.*, 33:L8402, April 2006. doi: 10.1029/2005GL025285.

- 1745 [38] B. Wouters and E. J. O. Schrama. Improved accuracy of GRACE gravity solutions
1746 through empirical orthogonal function filtering of spherical harmonics. *Geophys.*
1747 *Res. Lett.*, 34:23711–+, December 2007. doi: 10.1029/2007GL032098.
- 1748 [39] J. Kusche. Approximate decorrelation and non-isotropic smoothing of time-
1749 variable GRACE-type gravity field models. *J. Geodesy*, pages 80–+, February
1750 2007. doi: 10.1007/s00190-007-0143-3.
- 1751 [40] R. Klees, E. A. Revtova, B. C. Gunter, P. Ditmar, E. Oudman, H. C. Winsemius,
1752 and H. H. G. Savenije. The design of an optimal filter for monthly GRACE gravity
1753 models. *Geophys. J. Int.*, 175:417–432, November 2008. doi: 10.1111/j.1365-246X.
1754 2008.03922.x.
- 1755 [41] D. P. Chambers. Observing seasonal steric sea level variations with GRACE
1756 and satellite altimetry. *J. Geophys. Res. (Oceans)*, 111:C3010, March 2006. doi:
1757 10.1029/2005JC002914.
- 1758 [42] J. L. Chen, C. R. Wilson, J. S. Famiglietti, and M. Rodell. Attenuation effect on
1759 seasonal basin-scale water storage changes from GRACE time-variable gravity. *J.*
1760 *Geodesy*, 81:237–245, April 2007. doi: 10.1007/s00190-006-0104-2.
- 1761 [43] S. C. Swenson and J. M. Wahr. Estimating signal loss in regularized GRACE
1762 gravity field solutions. *Geophys. J. Int.*, 185:693–702, May 2011. doi: 10.1111/j.
1763 1365-246X.2011.04977.x.
- 1764 [44] F. W. Landerer and S. C. Swenson. Accuracy of scaled GRACE terrestrial
1765 water storage estimates. *Water Resour. Res.*, 48:W04531, April 2012. doi:
1766 10.1029/2011WR011453.
- 1767 [45] H. Save, S. Bettadpur, and B. D. Tapley. Reducing errors in the GRACE gravity
1768 solutions using regularization. *J. Geodesy*, 86:695–711, September 2012. doi:
1769 10.1007/s00190-012-0548-5.
- 1770 [46] I. Velicogna and J. Wahr. Greenland mass balance from GRACE. *Geophys. Res.*
1771 *Lett.*, 32:18505–+, September 2005. doi: 10.1029/2005GL023955.
- 1772 [47] J. A. Bonin and D. P. Chambers. Evaluation of high-frequency oceanographic
1773 signal in GRACE data: Implications for de-aliasing. *Geophys. Res. Lett.*, 381:
1774 L17608, September 2011. doi: 10.1029/2011GL048881.
- 1775 [48] S. Bruinsma, J.-M. Lemoine, R. Biancale, and N. Valès. CNES/GRGS 10-day
1776 gravity field models (release 2) and their evaluation. *Adv. Spac. Res.*, 45:587–601,
1777 February 2010. doi: 10.1016/j.asr.2009.10.012.
- 1778 [49] F. Flechtner, C. Dahle, K. H. Neumayer, R. König, and C. Förste. The
1779 Release 04 CHAMP and GRACE EIGEN Gravity Field Models. In F. Flechtner,
1780 T. Gruber, A. Güntner, M. Manda, M. Rothacher, T. Schöne, and J. Wickert,
1781 editors, *System Earth via Geodetic-Geophysical Space Techniques*, pages 41–
1782 58. Springer, Berlin, Heidelberg, 2010. ISBN ISBN 978-3-642-10227-1. doi:
1783 10.1007/978-3-642-10228-84.

- 1784 [50] E. Kurtenbach, T. Mayer-Gürr, and A. Eicker. Deriving daily snapshots of the
1785 Earth's gravity field from GRACE L1B data using Kalman filtering. *Geophys.*
1786 *Res. Lett.*, 36:17102–+, September 2009. doi: 10.1029/2009GL039564.
- 1787 [51] T. H. Syed, J. S. Famiglietti, M. Rodell, J. Chen, and C. R. Wilson. Analysis of
1788 terrestrial water storage changes from GRACE and GLDAS. *Water Resour. Res.*
1789 , 44:2433–+, February 2008. doi: 10.1029/2006WR005779.
- 1790 [52] R. Schmidt, P. Schwintzer, F. Flechtner, C. Reigber, A. Güntner, P. Döll,
1791 G. Ramillien, A. Cazenave, S. Petrovic, H. Jochmann, and J. Wunsch. GRACE
1792 observations of changes in continental water storage. *Global Planet. Change*, 50:
1793 112–126, February 2006.
- 1794 [53] K.-W. Seo, C. R. Wilson, J. S. Famiglietti, J. L. Chen, and M. Rodell. Terrestrial
1795 water mass load changes from Gravity Recovery and Climate Experiment
1796 (GRACE). *Water Resour. Res.* , 42:5417–+, May 2006. doi: 10.1029/
1797 2005WR004255.
- 1798 [54] E. Rangelova, W. van der Wal, A. Braun, M. G. Sideris, and P. Wu. Analysis
1799 of Gravity Recovery and Climate Experiment time-variable mass redistribution
1800 signals over North America by means of principal component analysis. *J. Geophys.*
1801 *Res. (Earth Surface)*, 112:3002–+, July 2007. doi: 10.1029/2006JF000615.
- 1802 [55] R. Schmidt, S. Petrovic, A. Güntner, F. Barthelmes, J. Wunsch, and J. Kusche.
1803 Periodic components of water storage changes from GRACE and global hydrology
1804 models. *J. Geophys. Res. (Solid Earth)*, 113:8419–+, August 2008. doi: 10.1029/
1805 2007JB005363.
- 1806 [56] S. Swenson, P. J.-F. Yeh, J. Wahr, and J. Famiglietti. A comparison of terrestrial
1807 water storage variations from GRACE with in situ measurements from Illinois.
1808 *Geophys. Res. Lett.*, 33:16401–+, August 2006. doi: 10.1029/2006GL026962.
- 1809 [57] B. Creutzfeldt, A. Güntner, H. Thoss, B. Merz, and H. Wziontek. Measuring the
1810 effect of local water storage changes on in situ gravity observations: Case study
1811 of the Geodetic Observatory Wettzell, Germany. *Water Resources Research*, 46
1812 W08531, 2010. doi: 10.1029/2009WR008359.
- 1813 [58] M. Rodell, P. R. Houser, U. Jambor, J. Gottschalck, K. Mitchell, C.-J. Meng,
1814 K. Arsenault, B. Cosgrove, J. Radakovich, M. Bosilovich, J. K. Entin, J. P.
1815 Walker, D. Lohmann, and D. Toll. The Global Land Data Assimilation System.
1816 *Bulletin of the American Meteorological Society*, 85:381–394, March 2004. doi:
1817 10.1175/BAMS-85-3-381.
- 1818 [59] M. Rodell, J. Chen, H. Kato, J. S. Famiglietti, J. Nigro, and C. R. Wilson.
1819 Estimating groundwater storage changes in the Mississippi River basin (USA)
1820 using GRACE. *Hydrogeology Journal*, 15:159–166, February 2007. doi: 10.1007/
1821 s10040-006-0103-7.
- 1822 [60] S. Swenson, J. Famiglietti, J. Basara, and J. Wahr. Estimating profile soil
1823 moisture and groundwater variations using GRACE and Oklahoma Mesonet

- 1824 soil moisture data. *Water Resour. Res.* , 44:1413–+, January 2008. doi:
1825 10.1029/2007WR006057.
- 1826 [61] G. Strassberg, B. R. Scanlon, and M. Rodell. Comparison of seasonal terrestrial
1827 water storage variations from GRACE with groundwater-level measurements from
1828 the High Plains Aquifer (USA). *Geophys. Res. Lett.*, 34:14402–+, July 2007. doi:
1829 10.1029/2007GL030139.
- 1830 [62] J. L. Chen, C. R. Wilson, and B. D. Tapley. The 2009 exceptional Amazon flood
1831 and interannual terrestrial water storage change observed by GRACE. *Water*
1832 *Resour. Res.* , 46:12526–+, December 2010. doi: 10.1029/2010WR009383.
- 1833 [63] H. Wang, L. Jia, H. Steffen, P. Wu, L. Jiang, H. Hsu, L. Xiang, Z. Wang, and
1834 B. Hu. Increased water storage in North America and Scandinavia from GRACE
1835 gravity data. *Nature Geosci.*, 6:38–42, January 2013. doi: 10.1038/ngeo1652.
- 1836 [64] M.-H. Lo, J. S. Famiglietti, P. J.-F. Yeh, and T. H. Syed. Improving parameter
1837 estimation and water table depth simulation in a land surface model using GRACE
1838 water storage and estimated base flow data. *Water Resour. Res.* , 46:5517–+, May
1839 2010. doi: 10.1029/2009WR007855.
- 1840 [65] S. Werth and A. Güntner. Calibration analysis for water storage variability of the
1841 global hydrological model WGHM. *Hydrol. Earth. Syst. Sc.* , 14:59–78, January
1842 2010.
- 1843 [66] B. Li, M. Rodell, B. F. Zaitchik, R. H. Reichle, R. D. Koster, and T. M. van
1844 Dam. Assimilation of GRACE terrestrial water storage into a land surface model:
1845 Evaluation and potential value for drought monitoring in western and central
1846 Europe. *J. Hydrology*, 446:103–115, June 2012. doi: 10.1016/j.jhydrol.2012.04.035.
- 1847 [67] B. F. Zaitchik, M. Rodell, and R. H. Reichle. Assimilation of GRACE terrestrial
1848 water storage data into a land surface model: results for the Mississippi River
1849 Basin. *J. Hydrometeorology*, 9:535–548, June 2008. doi: 10.1175/2007JHM951.1.
- 1850 [68] G.-Y. Niu and Z.-L. Yang. Assessing a land surface model’s improvements
1851 with GRACE estimates. *Geophys. Res. Lett.*, 33:7401–+, April 2006. doi:
1852 10.1029/2005GL025555.
- 1853 [69] G.-Y. Niu, K.-W. Seo, Z.-L. Yang, C. Wilson, H. Su, J. Chen, and M. Rodell.
1854 Retrieving snow mass from GRACE terrestrial water storage change with a
1855 land surface model. *Geophys. Res. Lett.*, 34:15704–+, August 2007. doi:
1856 10.1029/2007GL030413.
- 1857 [70] R. Houborg, M. Rodell, B. Li, R. Reichle, and B. F. Zaitchik. Drought indicators
1858 based on model-assimilated Gravity Recovery and Climate Experiment (GRACE)
1859 terrestrial water storage observations. *Water Resour. Res.* , 48:W07525, July 2012.
1860 doi: 10.1029/2011WR011291.
- 1861 [71] A. Güntner. Improvement of global hydrological models using GRACE data.
1862 *Surveys in Geophysics*, 29(4-5):375–397, 2008. doi: 10.1007/s10712-008-9038-y.

- 1863 [72] P. Döll, H. Hoffmann-Dobrev, F. T. Portmann, S. Siebert, A. Eicker, M. Rodell,
1864 G. Strassberg, and B. R. Scanlon. Impact of water withdrawals from groundwater
1865 and surface water on continental water storage variations. *J. geodyn.*, 59:143–156,
1866 September 2012. doi: 10.1016/j.jog.2011.05.001.
- 1867 [73] H. Gao, Q. Tang, C. Ferguson, E. Wood, and D. Lettenmaier. Estimating the
1868 water budget of major US river basins via remote sensing. *Int. J. Remote Sens.*,
1869 31:3955–3978, April 2010. doi: 10.1080/01431161.2010.483488.
- 1870 [74] J. Huang, J. Halpenny, W. van der Wal, C. Klatt, T. S. James, and A. Rivera.
1871 Detectability of groundwater storage change within the Great Lakes Water
1872 Basin using GRACE. *J. Geophys. Res. (Solid Earth)*, 117:8401, 2012. doi:
1873 10.1029/2011JB008876.
- 1874 [75] S. Z. Yirdaw, K. R. Snelgrove, and C. O. Agboma. GRACE satellite observations
1875 of terrestrial moisture changes for drought characterization in the Canadian
1876 Prairie. *J. Hydrology*, 356:84–92, July 2008.
- 1877 [76] D. Alsdorf, S.-C. Han, P. Bates, and J. Melack. Seasonal water storage on the
1878 amazon floodplain measured from satellites. *Remote Sens. Environ.* , 114(11):
1879 2448–2456, 2010. ISSN0034-4257. doi: 10.1016/j.rse.2010.05.020.
- 1880 [77] J. L. Chen, C. R. Wilson, B. D. Tapley, L. Longuevergne, Z. L. Yang, and
1881 B. R. Scanlon. Recent La Plata basin drought conditions observed by satellite
1882 gravimetry. *J. Geophys. Res. (Atmospheres)*, 115:22108–+, November 2010. doi:
1883 10.1029/2010JD014689.
- 1884 [78] F. Frappart, F. Papa, A. Güntner, S. Werth, J. Santos da Silva, J. Tomasella,
1885 F. Seyler, C. Prigent, W. B. Rossow, S. Calmant, and M.-P. Bonnet. Satellite-
1886 based estimates of groundwater storage variations in large drainage basins with
1887 extensive floodplains. *Remote Sens. Environ.* , 115(6):1588–1594, 2011. doi:
1888 10.1016/j.rse.2011.02.003.
- 1889 [79] A. Pereira and M. C. Pacino. Annual and seasonal water storage changes detected
1890 from GRACE data in the La Plata Basin. *Phys. Earth Planet. In.* , 212:88–99,
1891 December 2012. doi: 10.1016/j.pepi.2012.09.005.
- 1892 [80] M. Ahmed, M. Sultan, J. Wahr, E. Yan, A. Milewski, W. Sauck, R. Becker, and
1893 B. Welton. Integration of GRACE (Gravity Recovery and Climate Experiment)
1894 data with traditional data sets for a better understanding of the time-dependent
1895 water partitioning in African watersheds. *Geology*, pages 479–482, 2011. doi:
1896 10.1130/G31812.1.
- 1897 [81] M. Becker, W. Llovel, A. Cazenave, A. Güntner, and J.-F. Crétaux. Recent
1898 hydrological behavior of the East African great lakes region inferred from GRACE,
1899 satellite altimetry and rainfall observations. *Comptes Rendus Geoscience*, 342:
1900 223–233, March 2010.
- 1901 [82] J. W. Crowley, J. X. Mitrovica, R. C. Bailey, M. E. Tamisiea, and J. L.
1902 Davis. Land water storage within the Congo Basin inferred from GRACE

- 1903 satellite gravity data. *Geophys. Res. Lett.*, 33:19402–+, October 2006. doi:
1904 10.1029/2006GL027070.
- 1905 [83] Hyongki Lee, R. Edward Beighley, Douglas Alsdorf, Hahn Chul Jung, C.K.
1906 Shum, Jianbin Duan, Junyi Guo, Dai Yamazaki, and Konstantinos Andreadis.
1907 Characterization of terrestrial water dynamics in the congo basin using {GRACE}
1908 and satellite radar altimetry. *Remote Sens. Environ.* , 115(12):3530 – 3538, 2011.
1909 ISSN 0034-4257. doi: 10.1016/j.rse.2011.08.015.
- 1910 [84] H. C. Winsemius, H. H. G. Savenije, N. C. van de Giesen, B. J. J. M. van den
1911 Hurk, E. A. Zapreeva, and R. Klees. Assessment of Gravity Recovery and Climate
1912 Experiment (GRACE) temporal signature over the upper Zambezi. *Water Resour.*
1913 *Res.* , 42:12201–+, December 2006. doi: 10.1029/2006WR005192.
- 1914 [85] F. Seitz, M. Schmidt, and C. K. Shum. Signals of extreme weather conditions in
1915 Central Europe in GRACE 4-D hydrological mass variations. *Earth Planet. Sc.*
1916 *Lett.* , 268:165–170, April 2008. doi: 10.1016/j.epsl.2008.01.001.
- 1917 [86] E. Forootan and J. Kusche. Separation of global time-variable gravity signals
1918 into maximally independent components. *J. Geodesy*, 86:477–497, July 2012. doi:
1919 10.1007/s00190-011-0532-5.
- 1920 [87] M. J. Leblanc, P. Tregoning, G. Ramillien, S. O. Tweed, and A. Fakes. Basin-
1921 scale, integrated observations of the early 21st century multiyear drought in
1922 southeast Australia. *Water Resour. Res.* , 45:4408–+, April 2009. doi: 10.1029/
1923 2008WR007333.
- 1924 [88] D. Rieser, M. Kuhn, R. Pail, I. M. Anjasmara, and J. Awange. Relation between
1925 GRACE-derived surface mass variations and precipitation over Australia. *Aust.*
1926 *J. Earth Sci.*, 57:887–900, October 2010. doi: 10.1080/08120099.2010.512645.
- 1927 [89] O. Andersen, P. Berry, J. Freeman, F. G. Lemoine, S. Luthcke, K. Jakobsen,
1928 and M. Butts. Satellite Altimetry and GRACE Gravimetry for Studies of Annual
1929 Water Storage Variations in Bangladesh. *Terr. Atmos. Ocean Sci.*, 19:47–52, 2008.
1930 doi: 10.3319/TAO.2008.19.1-2.47(SA).
- 1931 [90] J. P. Moiwo, Y. Yang, F. Tao, W. Lu, and S. Han. Water storage change in the
1932 Himalayas from the Gravity Recovery and Climate Experiment (GRACE) and
1933 an empirical climate model. *Water Resour. Res.* , 470:W07521, July 2011. doi:
1934 10.1029/2010WR010157.
- 1935 [91] M. Rodell, I. Velicogna, and J. S. Famiglietti. Satellite-based estimates of
1936 groundwater depletion in India. *Nature*, 460:999–1002, August 2009. doi:
1937 10.1038/nature08238.
- 1938 [92] V. M. Tiwari, J. Wahr, and S. Swenson. Dwindling groundwater resources in
1939 northern India, from satellite gravity observations. *Geophys. Res. Lett.*, 36:18401–
1940 +, September 2009. doi: 10.1029/2009GL039401.
- 1941 [93] K. Yamamoto, Y. Fukuda, T. Nakaegawa, and J. Nishijima. Landwater variation

- 1942 in four major river basins of the Indochina peninsula as revealed by GRACE.
 1943 *Earth Planets Space*, 59:193–200, 2007.
- 1944 [94] F. Frappart, G. Ramillien, and J. Famiglietti. Water balance of the Arctic drainage
 1945 system using GRACE gravimetry products. *Int. J. Remote Sens.*, 32:431–453,
 1946 January 2011. doi: 10.1080/01431160903474954.
- 1947 [95] F. W. Landerer, J. O. Dickey, and A. Güntner. Terrestrial water budget
 1948 of the Eurasian pan-Arctic from GRACE satellite measurements during 2003–
 1949 2009. *J. Geophys. Res. (Atmospheres)*, 115:23115–+, December 2010. doi:
 1950 10.1029/2010JD014584.
- 1951 [96] David García-García, Caroline C. Ummenhofer, and Victor Zlotnicki. Australian
 1952 water mass variations from grace data linked to indo-pacific climate variability.
 1953 *Remote Sens. Environ.* , 115(9):2175 – 2183, 2011. ISSN 0034-4257. doi:
 1954 10.1016/j.rse.2011.04.007.
- 1955 [97] W. Llovel, M. Becker, A. Cazenave, J.-F. Crétaux, and G. Ramillien. Global
 1956 land water storage change from GRACE over 2002–2009; Inference on sea level.
 1957 *Comptes Rendus Geoscience*, 342:179–188, March 2010.
- 1958 [98] Y. Morishita and K. Heki. Characteristic precipitation patterns of El Niño/La
 1959 Niña in time-variable gravity fields by GRACE. *Earth Planet. Sc. Lett.* , 272:
 1960 677–682, August 2008. doi: 10.1016/j.epsl.2008.06.003.
- 1961 [99] T. Phillips, R. S. Nerem, B. Fox-Kemper, J. S. Famiglietti, and B. Rajagopalan.
 1962 The influence of ENSO on global terrestrial water storage using GRACE. *Geophys.*
 1963 *Res. Lett.*, 39:L16705, August 2012. doi: 10.1029/2012GL052495.
- 1964 [100] T. van Dam, J. Wahr, and D. Lavallée. A comparison of annual vertical
 1965 crustal displacements from GPS and Gravity Recovery and Climate Experiment
 1966 (GRACE) over Europe. *J. Geophys. Res. (Solid Earth)*, 1112:B03404, March 2007.
 1967 doi: 10.1029/2006JB004335.
- 1968 [101] M. S. Steckler, S. L. Nooner, S. H. Akhter, S. K. Chowdhury, S. Bettadpur,
 1969 L. Seeber, and M. G. Kogan. Modeling Earth deformation from monsoonal
 1970 flooding in Bangladesh using hydrographic, GPS, and Gravity Recovery and
 1971 Climate Experiment (GRACE) data. *J. Geophys. Res. (Solid Earth)*, 115:8407–+,
 1972 August 2010. doi: 10.1029/2009JB007018.
- 1973 [102] J. Kusche and E. J. O. Schrama. Surface mass redistribution inversion from
 1974 global GPS deformation and Gravity Recovery and Climate Experiment (GRACE)
 1975 gravity data. *J. Geophys. Res. (Solid Earth)*, 110:9409–+, September 2005. doi:
 1976 10.1029/2004JB003556.
- 1977 [103] P. Tregoning, C. Watson, G. Ramillien, H. McQueen, and J. Zhang. Detecting
 1978 hydrologic deformation using GRACE and GPS. *Geophys. Res. Lett.*, 36:15401,
 1979 August 2009. doi: 10.1029/2009GL038718.
- 1980 [104] V. Tesmer, P. Steigenberger, T. van Dam, and T. Mayer-Gürr. Vertical

- 1981 deformations from homogeneously processed GRACE and global GPS long-term
1982 series. *J. Geodesy*, 85:291–310, May 2011. doi: 10.1007/s00190-010-0437-8.
- 1983 [105] P. Valty, O. de Viron, I. Panet, M. Van Camp, and J. Legrand. Assessing
1984 the precision in loading estimates by geodetic techniques in Southern Europe
1985 *Geophysical Journal International*, 194:1441–1454, 2013. doi: 10.1093/gji/ggt173.
- 1986 [106] P. Döll, K. Fiedler, and J. Zhang. Global-scale analysis of river flow alterations
1987 due to water withdrawals and reservoirs. *Hydrol. Earth. Syst. Sc. Discuss.*, 6:
1988 4773–4812, July 2009.
- 1989 [107] P. Döll and K. Fiedler. Global-scale modeling of groundwater recharge. *Hydrol.*
1990 *Earth. Syst. Sc.*, 12:863–885, May 2008.
- 1991 [108] I. Haddeland, T. Skaugen, and D. P. Lettenmaier. Anthropogenic impacts on
1992 continental surface water fluxes. *Geophys. Res. Lett.*, 33:L08406, April 2006. doi:
1993 10.1029/2006GL026047.
- 1994 [109] Y. Wada, L. P. H. van Beek, C. M. van Kempen, J. W. T. M. Reckman, S. Vasak,
1995 and M. F. P. Bierkens. Global depletion of groundwater resources. *Geophys. Res.*
1996 *Lett.*, 37:L20402, October 2010. doi: 10.1029/2010GL044571.
- 1997 [110] T. Jacob, J. Wahr, W. T. Pfeffer, and S. Swenson. Recent contributions of
1998 glaciers and ice caps to sea level rise. *Nature*, 482:514–518, February 2012. doi:
1999 10.1038/nature10847.
- 2000 [111] J. S. Famiglietti, M. Lo, S. L. Ho, J. Bethune, K. J. Anderson, T. H. Syed,
2001 S. C. Swenson, C. R. de Linage, and M. Rodell. Satellites measure recent rates
2002 of groundwater depletion in California’s Central Valley. *Geophys. Res. Lett.*, 38:
2003 3403–+, February 2011. doi: 10.1029/2010GL046442.
- 2004 [112] A.L. Berger. Support for the astronomical theory of climatic change. *Nature*, 269
2005 (5623):44–45, 1977.
- 2006 [113] G. H. Roe and M. R. Allen. A comparison of competing explanations for the
2007 100,000-yr ice age cycle. *Geophys. Res. Lett.*, 26:2259–2262, 1999.
- 2008 [114] Didier Paillard. Glacial cycles: Toward a new paradigm. *Rev. Geophys.*, 39(3):
2009 325–346, 2001. ISSN 1944-9208. doi: 10.1029/2000RG000091.
- 2010 [115] A. Celsius. Anmärkningar om vatnets förminskande så i östersjön som
2011 vesterhafvet. *Kungl. Vet. Akad. Handl.*, pages 33–50, 1743.
- 2012 [116] Charles Lyell. The bakerian lecture: On the proofs of a gradual rising of the
2013 land in certain parts of sweden. *Philos. T. Roy. Soc.*, 125:pp. 1–38, 1835. ISSN
2014 02610523.
- 2015 [117] W. E. Farrell and J. A. Clark. On postglacial sea level. 46:647–667, 1976.
- 2016 [118] R.S. Woodward. On the form of and position of mean sea level. *US Geol. Surv.*
2017 *Bull.*, 48:87–170, 1888.
- 2018 [119] Roblyn A. Kendall, Konstantin Latychev, Jerry X. Mitrovica, Jonathan E.
2019 Davis, and Mark E. Tamisiea. Decontaminating tide gauge records for the

- influence of glacial isostatic adjustment: The potential impact of 3-D Earth structure. *Geophys. Res. Lett.*, 33(24), DEC 30 2006. ISSN 0094-8276. doi: 10.1029/2006GL028448.
- [120] G. Spada, V. R. Barletta, V. Klemann, R. E. M. Riva, Z. Martinec, P. Gasperini, B. Lund, D. Wolf, L. L. A. Vermeersen, and M. A. King. A benchmark study for glacial isostatic adjustment codes. *Geophys. J. Int.*, 185(1):106–132, APR 2011. ISSN 0956-540X. doi: 10.1111/j.1365-246X.2011.04952.x.
- [121] A. M. Dziewonski and D. L. Anderson. Preliminary Reference Earth Model. *Phys. Earth Planet. Inter.*, 25:297–356, 1981.
- [122] Holger Steffen and Patrick Wu. Glacial isostatic adjustment in Fennoscandia-A review of data and modeling. *J. Geodyn.*, 52(3-4):169–204, OCT 2011. ISSN 0264-3707. doi: 10.1016/j.jog.2011.03.002.
- [123] N. A. Haskell. The motion of a viscous fluid under a surface load. *Physics*, 6: 265–369, 1935.
- [124] W. R. Peltier. The impulse response of a Maxwell earth. *Rev. Geophys. Space Phys.*, 12:649–669, 1974.
- [125] L. M. Cathles. *The Viscosity of the Earth's Mantle*. Princeton University Press, Princeton, 1975.
- [126] Patrick Wu and W. R. Peltier. Viscous gravitational relaxation. 70:435–485, 1982.
- [127] K. Lambeck, P. Johnston, and M. Nakada. Holocene glacial rebound and sea level change in NW Europe. *Geophys. J. Int.* 103:451–468, 1990.
- [128] J. X. Mitrovica and W. R. Peltier. Constraints on mantle viscosity from relative sea level variations in Hudson Bay. *Geophys. Res. Lett.*, 19:1185–1188, 1992.
- [129] L. L. A. Vermeersen, R. Sabadini, and G. Spada. Analytical visco-elastic relaxation models. *Geophys. Res. Lett.*, 23:697–700, 1996.
- [130] Glenn A. Milne and Jerry X. Mitrovica. Postglacial sea-level change on a rotating earth. *Geophys. J. Int.* 133:1–19, 1998.
- [131] J. Hagedoorn, D. Wolf, and Z. Martinec. An estimate of global sea level rise inferred from tide-gauge measurements using glacial-isostatic adjustment models consistent with the relative sea level record. *Pure Appl. Geophys.*, 164(4):791–818, 2007.
- [132] J. O. Dickey, S. L. Marcus, O. de Viron, and I. Fukumori. Recent Earth oblateness variations: Unraveling climate and postglacial rebound effects. *Science*, 298(5600): 1975–1977, 2002.
- [133] JX. Mitrovica, J. Wahr, I. Matsuyama, and A. Paulson. The rotational stability of an ice-age earth. *Geophys. J. Int.*, 161:491–506, 2005.
- [134] Z. Martinec and J. Hagedoorn. Time-domain approach to linearized rotational response of a three-dimensional viscoelastic earth model induced by glacial-isostatic adjustment: I. inertia-tensor perturbations. *Geophys. J. Int.*, 163:443–462, 2005.

- 2060 [135] R. Sabadini and L. L. A. Vermeersen. *Long-term rotation instabilities of the*
2061 *Earth: A Reanalysis*, volume 29. In: Ice Sheets, Sea Level and the Dynamic
2062 Earth, American Geophys. Union, 2002.
- 2063 [136] Paolo Gasperini and Roberto Sabadini. Lateral heterogeneities on mantle viscosity
2064 and post-glacial rebound. *Geophys. J. Int.*, 98:413–428, 1989.
- 2065 [137] S. J. Zhong, A. Paulson, and J. Wahr. Three-dimensional finite-element modelling
2066 of earth's viscoelastic deformation: effects of lateral variations in lithospheric
2067 thickness. *Geophys. J. Int.*, 155:679–695, 2005.
- 2068 [138] Jeroen Tromp and Jerry X. Mitrovica. Surface loading of a viscoelastic earth—II.
2069 spherical models. 137:856–872, 1999.
- 2070 [139] Z. Martinec. Propagator-matrix technique for the viscoelastic response of a multi-
2071 layered sphere to surface toroidal traction. *Pure Appl. Geophys.*, 164:663–681,
2072 2007.
- 2073 [140] Volker Klemann, Erik R. Ivins, Zdenek Martinec, and Detlef Wolf. Models of
2074 active glacial isostasy roofing warm subduction: Case of the South Patagonian Ice
2075 Field. *J. GEOPHYSICAL RESEARCH-SOLID EARTH*, 112(B9), SEP 25 2007.
2076 ISSN 0148-0227. doi: 10.1029/2006JB004818.
- 2077 [141] Volker Klemann, Zdeněk Martinec, and Erik R. Ivins. Glacial isostasy and plate
2078 motions. *J. Geodyn.*, 46:95–103, 2008. doi: 10.1016/j.jog.2008.04.005.
- 2079 [142] Geruo A, John Wahr, and Shijie Zhong. Computations of the viscoelastic
2080 response of a 3-d compressible earth to surface loading: an application to glacial
2081 isostatic adjustment in antarctica and canada. *Geophys. J. Int.*, 2012. doi:
2082 10.1093/gji/ggs030.
- 2083 [143] C Giunchi and G. Spada. Postglacial rebound in a non-newtonian spherical earth.
2084 *Geophys. Res. Lett.*, 27:2065–2068, 2000.
- 2085 [144] W. van der Wal, P. Wu, H. Wang, and M.G. Sideris. "sea levels and uplift rate
2086 from composite rheology in glacial isostatic adjustment modeling". *J. Geodyn.*,
2087 50(1):38–48, 2010.
- 2088 [145] Y. Tanaka, V. Klemann, Z. Martinec, and R. E. M. Riva. Spectral-finite element
2089 approach to viscoelastic relaxation in a spherical compressible Earth: application
2090 to GIA modelling. *Geophys. J. Int.*, 184:220–234, 2011. doi: 10.1111/j.1365-246X.
2091 2010.04854.x. pdf.
- 2092 [146] Matt A. King, Rory J. Bingham, Phil Moore, Pippa L. Whitehouse, Michael J.
2093 Bentley, and Glenn A. Milne. Lower satellite-gravimetry estimates of Antarctic
2094 sea-level contribution. *Nature*, 491(7425):586–589, November 2012. doi: 10.1038/
2095 nature11621.
- 2096 [147] Andrew Shepherd, Erik R. Ivins, Geruo A, Valentina R. Barletta, Mike J. Bentley,
2097 Srinivas Bettadpur, Kate H. Briggs, David H. Bromwich, René Forsberg, Natalia
2098 Galin, Martin Horwath, Stan Jacobs, Ian Joughin, Matt A. King, Jan T. M.
2099 Lenaerts, Jilu Li, Stefan R. M. Ligtenberg, Adrian Luckman, Scott B. Luthcke,

- 2100 Malcolm McMillan, Rakia Meister, Glenn Milne, Jeremie Mouginot, Alan Muir,
2101 Julien P. Nicolas, John Paden, Antony J. Payne, Hamish Pritchard, Eric Rignot,
2102 Helmut Rott, Louise Sandberg Sørensen, Ted A. Scambos, Bernd Scheuchl, Ernst
2103 J. O. Schrama, Ben Smith, Aud V. Sundal, Jan H. van Angelen, Willem J. van de
2104 Berg, Michiel R. van den Broeke, David G. Vaughan, Isabella Velicogna, John
2105 Wahr, Pippa L. Whitehouse, Duncan J. Wingham, Donghui Yi, Duncan Young,
2106 and H. Jay Zwally. A reconciled estimate of ice-sheet mass balance. *Science*, 338
2107 (6111):1183–1189, 2012. doi: 10.1126/science.1228102.
- 2108 [148] I. Velicogna and J. Wahr. Measurements of time-variable gravity show mass loss in
2109 Antarctica. *Science*, 311:1754–1756, March 2006. doi: 10.1126/Science.1123785.
- 2110 [149] I. D. Thomas, M. A. King, M. J. Bentley, P. L. Whitehouse, N. T. Penna,
2111 S. D. P. Williams, R. E. M. Riva, D. A. Lavallee, P. J. Clarke, E. C. King,
2112 R. C. A. Hindmarsh, and H. Koivula. Widespread low rates of Antarctic glacial
2113 isostatic adjustment revealed by GPS observations. *Geophys. Res. Lett.*, 38:
2114 L22302, November 2011. doi: 10.1029/2011GL049277.
- 2115 [150] P. L. Whitehouse, M. J. Bentley, G. A. Milne, M. A. King, and I. D. Thomas. A
2116 new glacial isostatic adjustment model for Antarctica: calibrated and tested using
2117 observations of relative sea-level change and present-day uplift rates. *Geophys. J.*
2118 *Int.*, 190:1464–1482, September 2012. doi: 10.1111/j.1365-246X.2012.05557.x.
- 2119 [151] I. Sasgen, H. Konrad, E. R. Ivins, M. R. Van den Broeke, J. L. Bamber,
2120 Z. Martinec, and V. Klemann. Antarctic ice-mass balance 2003 to 2012: regional
2121 reanalysis of GRACE satellite gravimetry measurements with improved estimate
2122 of glacial-isostatic adjustment based on GPS uplift rates. *The Cryosphere*, 7(5):
2123 1499–1512, 2013. doi: 10.5194/tc-7-1499-2013.
- 2124 [152] W. R. Peltier. Global glacial isostasy and the surface of the ice-age earth: the
2125 ICE5G (VM2) model and GRACE. *Ann. Rev. Earth Planet. Sci.*, 32:111–149,
2126 2004.
- 2127 [153] M. E. Tamisiea, J. X. Mitrovica, and J. L. Davis. GRACE gravity data constrain
2128 ancient ice geometries and continental dynamics over Laurentia. *Science*, 316
2129 (5826):881–883, May 11 2007. ISSN 0036-8075. doi: 10.1126/science.1137157.
- 2130 [154] W. van der Wal, P. Wu, M. G. Sideris, and C. K. Shum. Use of GRACE determined
2131 secular gravity rates for glacial isostatic adjustment studies in North-America. *J.*
2132 *Geodyn.*, 46(3-5):144–154, 2008.
- 2133 [155] I. Sasgen, V. Klemann, and Z. Martinec. Towards the inversion of GRACE gravity
2134 fields for present-day ice-mass changes and glacial-isostatic adjustment in North
2135 America and Greenland. *Journal of Geodynamics*, 59:49–63, 2012.
- 2136 [156] J. Wahr, H. DaZhong, and A. Trupin. Predictions of vertical uplift caused by
2137 changing polar ice volumes on a viscoelastic Earth. *Geophys. Res. Lett.*, 22(8):
2138 977–980, 1995.

- 2139 [157] S. Mazzotti, A. Lambert, J. Henton, T. S. James, and N. Courtier. Absolute
2140 gravity calibration of GPS velocities and glacial isostatic adjustment in mid-
2141 continent North America. *Geophys. Res. Lett.*, 38(24), 2011. doi: 10.1029/
2142 2011GL049846.
- 2143 [158] Archie Paulson, Shijie Zhong, and John Wahr. Inference of mantle viscosity from
2144 GRACE and relative sea level data. *Geophys. J. Int.*, 171(2):497–508, NOV 2007.
2145 ISSN 0956-540X. doi: 10.1111/j.1365-246X.2007.03556.x.
- 2146 [159] J. L. Davis and members of BIFROST. GPS measurements to constrain
2147 geodynamic processes in Fennoscandia. *EOS*, 77:337–341, 1996.
- 2148 [160] H. G. Scherneck, J. M. Johansson, H. Koivula, T. van Dam, and J. L. Davis.
2149 Vertical crustal motion observed in the BIFROST project. *J. Geodyn.*, 35:425–
2150 441, 2003.
- 2151 [161] Holger Steffen, Patrick Wu, and Hansheng Wang. Determination of the Earth’s
2152 structure in Fennoscandia from GRACE and implications for the optimal post-
2153 processing of GRACE data. *Geophys. J. Int.*, 182(3):1295–1310, SEP 2010. ISSN
2154 0956-540X. doi: 10.1111/j.1365-246X.2010.04718.x.
- 2155 [162] E. M. Hill, J. L. Davis, M. E. Tamisiea, and M. Lidberg. Combination
2156 of geodetic observations and models for glacial isostatic adjustment fields in
2157 fennoscandia. *J. Geophys. Res.*, 115(B7):n/a–n/a, 2010. ISSN 2156-2202. doi:
2158 10.1029/2009JB006967.
- 2159 [163] V. Mikhailov, S. Tikhotsky, M. Diament, I. Panet, and V. Ballu. Can tectonic
2160 processes be recovered from new gravity satellite data? *Earth and Planetary
2161 Science Letters*, 228(34):281 – 297, 2004. doi: 10.1016/j.epsl.2004.09.035.
- 2162 [164] O. De Viron, I. Panet, V. Mikhailov, M. Van Camp, and M. Diament. Retrieving
2163 earthquake signature in grace gravity solutions. *Geophysical Journal International*,
2164 174(1):14–20+, 2008. doi: 10.1111/j.1365-246X.2008.03807.x.
- 2165 [165] A. Nur and J. R. Booker. Aftershocks Caused by Pore Fluid Flow? *Science*, 175:
2166 885–887, February 1972. doi: 10.1126/science.175.4024.885.
- 2167 [166] G. Peltzer, P. Rosen, F. Rogez, and K. Hudnut. Poroelastic rebound along the
2168 Landers 1992 earthquake surface rupture. *J. Geophys. Res.*, 103:30131, December
2169 1998. doi: 10.1029/98JB02302.
- 2170 [167] A. Nur and G. Mavko. Postseismic Viscoelastic Rebound. *Science*, 183:204–206,
2171 January 1974. doi: 10.1126/science.183.4121.204.
- 2172 [168] Roland Bürgmann and Georg Dresen. Rheology of the Lower Crust and Upper
2173 Mantle: Evidence from Rock Mechanics, Geodesy, and Field Observations. *Annu.
2174 Rev. Earth Pl. Sc.*, 36(1):531–567, 2008. doi: 10.1146/annurev.earth.36.031207.
2175 124326.
- 2176 [169] S.-C. Han, C. K. Shum, M. Bevis, C. Ji, and C.-Y. Kuo. Crustal dilatation
2177 observed by GRACE after the 2004 Sumatra-Andaman earthquake. *Science*, 313:
2178 658–662, August 2006. doi: 10.1126/science.1128661.

- 2179 [170] Y. Okada. Surface Deformation Due to Shear and Tensile Faults in a Half-Space.
2180 *Bull. Seis. Soc. Amer.*, 75(4):1135–1154, 1985.
- 2181 [171] Fred F. Pollitz. Coseismic Deformation From Earthquake Faulting On A Layered
2182 Spherical Earth. *Geophys. J. Int.*, 125(1):1–14, 1996. ISSN 1365-246X. doi:
2183 10.1111/j.1365-246X.1996.tb06530.x.
- 2184 [172] S.-C. Han, R. Riva, J. Sauber, and E. Okal. Source parameter inversion for
2185 recent great earthquakes from a decade-long observation of global gravity fields.
2186 *J. Geophys. Res. (Solid Earth)*, 118(3):1240–1267, 2013. ISSN 2169-9356. doi:
2187 10.1002/jgrb.50116.
- 2188 [173] G. Cambiotti, A. Bordonì, R. Sabadini, and L. Colli. GRACE gravity data help
2189 constraining seismic models of the 2004 Sumatran earthquake. *J. Geophys. Res.*
2190 *(Solid Earth)*, 116:B10403, October 2011. doi: 10.1029/2010JB007848.
- 2191 [174] D. B. T. Broerse, L. L. A. Vermeersen, R. E. M. Riva, and W. van der Wal. Ocean
2192 contribution to co-seismic crustal deformation and geoid anomalies: Application
2193 to the 2004 December 26 Sumatra–Andaman earthquake. *Earth Planet. Sc. Lett.*
2194 , 305:341–349, May 2011. doi: 10.1016/j.epsl.2011.03.011.
- 2195 [175] R. Ogawa and K. Heki. Slow postseismic recovery of geoid depression formed by
2196 the 2004 Sumatra-Andaman Earthquake by mantle water diffusion. *Geophys. Res.*
2197 *Lett.*, 34:6313–+, March 2007. doi: 10.1029/2007GL029340.
- 2198 [176] J. L. Chen, C. R. Wilson, B. D. Tapley, and S. Grand. GRACE detects coseismic
2199 and postseismic deformation from the Sumatra-Andaman earthquake. *Geophys.*
2200 *Res. Lett.*, 34:13302–+, July 2007. doi: 10.1029/2007GL030356.
- 2201 [177] I. Panet, V. Mikhailov, M. Diament, F. Pollitz, G. King, O. de Viron,
2202 M. Holschneider, R. Biancale, and J.-M. Lemoine. Coseismic and post-seismic
2203 signatures of the Sumatra 2004 December and 2005 March earthquakes in
2204 GRACE satellite gravity. *Geophys. J. Int.*, 171:177–190, October 2007. doi:
2205 10.1111/j.1365-246X.2007.03525.x.
- 2206 [178] S.-C. Han, J. Sauber, and S. Luthcke. Regional gravity decrease after the 2010
2207 Maule (Chile) earthquake indicates large-scale mass redistribution. *Geophys. Res.*
2208 *Lett.*, 37:23307–+, December 2010. doi: 10.1029/2010GL045449.
- 2209 [179] K. Heki and K. Matsuo. Coseismic gravity changes of the 2010 earthquake
2210 in central Chile from satellite gravimetry. *Geophys. Res. Lett.*, 37:24306–+,
2211 December 2010. doi: 10.1029/2010GL045335.
- 2212 [180] K. Matsuo and K. Heki. Coseismic gravity changes of the 2011 Tohoku-Oki
2213 earthquake from satellite gravimetry. *Geophys. Res. Lett.*, 38:L00G12, September
2214 2011. doi: 10.1029/2011GL049018.
- 2215 [181] S.-C. Han, J. Sauber, and R. Riva. Contribution of satellite gravimetry to
2216 understanding seismic source processes of the 2011 Tohoku-Oki earthquake.
2217 *Geophys. Res. Lett.*, 38:L24312, December 2011. doi: 10.1029/2011GL049975.

- 2218 [182] R. S. Stein. The role of stress transfer in earthquake occurrence. *Nature*, 402:
2219 605–609, December 1999. doi: 10.1038/45144.
- 2220 [183] S.-C. Han and F. J. Simons. Spatiospectral localization of global geopotential
2221 fields from the Gravity Recovery and Climate Experiment (GRACE) reveals
2222 the coseismic gravity change owing to the 2004 Sumatra-Andaman earthquake.
2223 *J. Geophys. Res. (Solid Earth)*, 113:1405–+, January 2008. doi: 10.1029/
2224 2007JB004927.
- 2225 [184] X. Zhou, W. Sun, B. Zhao, G. Fu, J. Dong, and Z. Nie. Geodetic observations
2226 detecting coseismic displacements and gravity changes caused by the Mw = 9.0
2227 Tohoku-Oki earthquake. *J. Geophys. Res. (Solid Earth)*, 117:B05408, May 2012.
2228 doi: 10.1029/2011JB008849.
- 2229 [185] G. Cambiotti and R. Sabadini. Gravitational seismology retrieving Centroid-
2230 Moment-Tensor solution of the 2011 Tohoku earthquake. *J. Geophys. Res. (Solid
2231 Earth)*, 118:183–194, January 2013. doi: 10.1029/2012JB009555.
- 2232 [186] L. Wang, C. K. Shum, F. J. Simons, A. Tassara, K. Erkan, C. Jekeli, A. Braun,
2233 C. Kuo, H. Lee, and D.-N. Yuan. Coseismic slip of the 2010 Mw 8.8 Great Maule,
2234 Chile, earthquake quantified by the inversion of GRACE observations. *Earth
2235 Planet. Sc. Lett.*, 335:167–179, June 2012. doi: 10.1016/j.epsl.2012.04.044.
- 2236 [187] L. Wang, C. K. Shum, F. J. Simons, B. Tapley, and C. Dai. Coseismic
2237 and postseismic deformation of the 2011 Tohoku-Oki earthquake constrained
2238 by GRACE gravimetry. *Geophys. Res. Lett.*, 39:L07301, April 2012. doi:
2239 10.1029/2012GL051104.
- 2240 [188] G. Cambiotti and R. Sabadini. A source model for the great 2011 Tohoku
2241 earthquake ($M_w=9.1$) from inversion of GRACE gravity data. *Earth Planet. Sc.
2242 Lett.*, 335:72–79, June 2012. doi: 10.1016/j.epsl.2012.05.002.
- 2243 [189] V. C. Tsai, M. Nettles, G. Ekström, and A. M. Dziewonski. Multiple CMT
2244 source analysis of the 2004 Sumatra earthquake. *Geophys. Res. Lett.*, 32:L17304,
2245 September 2005. doi: 10.1029/2005GL023813.
- 2246 [190] E. A. Okal and S. Stein. Observations of ultra-long period normal modes from the
2247 2004 Sumatra-Andaman earthquake. *Phys. Earth Planet. In.*, 175:53–62, June
2248 2009. doi: 10.1016/j.pepi.2009.03.002.
- 2249 [191] M. Hirschmann and D. Kohlstedt. Water in Earth’s mantle. *Phys. Today*, 65(3):
2250 030000, 2012. doi: 10.1063/PT.3.1476.
- 2251 [192] I. Panet, F. Pollitz, V. Mikhailov, M. Diament, P. Banerjee, and K. Grijalva.
2252 Upper mantle rheology from GRACE and GPS postseismic deformation after the
2253 2004 Sumatra-Andaman earthquake. *Geochem. Geophys. Geosy.*, 11:6008–+, June
2254 2010. doi: 10.1029/2009GC002905.
- 2255 [193] A. Hoechner, S. V. Sobolev, I. Einarsson, and R. Wang. Investigation on afterslip
2256 and steady state and transient rheology based on postseismic deformation and

- 2257 geoid change caused by the Sumatra 2004 earthquake. *Geochem. Geophys. Geosy.*,
2258 12:Q07010, July 2011. doi: 10.1029/2010GC003450.
- 2259 [194] F. F. Pollitz, R. Bürgmann, and P. Banerjee. Post-seismic relaxation following
2260 the great 2004 Sumatra-Andaman earthquake on a compressible self-gravitating
2261 Earth. *Geophys. J. Int.*, 167:397–420, October 2006. doi: 10.1111/j.1365-246X.
2262 2006.03018.x.
- 2263 [195] M. Hashimoto, N. Choosakul, M. Hashizume, S. Takemoto, H. Takiguchi,
2264 Y. Fukuda, and K. Fujimori. Crustal deformations associated with the great
2265 Sumatra-Andaman earthquake deduced from continuous GPS observation. *Earth
2266 Planets Space*, 58:127–139, February 2006.
- 2267 [196] W. Thatcher. Nonlinear strain buildup and the earthquake cycle on the San
2268 Andreas Fault. *J. Geophys. Res.*, 88:5893–5902, July 1983. doi: 10.1029/
2269 JB088iB07p05893.
- 2270 [197] M. van den Broeke, J. Bamber, J. Ettema, E. Rignot, E. Schrama, W.J. van
2271 de Berg, E. van Meijgaard, I. Velicogna, and B. Wouters. Partitioning Recent
2272 Greenland Mass Loss. *Science*, 326(5955):984–986, 2009. doi: 10.1126/science.
2273 1178176.
- 2274 [198] R. Thomas, C. Davis, E. Frederick, W. Krabill, Y. Li, S. Manizade, and C. Martin.
2275 A comparison of Greenland ice-sheet volume changes derived from altimetry
2276 measurements. *J. Glaciol.*, 54(185):203–212, March 2008. ISSN 0022-1430. doi:
2277 10.3189/002214308784886225.
- 2278 [199] E. Rignot and P. Kanagaratnam. Changes in the velocity structure of the
2279 Greenland ice sheet. *Science*, 311:986–990, February 2006. doi: 10.1126/science.
2280 1121381.
- 2281 [200] Andrew Shepherd and Duncan Wingham. Recent Sea-Level Contributions of the
2282 Antarctic and Greenland Ice Sheets. *Science*, 315(5818):1529–1532, 2007. doi:
2283 10.1126/science.1136776.
- 2284 [201] I. Velicogna and J. Wahr. Acceleration of Greenland ice mass loss in spring 2004.
2285 *Nature*, 443:329–331, September 2006. doi: 10.1038/nature05168.
- 2286 [202] B. Wouters, D. Chambers, and E.J.O. Schrama. GRACE observes small-scale
2287 mass loss in Greenland. *Geophys. Res. Lett.*, 35:L20501, October 2008. doi:
2288 10.1029/2008GL034816.
- 2289 [203] Ingo Sasgen, Michiel van den Broeke, Jonathan L. Bamber, Eric Rignot, Louise S.
2290 Sørensen, Bert Wouters, Zdeněk Martinec, Isabella Velicogna, and Sebastian B.
2291 Simonsen. Timing and origin of recent regional ice-mass loss in Greenland.
2292 *Earth Planet. Sc. Lett.*, 333-334:293–303, June 2012. ISSN 0012821X. doi:
2293 10.1016/j.epsl.2012.03.033.
- 2294 [204] Ch. Harig and F. J. Simons. Mapping Greenland’s mass loss in space and time.
2295 *PNAS*, 109:19934–19937, December 2012. doi: 10.1073/pnas.1206785109.

- 2296 [205] J. Bonin and D. Chambers. Uncertainty estimates of a GRACE inversion
2297 modelling technique over Greenland using a simulation. *Geophysical Journal*
2298 *International*, 2013. doi: 10.1093/gji/ggt091.
- 2299 [206] S. A. Khan, J. Wahr, M. Bevis, I. Velicogna, and E. Kendrick. Spread of ice mass
2300 loss into northwest Greenland observed by GRACE and GPS. *Geophys. Res. Lett.*,
2301 37:6501–+, March 2010. doi: 10.1029/2010GL042460.
- 2302 [207] M. Tedesco, X. Fettweis, T. Mote, J. Wahr, P. Alexander, J. E. Box, and
2303 B. Wouters. Evidence and analysis of 2012 Greenland records from spaceborne
2304 observations, a regional climate model and reanalysis data. *The Cryosphere*, 7(2):
2305 615–630, 2013. doi: 10.5194/tc-7-615-2013.
- 2306 [208] J. L. Chen, C. R. Wilson, D. D. Blankenship, and B. D. Tapley. Antarctic
2307 mass rates from GRACE. *Geophys. Res. Lett.*, 33:11502–+, June 2006. doi:
2308 10.1029/2006GL026369.
- 2309 [209] Brian Gunter, T. Urban, R. Riva, M. Helsen, R. Harpold, S. Poole, P. Nagel,
2310 B. Schutz, and B. Tapley. A comparison of coincident GRACE and ICESat
2311 data over Antarctica. *J. Geodesy*, 83(11):1051–1060, 2009. doi: 10.1007/
2312 s00190-009-0323-4.
- 2313 [210] M. Horwath, B. Legrésy, F. Rémy, F. Blarel, and J.-M. Lemoine. Consistent
2314 patterns of Antarctic ice sheet interannual variations from ENVISAT radar
2315 altimetry and GRACE satellite gravimetry. *Geophys. J. Int.*, 189:863–876, May
2316 2012. doi: 10.1111/j.1365-246X.2012.05401.x.
- 2317 [211] J. L. Chen, C. R. Wilson, B. D. Tapley, and D. Blankenship. Antarctic
2318 regional ice loss rates from GRACE. *Earth Planet. Sc. Lett.* , 2007. doi:
2319 10.1016/j.epsl.2007.10.057. in press.
- 2320 [212] M. Horwath and R. Dietrich. Signal and error in mass change inferences from
2321 GRACE: the case of Antarctica. *Geophys. J. Int.*, 177:849–864, June 2009. doi:
2322 10.1111/j.1365-246X.2009.04139.x.
- 2323 [213] I. Sasgen, H. Dobsław, Z. Martinec, and M. Thomas. Satellite gravimetry
2324 observation of Antarctic snow accumulation related to ENSO. *Earth and Planetary*
2325 *Science Letters*, 299:352–358, 2010. doi: 10.1016/j.epsl.2010.09.015.
- 2326 [214] J. L. Chen, C. R. Wilson, D. Blankenship, and B. D. Tapley. Accelerated Antarctic
2327 ice loss from satellite gravity measurements. *Nature Geosci.*, 2:859–862, December
2328 2009. doi: 10.1038/ngeo694.
- 2329 [215] C. Boening, M. Lebsock, F. Landerer, and G. Stephens. Snowfall-driven mass
2330 change on the East Antarctic ice sheet. *Geophys. Res. Lett.*, 39:L21501, November
2331 2012. doi: 10.1029/2012GL053316.
- 2332 [216] R. E. M. Riva, B. C. Gunter, T. J. Urban, B. L. A. Vermeersen, R. C. Lindenbergh,
2333 M. M. Helsen, J. L. Bamber, R. S. W. van de Wal, M. R. van den Broeke, and
2334 B. E. Schutz. Glacial Isostatic Adjustment over Antarctica from combined ICESat

- 2335 and GRACE satellite data. *Earth Planet. Sc. Lett.* , 288:516–523, November 2009.
2336 doi: 10.1016/j.epsl.2009.10.013.
- 2337 [217] I. Velicogna and J. Wahr. A method for separating Antarctic postglacial rebound
2338 and ice mass balance using future ICESat Geoscience Laser Altimeter System,
2339 Gravity Recovery and Climate Experiment, and GPS satellite data. *J. Geophys.*
2340 *Res. (Solid Earth)*, 107, October 2002. doi: 10.1029/2001JB000708.
- 2341 [218] E. R. Ivins and T. S. James. Antarctic glacial isostatic adjustment: a
2342 new assessment. *Antarct. Sci.*, 17(04):541–553, 2005. doi: 10.1017/
2343 S0954102005002968.
- 2344 [219] J. Ettema, M. R. van den Broeke, E. van Meijgaard, W. J. van de Berg, J. L.
2345 Bamber, J. E. Box, and R. C. Bales. Higher surface mass balance of the Greenland
2346 ice sheet revealed by high-resolution climate modeling. *Geophys. Res. Lett.*, 36:
2347 L12501, June 2009. doi: 10.1029/2009GL038110.
- 2348 [220] J. T. M. Lenaerts, M. R. van den Broeke, W. J. van de Berg, E. van Meijgaard,
2349 and P. Kuipers Munneke. A new, high-resolution surface mass balance map of
2350 Antarctica (1979-2010) based on regional atmospheric climate modeling. *Geophys.*
2351 *Res. Lett.*, 39:L04501, February 2012. doi: 10.1029/2011GL050713.
- 2352 [221] Andrew Shepherd, Erik R. Ivins, Geruo, Valentina R. Barletta, Mike J. Bentley,
2353 Srinivas Bettadpur, Kate H. Briggs, David H. Bromwich, René Forsberg, Natalia
2354 Galin, Martin Horwath, Stan Jacobs, Ian Joughin, Matt A. King, Jan T. M.
2355 Lenaerts, Jilu Li, Stefan R. M. Ligtenberg, Adrian Luckman, Scott B. Luthcke,
2356 Malcolm McMillan, Rakia Meister, Glenn Milne, Jeremie Mougnot, Alan Muir,
2357 Julien P. Nicolas, John Paden, Antony J. Payne, Hamish Pritchard, Eric Rignot,
2358 Helmut Rott, Louise S. Sørensen, Ted A. Scambos, Bernd Scheuchl, Ernst J. O.
2359 Schrama, Ben Smith, Aud V. Sundal, Jan H. van Angelen, Willem J. van de Berg,
2360 Michiel R. van den Broeke, David G. Vaughan, Isabella Velicogna, John Wahr,
2361 Pippa L. Whitehouse, Duncan J. Wingham, Donghui Yi, Duncan Young, and
2362 H. Jay Zwally. A Reconciled Estimate of Ice-Sheet Mass Balance. *Science*, 338
2363 (6111):1183–1189, November 2012. ISSN 1095-9203. doi: 10.1126/science.1228102.
- 2364 [222] B. Wouters, J. L. Bamber, M. R. van den Broeke, J. T. M. Lenaerts, and I. Sasgen.
2365 Limits in detecting acceleration of ice sheet mass loss due to climate variability.
2366 *Nature Geoscience*, 6:613–616, 2013. doi: 10.1038/ngeo1874.
- 2367 [223] I. Velicogna. Increasing rates of ice mass loss from the Greenland and Antarctic
2368 ice sheets revealed by GRACE. *Geophys. Res. Lett.*, 36:L19503, October 2009.
2369 doi: 10.1029/2009GL040222.
- 2370 [224] E. Rignot, I. Velicogna, M. R. van den Broeke, A. Monaghan, and J. Lenaerts.
2371 Acceleration of the contribution of the Greenland and Antarctic ice sheets to
2372 sea level rise. *Geophys. Res. Lett.*, 38:L05503, March 2011. doi: 10.1029/
2373 2011GL046583.
- 2374 [225] P. L. Svendsen, O. B. Andersen, and A. A. Nielsen. Acceleration of the Greenland

- ice sheet mass loss as observed by GRACE: Confidence and sensitivity. *Earth and Planetary Science Letters*, 364:24–29, 2013. doi: 10.1016/j.epsl.2012.12.010.
- [226] Roger J. Braithwaite. After six decades of monitoring glacier mass balance we still need data but it should be richer data. *Ann. Glaciol.*, 50(1):191–197. ISSN 0260-3055. doi: 10.3189/172756409787769573.
- [227] Anthony A. Arendt, Keith A. Echelmeyer, William D. Harrison, Craig S. Lingle, and Virginia B. Valentine. Rapid Wastage of Alaska Glaciers and Their Contribution to Rising Sea Level. *Science*, 297(5580):382–386, 2002. doi: 10.1126/science.1072497.
- [228] M. E. Tamisiea, E. W. Leuliette, J. L. Davis, and J. X. Mitrovica. Constraining hydrological and cryospheric mass flux in southeastern Alaska using space-based gravity measurements. *Geophys. Res. Lett.*, 32:20501–+, October 2005. doi: 10.1029/2005GL023961.
- [229] J. L. Chen, B. D. Tapley, and C. R. Wilson. Alaskan mountain glacial melting observed by satellite gravimetry. *Earth Planet. Sc. Lett.*, 248:368–378, August 2006. doi: 10.1016/j.epsl.2006.05.039.
- [230] S. B. Luthcke, A. A. Arendt, D. D. Rowlands, J. J. McCarthy, and C. F. Larsen. Recent glacier mass changes in the Gulf of Alaska region from GRACE mascon solutions. *J. Glaciol.*, 54:767–777, 2008. doi: 10.3189/002214308787779933.
- [231] A. Arendt, S. Luthcke, A. Gardner, S. O’Neel, D. Hill, G. Moholdt, and W. Abdalati. Analysis of a GRACE global mascon solution for Gulf of Alaska glaciers. *Journal of Glaciology*, 59:913–924, 2013. doi: 10.3189/2013JoG12J197.
- [232] Alex S. Gardner, Geir Moholdt, J. Graham Cogley, Bert Wouters, Anthony A. Arendt, John Wahr, Etienne Berthier, Regine Hock, W. Tad Pfeffer, Georg Kaser, Stefan R. M. Ligtenberg, Tobias Bolch, Martin J. Sharp, Jon Ove Hagen, Michiel R. van den Broeke, and Frank Paul. A Reconciled Estimate of Glacier Contributions to Sea Level Rise: 2003 to 2009. *Science*, 340(6134):852–857, 2013. doi: 10.1126/science.1234532.
- [233] A. S. Gardner, G. Moholdt, B. Wouters, G. J. Wolken, D. O. Burgess, M. J. Sharp, J. G. Cogley, C. Braun, and C. Labine. Sharply increased mass loss from glaciers and ice caps in the Canadian Arctic Archipelago. *Nature*, 473:357–360, May 2011. doi: 10.1038/nature10089.
- [234] A. S. Gardner, G. Moholdt, A. Arendt, and B. Wouters. Long-term contributions of Baffin and Bylot Island Glaciers to sea level rise: an integrated approach using airborne and satellite laser altimetry, stereoscopic imagery and satellite gravimetry. *The Cryosphere Discuss.*, 6:1563–1610, April 2012. doi: 10.5194/tcd-6-1563-2012.
- [235] Jan T. M. Lenaerts, Jan H. van Angelen, Michiel R. van den Broeke, Alex S. Gardner, Bert Wouters, and Erik van Meijgaard. Irreversible mass loss of

- 2414 Canadian Arctic Archipelago glaciers. *Geophys. Res. Lett.*, 40(5):870–874, 2013.
2415 ISSN 1944-8007. doi: 10.1002/grl.50214.
- 2416 [236] M. B. Dyurgerov. Reanalysis of Glacier Changes: From the IGY to the IPY,
2417 1960–2008. *Data of Glaciological Studies*, 108:1–116, 2010.
- 2418 [237] G. Moholdt, B. Wouters, and A. S. Gardner. Recent mass changes of glaciers
2419 in the Russian High Arctic. *Geophys. Res. Lett.*, 39:L10502, May 2012. doi:
2420 10.1029/2012GL051466.
- 2421 [238] E. Rignot, A. Rivera, and G. Casassa. Contribution of the Patagonia icefields of
2422 South America to sea level rise. *Science*, 302:434–437, October 2003.
- 2423 [239] J. L. Chen, C. R. Wilson, B. D. Tapley, D. D. Blankenship, and E. R.
2424 Ivins. Patagonia Icefield melting observed by Gravity Recovery and Climate
2425 Experiment (GRACE). *Geophys. Res. Lett.*, 34:22501–+, November 2007. doi:
2426 10.1029/2007GL031871.
- 2427 [240] M. J. Willis, A. K. Melkonian, M. E. Pritchard, and A. Rivera. Ice loss from the
2428 Southern Patagonian Ice Field, South America, between 2000 and 2012. *Geophys.
2429 Res. Lett.*, 39:L17501, September 2012. doi: 10.1029/2012GL053136.
- 2430 [241] Erik R. Ivins, Michael M. Watkins, Dah-Ning Yuan, Reinhard Dietrich, Gino
2431 Casassa, and Axel Rülke. On-land ice loss and glacial isostatic adjustment at the
2432 Drake Passage: 2003–2009. *J. Geophys. Res. (Solid Earth)*, 116(B2), 2011. ISSN
2433 2156-2202. doi: 10.1029/2010JB007607.
- 2434 [242] K. Matsuo and K. Heki. Time-variable ice loss in Asian high mountains from
2435 satellite gravimetry. *Earth Planet. Sc. Lett.*, 290:30–36, February 2010. doi:
2436 10.1016/j.epsl.2009.11.053.
- 2437 [243] C. Wunsch and E. M. Gaposchkin. On Using Satellite Altimetry to Determine
2438 the General Circulation of the Oceans With Application to Geoid Improvement
2439 (Paper 80R0631). *Rev. Geophys. and Space Phys.*, 18:725, November 1980. doi:
2440 10.1029/RG018i004p00725.
- 2441 [244] D. Stammer and C. Wunsch. Preliminary assessment of the accuracy and precision
2442 of TOPEX/POSEIDON altimeter data with respect to the large-scale ocean
2443 circulation. *J. Geophys. Res.*, 99:24584, December 1994. doi: 10.1029/94JC00919.
- 2444 [245] B. D. Tapley, D. P. Chambers, C. K. Shum, R. J. Eanes, J. C. Ries, and R. H.
2445 Stewart. Accuracy assessment of the large-scale dynamic ocean topography from
2446 TOPEX/POSEIDON altimetry. *J. Geophys. Res.*, 99:24605, December 1994. doi:
2447 10.1029/94JC01827.
- 2448 [246] F. G. Lemoine, S. C. Kenyon, J. K. Factor, R.G. Trimmer, N. K. Pavlis, D. S.
2449 Chinn, C. M. Cox, S. M. Klosko, S. B. Luthcke, M. H. Torrence, Y. M. Wang,
2450 R. G. Williamson, E. C. Pavlis, R. H. Rapp, and T. R. Olson. The Development of
2451 the Joint NASA GSFC and the NIMA Geopotential Model EGM96. NASA/TP-
2452 1998-206861, July 1998.

- 2453 [247] B. D. Tapley, D. P. Chambers, S. Bettadpur, and J. C. Ries. Large scale
2454 ocean circulation from the GRACE GGM01 Geoid. *Geophys. Res. Lett.*, 30:2163,
2455 November 2003. doi: 10.1029/2003GL018622.
- 2456 [248] R. J. Bingham, P. Knudsen, O. Andersen, and R. Pail. An initial estimate of the
2457 North Atlantic steady-state geostrophic circulation from GOCE. *Geophys. Res.*
2458 *Lett.*, 38:L01606, January 2011. doi: 10.1029/2010GL045633.
- 2459 [249] P. Knudsen, R. Bingham, O. Andersen, and M.-H. Rio. A global mean dynamic
2460 topography and ocean circulation estimation using a preliminary GOCE gravity
2461 model. *J. Geodesy*, 85:861–879, November 2011. doi: 10.1007/s00190-011-0485-8.
- 2462 [250] N. K. Pavlis, S. A. Holmes, S. C. Kenyon, and J. K. Factor. The development and
2463 evaluation of the Earth Gravitational Model 2008 (EGM2008). *J. Geophys. Res.*
2464 *(Solid Earth)*, 117:B04406, April 2012. doi: 10.1029/2011JB008916.
- 2465 [251] T. Kanzow, F. Flechtner, A. Chave, R. Schmidt, P. Schwintzer, and U. Send.
2466 Seasonal variation of ocean bottom pressure derived from Gravity Recovery and
2467 Climate Experiment (GRACE): Local validation and global patterns. *J. Geophys.*
2468 *Res. (Oceans)*, 110:C9001, September 2005. doi: 10.1029/2004JC002772.
- 2469 [252] D.P. Chambers, J. Wahr, and R.S. Nerem. Preliminary observations of global
2470 ocean mass variations with GRACE. *Geophys. Res. Lett.*, 31:L13310, 2004. doi:
2471 10.1029/2004GL020461.
- 2472 [253] R. M. Ponte. Oceanic Response to Surface Loading Effects Neglected in Volume-
2473 Conserving Models. *J. Phys. Oceanogr.*, 36:426–434, June 2006. doi: 10.1175/
2474 JPO2843.1.
- 2475 [254] K. Lorbacher, S. J. Marsland, J. A. Church, S. M. Griffies, and D. Stammer.
2476 Rapid barotropic sea level rise from ice sheet melting. *J. Geophys. Res. (Oceans)*,
2477 117:C06003, June 2012. doi: 10.1029/2011JC007733.
- 2478 [255] W. R. Peltier. Closure of the budget of global sea level rise over the GRACE
2479 era: the importance and magnitudes of the required corrections for global glacial
2480 isostatic adjustment. *Quaternary Sci. Rev.*, 28:1658–1674, August 2009. doi:
2481 10.1016/j.quascirev.2009.04.004.
- 2482 [256] D. P. Chambers, J. Wahr, M. E. Tamisiea, and R. S. Nerem. Ocean mass from
2483 GRACE and glacial isostatic adjustment. *J. Geophys. Res. (Solid Earth)*, 115:
2484 B11415, November 2010. doi: 10.1029/2010JB007530.
- 2485 [257] W. R. Peltier, R. Drummond, and K. Roy. Comment on "Ocean mass from
2486 GRACE and glacial isostatic adjustment" by D. P. Chambers et al. *J. Geophys.*
2487 *Res. (Solid Earth)*, 117:B11403, November 2012. doi: 10.1029/2011JB008967.
- 2488 [258] D. P. Chambers, J. Wahr, M. E. Tamisiea, and R. S. Nerem. Reply to comment
2489 by W. R. Peltier et al. on "Ocean mass from GRACE and glacial isostatic
2490 adjustment". *J. Geophys. Res. (Solid Earth)*, 117:B11404, November 2012. doi:
2491 10.1029/2012JB009441.

- 2492 [259] J. L. Chen, C. R. Wilson, D. P. Chambers, R. S. Nerem, and B. D. Tapley.
2493 Seasonal global water mass budget and mean sea level variations. *Geophys. Res.*
2494 *Lett.*, 25:3555–3558, 1998. doi: 10.1029/98GL02754.
- 2495 [260] J.F. Minster, A. Cazenave, Y.V. Serafini, F. Mercier, M.C. Gennero, and P. Rogel.
2496 Annual cycle in mean sea level from topexposeidon and ers-1: inference on the
2497 global hydrological cycle. *Global Planet. Change*, 20(1):57 – 66, 1999. ISSN 0921-
2498 8181. doi: 10.1016/S0921-8181(98)00058-7.
- 2499 [261] J. K. Willis, D. P. Chambers, and R. S. Nerem. Assessing the globally averaged
2500 sea level budget on seasonal to interannual timescales. *J. Geophys. Res.*, 2008.
2501 doi: 10.1029/2007JC004517. in press.
- 2502 [262] A. Cazenave and R.S. Nerem. Present-day sea level change: observations and
2503 causes. *ROG*, 42:RG3001, 2004.
- 2504 [263] J. K. Willis, D. Roemmich, and B. Cornuelle. Interannual variability in
2505 upper ocean heat content, temperature, and thermosteric expansion on global
2506 scales. *J. Geophys. Res. (Oceans)*, 109:C12036, December 2004. doi: 10.1029/
2507 2003JC002260.
- 2508 [264] A. Lombard, D. Garcia, G. Ramillien, A. Cazenave, R. Biancale, J. M. Lemoine,
2509 F. Flechtner, R. Schmidt, and M. Ishii. Estimation of steric sea level variations
2510 from combined GRACE and Jason-1 data. *Earth Planet. Sc. Lett.* , 254:194–202,
2511 February 2007. doi: 10.1016/j.epsl.2006.11.035.
- 2512 [265] E. W. Leuliette and L. Miller. Closing the sea level rise budget with altimetry,
2513 Argo, and GRACE. *Geophys. Res. Lett.*, 36:4608–+, February 2009. doi:
2514 10.1029/2008GL036010.
- 2515 [266] A. Cazenave, K. Dominh, S. Guinehut, E. Berthier, W. Llovel, G. Ramillien,
2516 M. Ablain, and G. Larnicol. Sea level budget over 2003-2008: A reevaluation from
2517 GRACE space gravimetry, satellite altimetry and Argo. *Global Planet. Change*,
2518 65:83–88, January 2009.
- 2519 [267] R. S. Nerem, D. P. Chambers, C. Choe, and G. T. Mitchum. Estimating Mean Sea
2520 Level Change from the TOPEX and Jason Altimeter Missions. *Marine Geodesy*,
2521 33(sup1):435–446, 2010. doi: 10.1080/01490419.2010.491031.
- 2522 [268] J.K. Willis, D. P. Chambers, C.-Y. Kuo, and C. K. Shum. Global Sea Level Rise:
2523 Recent Progress and Challenges for the Decade to Come. *Oceanography*, 23:26–35,
2524 2010. doi: 10.5670/oceanog.2010.03.
- 2525 [269] E. W. Leuliette and J. K. Willis. Balancing the Sea Level Budget. *Oceanography*,
2526 24:122–129, 2011. doi: 10.5670/oceanog.2011.32.
- 2527 [270] C. Boening, J. K. Willis, F. W. Landerer, R. S. Nerem, and J. Fasullo. The 2011
2528 La Niña: So strong, the oceans fell. *Geophys. Res. Lett.*, 39:L19602, October 2012.
2529 doi: 10.1029/2012GL053055.
- 2530 [271] J. T. Fasullo, C. Boening, F. W. Landerer, and R. S. Nerem. Australia’s unique

- 2531 influence on global sea level in 2010–2011. *Geophys. Res. Lett.*, 40(16):4368–4373,
2532 2013. doi: 10.1002/grl.50834.
- 2533 [272] D. P. Chambers, J. Chen, R. S. Nerem, and B. D. Tapley. Interannual mean
2534 sea level change and the Earth’s water mass budget. *Geophys. Res. Lett.*, 27:
2535 3073–3076, 2000. doi: 10.1029/2000GL011595.
- 2536 [273] T. Ngo-Duc, K. Laval, J. Polcher, A. Lombard, and A. Cazenave. Effects of land
2537 water storage on global mean sea level over the past half century. *Geophys. Res.
2538 Lett.*, 32(9):n/a–n/a, 2005. ISSN 1944-8007. doi: 10.1029/2005GL022719.
- 2539 [274] D. P. Chambers and J. Schröter. Measuring ocean mass variability from satellite
2540 gravimetry. *J. geodyn.*, 52:333–343, December 2011. doi: 10.1016/j.jog.2011.04.
2541 004.
- 2542 [275] J. Morison, J. Wahr, R. Kwok, and C. Peralta-Ferriz. Recent trends in Arctic
2543 Ocean mass distribution revealed by GRACE. *Geophys. Res. Lett.*, 34:7602–+,
2544 April 2007. doi: 10.1029/2006GL029016.
- 2545 [276] James Morison, Ron Kwok, Cecilia Peralta-Ferriz, Matt Alkire, Ignatius Rigor,
2546 Roger Andersen, and Mike Steele. Changing Arctic Ocean freshwater pathways.
2547 *Nature*, 481(7379):66–70, January 2012. doi: 10.1038/nature10705.
- 2548 [277] R. M. Ponte. A preliminary model study of the large-scale seasonal cycle in
2549 bottom pressure over the global ocean. *J. Geophys. Res.*, 104:1289–1300, 1999.
2550 doi: 10.1029/1998JC900028.
- 2551 [278] R. J. Bingham and C. W. Hughes. Observing seasonal bottom pressure variability
2552 in the North Pacific with GRACE. *Geophys. Res. Lett.*, 33:L8607, April 2006. doi:
2553 10.1029/2005GL025489.
- 2554 [279] Y. T. Song and V. Zlotnicki. Subpolar ocean bottom pressure oscillation and its
2555 links to the tropical enso. *Int. J. Remote Sens.*, 29(21):6091–6107, 2008. doi:
2556 doi:10.1080/01431160802175538.
- 2557 [280] D. P. Chambers and J. K. Willis. Analysis of large-scale ocean bottom pressure
2558 variability in the North Pacific. *J. Geophys. Res. (Oceans)*, 113:11003–+,
2559 November 2008. doi: 10.1029/2008JC004930.
- 2560 [281] D. P. Chambers. ENSO-correlated fluctuations in ocean bottom pressure and
2561 wind-stress curl in the North Pacific. *Ocean Science*, 7(5):685–692, 2011. doi:
2562 10.5194/os-7-685-2011.
- 2563 [282] D. Stammer, R. Tokmakian, A. Semtner, and C Wunsch. How well does a 1/4°
2564 global circulation model simulate large-scale oceanic observations? *J. Geophys.
2565 Res.*, 101:25779, November 1996. doi: 10.1029/96JC01754.
- 2566 [283] V. N. Stepanov and C. W. Hughes. Propagation of signals in basin-scale ocean
2567 bottom pressure from a barotropic model. *J. Geophys. Res. (Oceans)*, 111:C12002,
2568 December 2006. doi: 10.1029/2005JC003450.

- 2569 [284] D. P. Chambers and J. K. Willis. Low-frequency exchange of mass between
2570 ocean basins. *J. Geophys. Res. (Oceans)*, 114:11008–+, November 2009. doi:
2571 10.1029/2009JC005518.
- 2572 [285] S. A. Cunningham, S. G. Alderson, B. A. King, and M. A. Brandon. Transport and
2573 variability of the Antarctic Circumpolar Current in Drake Passage. *J. Geophys.
2574 Res. (Oceans)*, 108:8084, May 2003. doi: 10.1029/2001JC001147.
- 2575 [286] C. W. Hughes, P. L. Woodworth, M. P. Meredith, V. Stepanov, T. Whitworth,
2576 and A. R. Pyne. Coherence of Antarctic sea levels, Southern Hemisphere Annular
2577 Mode, and flow through Drake Passage. *Geophys. Res. Lett.*, 30:1464, May 2003.
2578 doi: 10.1029/2003GL017240.
- 2579 [287] J. C. Fyfe and O. A. Saenko. Simulated changes in the extratropical Southern
2580 Hemisphere winds and currents. *Geophys. Res. Lett.*, 33:L06701, March 2006. doi:
2581 10.1029/2005GL025332.
- 2582 [288] V. Zlotnicki, J. Wahr, I. Fukumori, and Y. Song. Antarctic circumpolar current
2583 transport variability during 2003–05 from GRACE. *J. Phys. Oceanogr.*, 37(2):
2584 230–244, 2007.
- 2585 [289] C. ning, R. Timmermann, S. Danilov, and J. Schröter. Antarctic circumpolar
Bö
2586 current transport variability in grace gravity solutions and numerical ocean model
2587 simulations. In F. Flechtner, T. Gruber, A. Güntner, M. Manda, M. Rothacher,
2588 T. Schöne, and J. Wickert, editors, *System Earth via Geodetic-Geophysical Space
2589 Techniques*, pages 187–199. Springer, Berlin, Heidelberg, 2010. ISBN ISBN 978-
2590 3-642-10227-1. doi: 10.1007/978-3-642-10228-8_15.
- 2591 [290] I. Bergmann and H. Dobslaw. Short-term transport variability of the Antarctic
2592 Circumpolar Current from satellite gravity observations. *J. Geophys. Res.
2593 (Oceans)*, 117:C05044, May 2012. doi: 10.1029/2012JC007872.
- 2594 [291] P. Tregoning, K. Lambeck, and G. Ramillien. GRACE estimates of sea surface
2595 height anomalies in the Gulf of Carpentaria, Australia. *Earth Planet. Sc. Lett.* ,
2596 271:241–244, July 2008. doi: 10.1016/j.epsl.2008.04.018.
- 2597 [292] B. Wouters and D. Chambers. Analysis of seasonal ocean bottom pressure
2598 variability in the Gulf of Thailand from GRACE. *Global Planet. Change*, 74: 76–
2599 81, November 2010.
- 2600 [293] R.E.M. Riva, J.L. Bamber, D. A. Lavalley, and B. Wouters. Sea-level fingerprint
2601 of continental water and ice mass change from GRACE. *Geophys. Res. Lett.*, 37:
2602 L19605, 2010. doi: 10.1029/2010GL044770.
- 2603 [294] N. T. Vinogradova, R. M. Ponte, M. E. Tamisiea, K. J. Quinn, E. M. Hill, and
2604 J. L. Davis. Self-attraction and loading effects on ocean mass redistribution at
2605 monthly and longer time scales. *J. Geophys. Res. (Oceans)*, 116:C08041, August
2606 2011. doi: 10.1029/2011JC007037.
- 2607 [295] B. Wouters, R. E. M. Riva, D. A. Lavallée, and J. L. Bamber. Seasonal variations

- 2608 in sea level induced by continental water mass: First results from GRACE.
2609 *Geophys. Res. Lett.*, 38:3303–+, February 2011. doi: 10.1029/2010GL046128.
- 2610 [296] B. Killett, J. Wahr, S. Desai, D. Yuan, and M. Watkins. Arctic Ocean tides from
2611 GRACE satellite accelerations. *J. Geophys. Res. (Oceans)*, 116:C11005, November
2612 2011. doi: 10.1029/2011JC007111.
- 2613 [297] R. D. Ray, S. B. Luthcke, and J.-P. Boy. Qualitative comparisons of global ocean
2614 tide models by analysis of intersatellite ranging data. *J. Geophys. Res. (Oceans)*,
2615 114:9017–+, September 2009. doi: 10.1029/2009JC005362.
- 2616 [298] D. Ren, R. Fu, L. M. Leslie, D. J. Karoly, J. Chen, and C. Wilson. A multirheology
2617 ice model: Formulation and application to the Greenland ice sheet. *J. Geophys.*
2618 *Res.*, 116:D05112, March 2011. doi: 10.1029/2010JD014855.
- 2619 [299] Armin Köhl, Frank Siegmund, and Detlef Stammer. Impact of assimilating
2620 bottom pressure anomalies from GRACE on ocean circulation estimates. *J.*
2621 *Geophys. Res.*, 117(C4):C04032, 2012. ISSN 2156-2202. doi: 10.1029/
2622 2011JC007623.
- 2623 [300] A. Hu, G. Meehl, W. Han, and J. Yin. Effect of the potential melting of
2624 the Greenland Ice Sheet on the Meridional Overturning Circulation and global
2625 climate in the future. *Deep-Sea Res. Pt. II*, 58(17-18):1914–1926, 2011. doi:
2626 10.1016/j.dsr2.2010.10.069.
- 2627 [301] D. N. Wiese, R. S. Nerem, and F. G. Lemoine. Design considerations for a
2628 dedicated gravity recovery satellite mission consisting of two pairs of satellites.
2629 *J. Geodesy*, 86:81–98, February 2012. doi: 10.1007/s00190-011-0493-8.
- 2630 [302] I Panet, J Flury, R Biancale, T Gruber, J Johannessen, MR van den Broeke, T van
2631 Dam, P Gegout, CW Hughes, G Ramillien, et al. Earth system mass transport
2632 mission (e. motion): A concept for future earth gravity field measurements from
2633 space. *Surveys in Geophysics*, 34(2):141–163, 2013.
- 2634 [303] NG2 Team. Assessment of a Next Generation Gravity Mission to Monitor the
2635 Variations of Earth’s Gravity Field Technical Report NG2-ASG-FR, Astrium,
2636 2011.
- 2637 [304] G. A, J. Wahr, and S. Zhong. Computations of the viscoelastic response of a
2638 3-D compressible Earth to surface loading: an application to Glacial Isostatic
2639 Adjustment in Antarctica and Canada. *Geophys. J. Int.*, 192:557–572, February
2640 2013. doi: 10.1093/gji/ggs030.
- 2641 [305] O. B. Andersen and P. Knudsen. DNSCO8 mean sea surface and mean dynamic
2642 topography models. *J. Geophys. Res. (Oceans)*, 114:C11001, November 2009. doi:
2643 10.1029/2008JC005179.
- 2644 [306] S. Levitus, J. I. Antonov, T. P. Boyer, O. K. Baranova, H. E. Garcia, R. A.
2645 Locarnini, A. V. Mishonov, J. R. Reagan, D. Seidov, E. S. Yarosh, and M. M.
2646 Zweng. World ocean heat content and thermosteric sea level change (0-2000

2647
2648

m), 1955-2010. *Geophys. Res. Lett.*, 39:L10603, May 2012. doi: 10.1029/2012GL051106.